EUROPEAN Journal of Molecular Biotechnology

Has been issued since 2013.
E-ISSN 2409-1332
2019. 7(2). Issued 2 times a year

Journal is indexed by: **Chemical Abstracts Service** (USA), **CiteFactor** – Directory of International Reseach Journals (Canada), **Cross Ref** (UK), **EBSCOhost Electronic Journals Service** (USA), **Global Impact Factor** (Australia), **Journal Index** (USA), **Electronic scientific library** (Russian Federation), **Open Academic Journals Index** (USA), **Sherpa Romeo** (Spain), **ULRICH's WEB** (USA).

All manuscripts are peer reviewed by experts in the respective field. Authors of the manuscripts bear responsibility for their content, credibility and reliability.

Editorial board doesn't expect the manuscripts' authors to always agree with its opinion.

Postal Address: 1367/4, Stara Vajnorska str., Bratislava – Nove Mesto, Slovakia, 831 04

Website: http://ejournal8.com/
E-mail: aphr.sro@gmail.com

Founder and Editor: Academic Publishing House Researcher s.r.o.

Release date 15.12.19
Format 21 × 29,7/4.

Headset Georgia.

Order № 20.

European Journal of Molecular Biotechnology

2019

Is. 2

C O N T E N T S

Articles

Letters to the Editorial

Published in the Slovak Republic
European Journal of Molecular Biotechnology
Has been issued since 2013.
E-ISSN: 2409-1332
2019, 7(2): 49-62

DOI: 10.13187/ejmb.2019.2.49
www.ejournal8.com

Articles

Modern Nanomaterials and Nanotechnology in Diagnosis and Treatment of Malignant Tumors of Gastrointestinal Tract

Ahmad H. Al-Humairi [a, b, *]

[a] University of Babylon, Iraq
[b] Volgograd State University, Russian Federation

Abstract

This review aims to systematize current achievements in the use of nanotechnology for the detection, diagnosis, treatment and prognosis of gastrointestinal (GI) malignant tumors. Information about the use of nanovesicles isolated from the body (exosomes) and synthesized (liposomes) for targeted delivery of drugs and imaging agents to cancer cells for this purpose is presented. A separate section of the review deals with revealing the laws of transport and interaction of nanoparticles with tumor cells to diagnose and treat GI malignant tumors. Here we present modern research to determine the effectiveness of micelles, liposomes, solid lipid nanoparticles, mesoporous silica nanoparticles and particles containing perfluorocarbon. The problems and achievements in the use of nanoparticles for targeted delivery of chemotherapy drugs to cancer cells using ultrasound are considered. The authors conclude the review with a list of the most promising areas of development in this field of molecular medicine and biotechnology, including combinations of direct cytotoxic action, immunomodulation, impact on tumor vessels (1), and combination of diagnostic component with facilitating the detection of tumor cells well-known as teranostics.

Keywords: nanotechnologies, nanoparticles, nanovesicles, gastrointestinal tract, malignant tumors, teranostics, target therapy, target drug delivery.

1. Introduction

Nanomaterials, literally, meaning materials with a dimension of 10^{-9}, in fact include all natural, modified or completely artificial objects that have their own dimensions, or surface profile, or pores smaller than 100 nm. They have now revolutionized materials science and became one of the main drivers of technological progress. Complexes of processes based on these materials, defined as nanotechnologies, have led to the rapid development of energy, electronics, computer technologies, and many other branches of human activity (Breding et al., 2014; Lapčík et al., 2019; Madamsetty et al., 2019; Shi, Lammers, 2019).

Applied to biology and medicine, nanotechnology proved to be a great tool for understanding life at the molecular level, and immediately after their first application for this purpose, scientists began to develop technologies for active intervention in biological systems. As a result, we have genetic engineering, molecular diagnostics, and high-precision (targeted, personified drug delivery to target cells) technologies for treating diseases. Moreover, at a certain stage, it turned out to be

* Corresponding author
E-mail addresses: ahmed.h.mneahil@gmail.com (A.H. Al-Humairi)

very effective to combine these two directions. As a result, a new modern direction appeared in medicine, named as teranostics, like the combination of treatment and diagnosis in one technology (Ai et al., 2016; Deyev, Lebedenko, 2017; Sokolov et al., 2017).

Modern nanotechnologies have significantly improved the diagnostics and treatment of cardiovascular, autoimmune, endocrine diseases (primarily diabetes and thyroid diseases), infections, injuries and disorders of the musculoskeletal system, dental pathology, etc. (Sharma et al., 2015; Melerzanov et al., 2016; Kalita et al., 2016; Novochadov et al., 2016; Mukherjee et al., 2019).

Teranostic agents can be obtained using the following strategies: screening plant extracts for nanomaterial synthesis (1); standardization of various physical and chemical parameters for biosynthesis (2); addition of therapeutic and imaging agents (3); and characterization of nanocarriers using analytical methods (4) (Duan et al., 2015; Madamsetty et al., 2019).

Of particular interest is the progress caused by the introduction of theranostics of nanotechnology in experimental and clinical oncology. The vector of development in antitumor therapy is aimed at an approach called precision personified medicine with the most integrated and versatile effect on the tumor (Arnedos et al., 2015; Lloyd et al., 2015). The acquired knowledge and technologies are actively used to create new methods and tools for cancer diagnosis and therapy based on compounds selectively acting on specific molecular targets, as well as new systems for delivering these agents to cancer cells that do not affect healthy organs and tissues.

2. Discussion

Nanotechnology teranostics of GI malignant tumors: The common principles

In this review, we focused on the systematization of recent successes in this direction on the example of malignant GI tumors. These tumors are among the most common and deadly malignancies worldwide, mainly due to late diagnosis and lack of effective treatment methods. The most typical tumors of this localization are esophageal squamous cell carcinoma (ESCC), gastric cancer (GC), colorectal cancer (CRC), and peritoneal carcinomatosis (PC) (Bray et al., 2018). It is these models are the base to develop new technologies for influencing GI tumors (Huang et al., 2019).

Special attention should be paid to CRC, because due to its relatively slow and hidden progression, as well as its high prevalence, the early detection and effective treatment of this tumor constitute not only a medical but also a social problem in the modern world.

Thus, the problem is to accurately identify, diagnose, and prescribe therapy at the earliest possible stages of tumor progression. The appearance of precancerous lesions that result from abnormal cell growth indicates a precancerous condition with high risk to develop into tumors. These conditions include atrophic gastritis, chronic ulcerative colitis, various variants of epithelial metaplasia and dysplasia (Li et al., 2018b; Rentien et al., 2018; Huang et al., 2019).

A serious point in the treatment of tumors is the situation when cancer cells develop drug resistance and stop responding to chemotherapy. It resulted in necessity to increase the dose (and toxicity) or provide targeted delivery of the drug to the tumor cell (Lian et al., 2017; Li et al., 2019).

There are four critical aspects to consider when developing an effective teranostic nanoplatform: choosing an effective therapeutic agent (1), choosing a stable carrier (2); implementing a targeted and sustainable approach to drug release (3); choosing a imaging agent carefully (4) (Muthuraj et al., 2016; Chi et al., 2017).

Special attention is paid to NPs obtained from plant viruses. They are attractive because they are both biocompatible and biodegradable, and their antigenicity can be weakened by a polymer coating (Pitek et al., 2016; Czapar, Steinmetz, 2017). Viral NPs can be designed and constructed using genetic and chemical protocols. Plant viruses (as opposed to animal or human viruses) are a safe platform because they do not cause diseases in humans. Their size is in the nanometer range, which helps to increase tissue permeability and retention in tumors. Multivalent nature of these NPs allows the incorporation of several molecules with different functions, which allows, for example, combining a cell targeting ligand and an imaging agent on the same nanoparticle (Gamper et al., 2019).

Nanovesicles (NVs), which will be discussed first, may have different origins. One group includes natural NVs (exosomes), which have a diameter from 25 to 1000 nm, and therefore the largest of them, strictly speaking, no longer belong to nanoobjects. Exosomes can be found in body

fluids, where they are involved in antigen presentation, immune response, intercellular signaling, and RNA and protein transport (Sun et al., 2018; Zhu et al., 2018). Second group unites synthetic vesicles, which can be exclusively synthetic biomimetic materials or combined into hybrids with natural NVs (Atay et al., 2018; Danaei et al., 2018; Li et al., 2018a).

Of particular note are the so-called tumor exosomes containing proteins and RNA (including microRNAs and messenger RNAS), which are malignant vesicles that are found in the blood serum and other biological fluids of cancer patients. These exosomes have great promise in diagnosing and predicting diseases, as they can protect labile cancer biomarkers from degradation (Boyiadzis et al., 2017; Arenaccio et al., 2019).

Success in using NVs for precancerous and malignant GI diseases

Both body-derived NPs and synthesized NVs are widely used in the detection, diagnosis, treatment and prognosis of different GI tumors, especially in primary focal lesions. Figure 1 demonstrates the working classification of NVs (Huang et al., 2019) and variants with achieved success in GI malignant diseases using NVs.

Analyzing the general problems of targeted use of NVs, it is necessary to point out the need to comply with the basic principles of biofunctionality, biomimetics and biocompatibility. Only in this case, a specific delivery system will be able to transport microRNA, mRNA, siRNA, lncRNA, peptides and synthetic drugs to the target cells (Barile, Vassalli, 2017; Zhang et al., 2018b).

NVs should ideally not exhibit significant cytotoxicity or activate the body's defense systems (Tagalakis et al., 2017). Implantation of NVs carrying targeted molecules can be performed indirectly (penetration through a concentration gradient) (Roma-Rodrigues et al., 2017) or using direct methods (electroporation) (Ye et al., 2018). This method involves direct NVs injection into the cytoplasm, bypassing the endocytosis pathway. For example, the 3DNEP chip was designed to deliver extremely small biological elements to huge plasmids with almost zero negative effects on target cells (Ye et al., 2018).

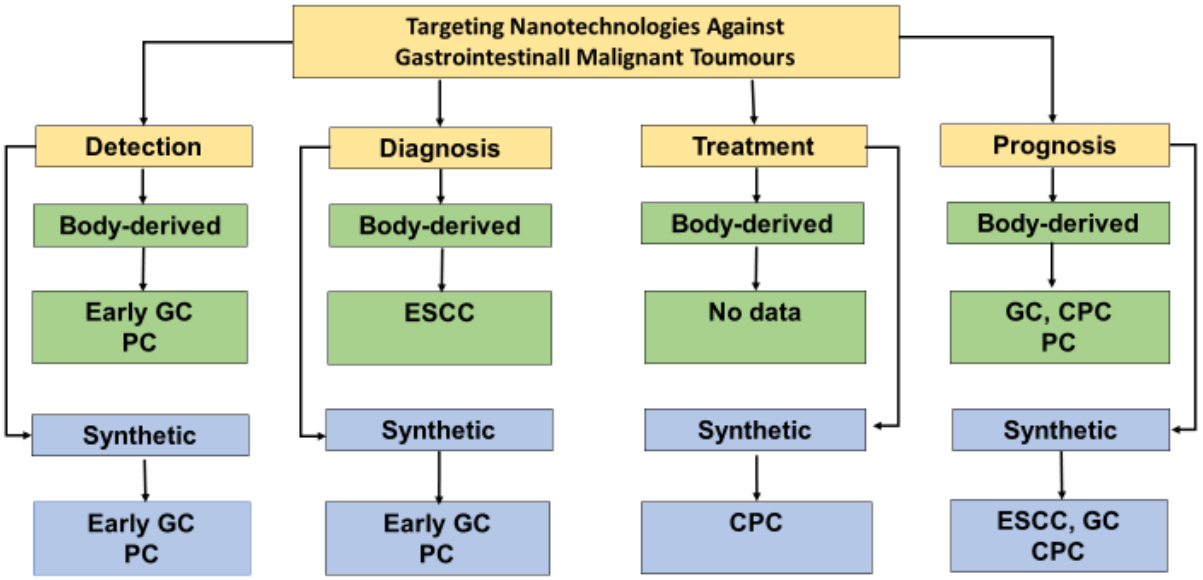

Fig. 1. Targeted using NVs of various origins in the most common malignant GI tumors

For primary detection of GI tumors, both NVs isolated from the body and synthetic ones are used. Thus, Lin et al. (2018) described that the tumor factor lncU EGC1, encapsulated in exosomes, can be the basis for highly sensitive, stable, and non-invasive diagnosis of precancerous chronic atrophic gastritis. MicroRNAs, lncRNAs, and multiple proteins in tumor exosomes can be used as non-invasive disease biomarkers for early GC diagnosis (Wang et al., 2018). Exosomes released into the serum by cancer cells protect their contents from degradation and can be used to detect PC at the earliest, most treatable stage (McMullen et al., 2017). Among the synthetic NVs used for the detection of GI tumors, it should be noted that they are used in the composition of liposomes as contrast agents for screening and detecting the early GC stage (Zhang et al., 2018a) and effective

use of NVs loaded with superparamagnetic iron oxide as new contrast agents for human CRC imaging (Feng et al., 2016).Diagnostic use of NVs is to specify the location, stage, and degree of tumor malignancy. Yan et al. (2018) described the possibility of diagnosing and predicting further human ESCC progress by analysis of oncogenic exosomes expressing Stathmin-1. Similarly, increased expression of MicroRNA 296-5p in exosomes may be a promising diagnostic biomarker for early GC (Huang et al., 2017). A synthetic pegylated liposome modified with the Arg-Gly-Asp peptide and containing Indocyanine Green can accumulate in tumor tissues for the diagnosis of early GC (Ding et al., 2015). The near-infrared fluorescent liposomal probes effectively targeting peritoneal disseminated tumors for accurate GC diagnosis may be another example of effective NVs application (Hoshino et al., 2015).

We have met few successful examples of NVs using for treatment of malignant GI tumors. Pegylated melanin-like liposomes were able to carry enough doxorubimicin (DOX) for targeted delivery to human CRC cells. As the size of the particles that were synthesized at a pH of approximately 7.5-8 increased, the loading efficiency of the drug also increased due to the expanded internal volume for the drugs. However, in contrast to the loading efficiency, the release of the drug occurred much faster from smaller particles that were synthesized at pH 9. The developed NVs are able to overcome drug resistance during long-term chemotherapy (Wang et al., 2016; Li et al., 2017).

Studying the possibilities of NVs using for tumor prognosis Sun et al. (2017) found that microRNA in exosomes secreted by both cancer stem cells and differentiated cells may reflect the stage of GC progression and metastasis, as well as indirectly act like an indicator for measuring the likelihood of GC recurrence after therapy. Exosomal microRNAs from lavage peritoneal fluid are potential predictive biomarkers for peritoneal metastasis in GC (Tokuhisa et al., 2015).

Exosomal microRNA 19a in serum is an early predictive biomarker of relapses in human CRC (Matsumura et al., 2015). There are examples of successful use of synthetic NVs for predicting the course of GC. Thus, liposomes transfected with the PEGfp-N1 Kangai 1 plasmid can inhibit migration and invasion of GC cells and improve tumor prognosis (Guo et al., 2015). Nanoliposomal quercetin in combination with CD133 antiserum may be a prognostic marker in human ESCC cases (Zheng et al., 2014). NVs obtained by "green chemistry" methods using grapefruit juice can improve the prognosis of colitis caused by dextran sulfate sodium in mice, which is a model of precancerous colitis in humans (Wang et al., 2014).

Nanocapsulation of chemotherapeutic agents in biocompatible polymer or lipid matrices has great potential for improving the pharmacokinetics and effectiveness of traditional chemotherapy while reducing the systemic toxicity of anti-cancer drugs. Labeling the surface of nanoparticles with specific ligands for cancer cells, namely monoclonal antibodies or antibody fragments, provides a means to target more aggressive clones. This increases the effectiveness of nanopreparations, while reducing their side effects. Other ligands, such as peptides/small proteins and antibodies/antibody fragments that have an affinity for either the tumor cells or its vascular system, are also widely and successfully used for targeting GI carcinomas. To date, two nanocomplexes have advanced beyond the preclinical stages for advanced solid tumor metastases: MCC-465, an anti-myosin heavy chain(a) as an immunoliposome (1); and MBP-426, a transferrin-liposome-oxaliplatin conjugate (2). However, none of them have yet been approved for clinical use (Fernandes et al., 2015).

Success in using NPs for precancerous and malignant GI diseases

Chemotherapy drugs such as doxorubicin (DOX) are usual approach to first-line therapy against CRC and lung cancer, but the effectiveness of these drugs is limited by the development of drug resistance. One way to overcome this disadvantage is to synthesize new compounds suitable for targeted selective delivery of the drug to cancer cells (Martins et al., 2016; Ma et al., 2016; Lenis-Rojas et al., 2017).

In the last 10 years, nanoscale drug delivery systems such as liposomes, solid lipid nanoparticles, polymer micelles, mesoporous silica, carbon nanomaterial, and gold NPs have emerged that have increased the selectivity of anti-cancer therapy and reduced the toxicity of drugs (Qu et al., 2014; Hou et al., 2016; Tang et al., 2017; Millard et al., 2017). For example, Huo et al. (2014a) presented platform on gold NPs with different sizes, and they found that small gold NPs can effectively enter the cell nucleus. Similarly, DNA nanotechnology is widely studied in various

biomedical fields, including as a promising drug delivery system for cancer treatment (Miao et al., 2015; Xia et al., 2016; Wang et al., 2017).

Although ultrasound is most widely known for its use in diagnostic imaging, its energy can be used to influence cell function and drug delivery. In recent years, increasing attention has been paid to drug delivery using ultrasound, as it allows spatially limited delivery of the therapeutic compound to target areas such as tumors (Xhu et al., 2013). The combination of ultrasound and nanocomposition drug delivery systems eliminates the main limitations of traditional drug delivery systems, including: insufficient absorption and accumulation of nanoparticles by cells (1); limited amount of drug delivered or released from nanoparticles (2); specific targeted drug-delivery carriers nanoparticles (3) (Tharkar et al., 2019).

In addition, the NPs combination with ultrasound has significant potential to improve drug delivery efficiency and reduce drug side effects by better overcoming physiological barriers such as endothelial lining of blood vessels, endothelium of target tissues, dense epithelial cell layers, tissue interstitial, plasma cell membrane, diffusion through the cytoplasm, and penetration into the nucleus through the nuclear membrane (Barua, Mitragotri, 2014; Rosenblum et al., 2018; Thakkar et al., 2019).

Figure 2 summarized more interesting information about the properties of different NPs used in ultrasound techniques to facilitate the delivery of anti-cancer drugs to target cells based on open sources (You et al., 2016; Horise et al., 2019; Özdemir et al., 2019; Sadegh Malvajerd et al., 2019; Tharkar et al., 2019).

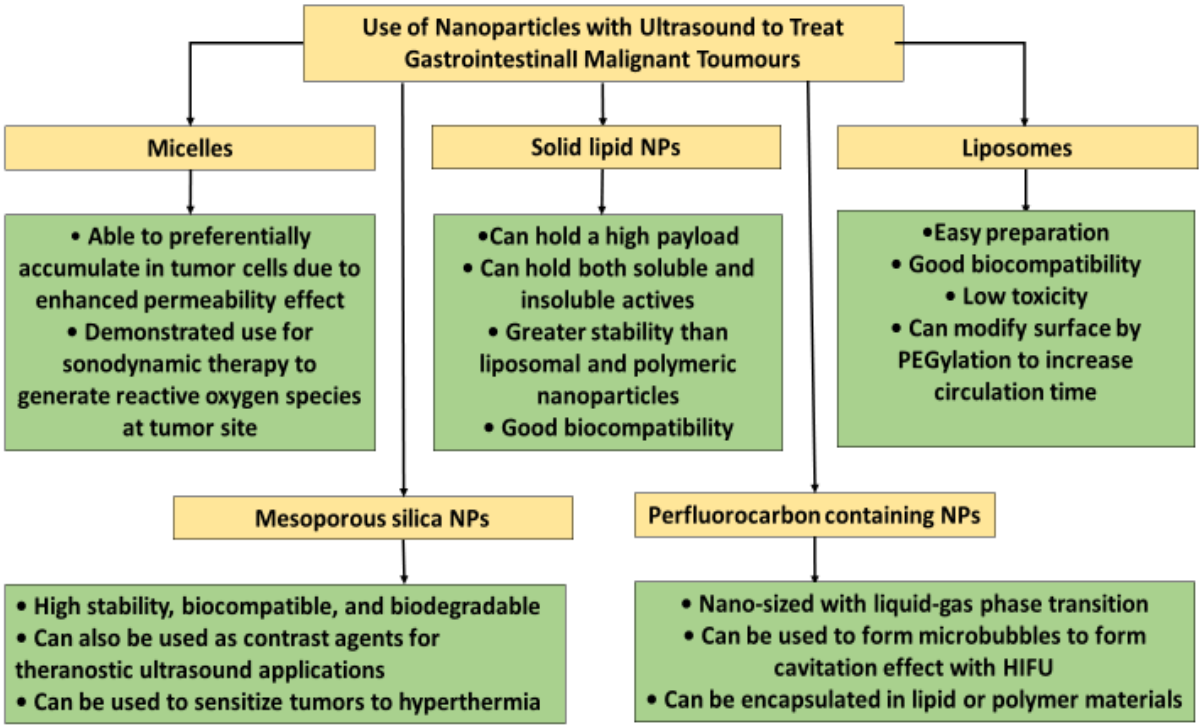

Fig. 2. Joint use of nanoparticles and ultrasound in the treatment of GI tumors: properties of different variants of nanoparticles

The most used tumor-specific fragments for targeting are abnormally overexpressed tumor receptors. These substances include endothelial growth factor receptor (VEGFR), epidermal growth factor receptor (EGFR integrin receptor vascular), folate receptor (FR), and human epidermal growth factor receptor 2 (HER2) (Ko et al., 2019).

Encapsulation of therapeutic drug molecules in nanoparticles can improve their bioavailability, bio-distribution, and can also improve internalization in the target cell. However, despite recent advances in nanotechnology, only ~1 % of nanoparticles accumulate in tumors (Wilhelm et al., 2016).

The effective extravasation of NPs through the tumor microenvironment is a serious barrier. Tumor tissue usually have abnormal vascularization, exhibit excessive extracellular matrix density, which resists the diffusion of therapeutic NPs to cancer cells. In addition, increased interstitial fluid pressure, which is the result of rapid cell proliferation, leads to ineffective anti-cancer treatment activity (Sriraman et al., 2014; Zhang et al., 2019a). Mucus becom another barrier to drug/nanoparticle delivery to GI tumors (Chen et al., 2017).

Ultrasound delivery of drug-loaded NPs eliminates the above limitations by increasing the accumulation and uptake of NPs by cells, as well as stimulating the release of the drug only at the target cells. We can achieve these effects through various processes, such as sonoporosis, cavitation, or hyperthermia (Mullick Chowdhury et al., 2017).

Khaled et al. (2019) developed a new type of composite of silver nanoparticles, including pegylated graphene quantum dots and decorated silver nanoprisms (pGAgNPs), which demonstrated good intracellular absorption and radiosensitization *in vitro* in radiation-sensitive HCT116 cells and relatively radiation-resistant HT29 cells of human CRCr.

To improve the treatment of CRC Zhong et al. (2019) prepared paclitaxel-loaded NPs from PLGA (PLGA-PTX) and evaluated their anti-cancer activity in co-administered protocol with the iRGD peptide. Compared to free PTX, encapsulated ones retained preferential cytotoxicity in relation to various CRC cells, effectively sparing healthy cells. Treatment with PLGA-PTX resulted in stopping the cell cycle in the G2/M phase and apoptosis, which led to inhibition of migration and invasion of cancer cells. The proposed co-administration system, devoid of covalent conjugation, provided more convenient means to combine various therapeutic agents with iRGD achieving personalized nanotherapy (Zhong et al., 2019).

The development of multi-functional teranostic NPs presents a number of challenges, including visualization quality, 'load capacity', toxicity of internal ingredients, storage and stability *in vivo*, complexity of synthesis, batch repeatability, production costs, and regulatory barriers. By varying the size, shape, and surface properties of NPs, we can adjust their biocompatibility and specificity with target cells. Current interests are mainly related to noninvasive deep tissue imaging and targeted drug therapy (Yang et al., 2019).

Selective and complex effects on the tumor: recent findings and directions of development

NPs can effectively enhance immunomodulatory effects and modulate the immune response by manipulating immune cells to facilitate targeted delivery (Riley et al., 2019; Nam et al., 2019; Sun et al., 2019).

They can act as immunoactive agents to program the tumor cells themselves (Feng et al., 2018; Chen et al., 2019), antigen-presenting cells (Kuai et al., 2016; Zhu et al., 2017), T cells (Tang et al., 2018), or affect tumor-associated macrophages (Zanganeh et al., 2016).

The method of directed radionuclide therapy is based on the selective accumulation of a pharmaceutical containing a radioactive isotope only in the tumorous tissues (Bronte et al., 2015; Vodeneev et al., 2015). Directed radionuclide therapy should only affect tumor cells and not affect normal cells. This condition makes it possible to create a pharmaceutical product with a large, and in the ideal case – with an infinitely large therapeutic index, which will allow you to get high efficiency with minimal side effects (Golden, Apetoh, 2015; Pouget et al., 2015). Creating a pharmaceutical with a prolonged action and a high therapeutic index requires the selection of a radioisotope and a platform for its delivery to the tumor.

Tumor-induced angiogenesis has been one of the focuses of anti-tumor therapy for several decades. The immature and fenestrated vascular network of the tumors contributes to the intravasation of cancer cells and the spread of metastases, while preventing the antitumor effectiveness of immune cells and the effective diffusion of chemotherapy drugs (Mattheolabakis, Mikelis, 2019).

In recent years, starvation therapy has become an effective method of suppressing tumor growth and survival by blocking blood flow or depriving them of essential nutrients or oxygen (Chung et al., 2015; Selwan et al., 2016; Yu et al., 2019). Nutrient transport can be blocked by stopping the blood supply to the tumor through treatment with angiogenesis-inhibiting agents or vascular disrupting agents (Chase et al., 2017) and transarterial chemoembolization (Lin et al., 2016). In addition, agents that can consume intracellular nutrients, oxygen, or mediate the uptake of necessary substances by tumor cells leading to tumor starvation and necrosis (Zhang et al., 2017).

Most in vivo model experiments use mice carrying implanted human tumor cells to develop these platforms. Against GI tumors are the most popular cell line CT26 tumor bearing mice (Song et al., 2016; Liu et al., 2017; Chen et al., 2018). HT-29, C8161 tumor bearing mice and other models are also used to define therapeutic index and possible side effects (Pouget et al., 2015; Sui et al., 2017; Yu et al., 2019). The use of directed radionuclide therapy is convenient for the patient. After the introduction of the drug (within a few minutes), it affects the tumor for several days, the patient should not undergo additional procedures during this time (Golden, Apetoh, 2015). Creating a pharmaceutical with a prolonged action and a high therapeutic index requires the selection of a radioisotope and a platform for its delivery to the tumor.

Various NPs used as materials for starvation therapy can be natural and synthetic polymers (Zhang et al., 2019b; Yang et al., 2019), liposome (Zhang et al., 2018c), organometallic frameworks, or gold nanoparticles (Au-NPs) (Son et al., 2017) and NPs silica (Yang et al., 2018; Yu et al., 2019). All of they were used for co-delivery of carcinogenic agents and other therapeutic agents in order to reduce drug side effects, increase their target effectiveness, increase the stability and half-life of therapeutic agents, and co-delivery of multiple drugs to overcome drug resistance (Jing et al., 2018).

Thus, the epidermal growth factor receptor (EGFR) is often overexpressed in cancer cells and this can be used for selective exposure with the therapeutic monoclonal antibody cetuximab (approved by the FDA for the treatment of CRC). The drug blocks EGFR signaling transduction, leading to cell cycle arrest, induction of apoptosis, inhibition of angiogenesis, metastasis, internalization, and self-regulation (Pabla, 2015; Pedrosa et al., 2019).

Zinc is another such agent. One of these compounds, [Zn (DION)2] Cl2-ZnD (DION-1,10-phenanthroline-5,6-DION), showed high cytotoxic potential against cancer cell lines, with IC50 values 2 times and 70 times lower than doxorubicin (DOX) and cisplatin, respectively. Zn-DION has been described as highly cytotoxic to HCT116 colorectal carcinoma cells, compared to ZnCl2 or only DION. When exposed to IC50 Zn-DION cells, chromatin condensation and core fragmentation were observed for 48 hours, and the number of apoptotic cells increased fourfold during double staining with propidium iodide and V-FITC annexin. Together, these results confirm that Zn-DION induces HCT116 cell death through activation of the internal apoptotic pathway (Pedrosa et al., 2019).Molecular imaging technology is important for detecting tumors and monitoring prognosis as a result of its high accuracy and reliability for elucidating biological processes and monitoring pathological conditions (Zhan et al., 2017). Fortunately, magnetic resonance contrast agents may enhance contrast, thereby increasing the sensitivity of magnetic resonance diagnostics. Approximately 35 % of clinical magnetic resonance imaging devices require CAs (Lei et al., 2017).

Various T1 – or T2-MRI CAS based on NPS gadolinium, manganese, and iron oxide were developed to increase the contrast sensitivity of images. However, conventional drugs based on small-sized complexes usually suffer from short blood circulation times and severe in vivo toxicity, which can lead to nephrogenic systemic fibrosis and cerebral deposition (Xiang et al., 2018). So, researchers turned to superparamagnetic nanoparticles, especially Fe_3O_4 NPs. Over the past 20 years, several T2 contrast agents based on these NPs have been clinically tested and approved by the US Food and Drug Administration. Unfortunately, these NPs were somewhat limited in their clinical use due to their own dark signals and susceptibility artifacts in MRI (Neves et al., 2016).

Mn-based contrast agents are considered ideal substitutes because of their bright signals and good biocompatibility. manganese oxide NVs. Variants that have appeared in recent years have shown little toxicity and good contrast effects (Hsu et al., 2016), as well as chemical and magnetic resonance characteristics of reactive contrast agents based on Mn (Garcia-Hevia et al., 2019; Cai, Zhu, Zeng et al., 2019).

Based on previously identified complexes of integrin alpha-6 and E-cadherin on the surface of CRC cells, but not typical for normal colon cells, peptides of the composition CGIYRLRS and CGVYSLRS were created, being able to compete with angiopoietin-like protein 6 in CRC tissues. Modular nanosystems were created to obtain a visualization platform consisting of fluorescent silica-PEG NPs with these peptides on the surface. The NPs contained dye rhodamine A, cyanine 5, or both (two-color). The study silica NPs *in vivo* on model mice with a pseudo-metastatic tumor (human CRC cancer cells were implanted in the spleen of diabetic mice) using three-dimensional

confocal micrography showed that labeled these NPs were located very close to the tumor's blood vessels (Marchio, Bussolino, 2018).

3. Conclusion

In modern diagnostics and therapy of GI tumors, NPs of natural, synthetic and hybrid origin are actively used. They can have a solid or composite structure (shell + content), their composition is most often represented by proteins or peptides, DNA or RNA, polysaccharides, lipids, metals, usually in combination with each other. The effects of such NPs are very diverse and include direct cytotoxic action, immunomodulation, impact on tumor vessels, etc. The combination of these different influences and a diagnostic component associated with facilitating the identification of tumor cells is the most promising direction of development in this area being the essence of the new approach, theranostics.

References

Ai et al., 2016 – *Ai, X., Mu, J., Xing, B.* (2016). Recent advances of light-mediated theranostics. *Theranostics*. 6: 2439-2457.

Arenaccio et al., 2019 – *Arenaccio, C., Chiozzini, C., Ferrantelli, F. et al.* (2019). Exosomes in therapy: engineering, pharmacokinetics and future applications. *Curr Drug Targets*. 20(1): 87-95. DOI: 10.2174/1389450119666180521100409

Arnedos et al., 2015 – *Arnedos, M., Vicier, C., Loi, S., Lefebvre, C.* (2015). Precision medicine for metastatic breast cancer limitations and solutions. *Nat. Rev. Clin. Oncol.* 12: 693-704.

Atay et al., 2018 – *Atay, S., Wilkey, D.W., Milhem, M., et al.* (2018). Insights into the proteome of gastrointestinal stromal tumors-derived exosomes reveals new potential diagnostic biomarkers. *Mol. Cell. Proteomics*. 17(3): 495-515. DOI: 10.1074/mcp.RA117.000267

Barile, Vassalli, 2017 – *Barile, L., Vassalli, G.* (2017). Exosomes: therapy delivery tools and biomarkers of diseases. *Pharmacol. Ther*. 174: 63-78. DOI: 10.1016/j.pharmthera.2017.02.020

Barua, Mitragotri, 2014 – *Barua, S., Mitragotri, S.* (2014). Challenges associated with penetration of nanoparticles across cell and tissue barriers: a review of current status and future prospects. *Nano Today*. 9: 223-243. DOI: 10.1016/j.nantod.2014.04.008

Boyiadzis et al., 2017 – *Boyiadzis, M, Whiteside, T.L.* (2017). The emerging roles of tumor-derived exosomes in hematological malignancies. *Leukemia*. 31(6): 1259-1268. DOI: 10.1038/leu.2017.91

Breding et al., 2014 – *Breding, K., Jimbo, R., Hayashi, M. et al.* (2014). The effect of hydroxyapatite nanocrystals on osseointegration of titanium implants: an in vivo rabbit study. *Int. J. Dent.*: e171305.

Bray et al., 2018 – *Bray, F., Ferlay, J., Soerjomataram, I. et al.* (2018). Global cancer statistics 2018: GLOBOCAN estimates of incidence and mortality worldwide for 36 cancers in 185 countries. *CA-Cancer J. Clin*. 68: 394-424.

Bronte et al., 2015 – *Bronte, G., Sortino, G., Passiglia, F. et al.* (2015). Monoclonal antibodies for the treatment of non-haematological tumours: update of an expanding scenario. *Expert Opin. Biol. Ther*. 15(1): 45-59.

Cai et al., 2019 – *Cai, X., Zhu, Q., Zeng, Y. et al.* (2019). Manganese oxide nanoparticles as MRI contrast agents in tumor multimodal imaging and therapy. *Int. J. Nanomedicine*. 14: 8321-8344. DOI: 10.2147/IJN.S218085

Chang et al., 2016 – *Chang, L., Bertani, P., Gallego-Perez, D., et al.* (2016). 3D nanochannel electroporation for high-throughput cell transfection with high uniformity and dosage control. *Nanoscale*. 8(1): 243-252. DOI: 10.1039/c5nr03187g

Chase et al., 2017 – *Chase, D.M., Chaplin, D.J., Monk, B.J.* (2017). The development and use of vascular targeted therapy in ovarian cancer. *Gynecol. Oncol.* 145: 393-406. DOI: 10.1016/j.ygyno.2017.01.031

Chen et al., 2017 – *Chen, Q., Xiao, B., Merlin, D.* (2017). Low-frequency ultrasound may improve drug penetration in colonic mucosa. *Transl. Cancer Res.* 6(Suppl 2): S276-279. 10.21037/tcr.2017.03.62

Chen et al., 2018 – *Chen, Z.X., Liu, M.D., Zhang, M.K. et al.* (2018). Interfering with lactate-fueled respiration for enhanced photodynamic tumor therapy by a porphyrinic MOF nanoplatform. *Adv. Funct. Mater*. 28: 1803498.

Chen et al., 2019 – *Chen, Q., Wang, C., Zhang, X. et al.* (2019). *In situ* sprayed bioresponsive immunotherapeutic gel for post-surgical cancer treatment. *Nat. Nanotechnol.* 14: 89-97. DOI: 10.1038/s41565-018-0319-4

Chi et al., 2017 – *Chi, Y.H., Hsiao, J.K., Lin, M.H. et al.* (2017). Lung cancer-targeting peptides with multi-subtype indication for combinational drug delivery and molecular imaging. *Theranostics*. 7: 1612-1632. DOI: 10.7150/thno.17573

Chung et al., 2015 – *Chung, B.L., Toth, M.J., Kamaly, N. et al.* (2015). Nanomedicines for endothelial disorders. *Nano Today*. 10: 759-776. DOI: 10.1007/s12012-018-9491-x

Danaei et al., 2018 – *Danaei, M., Dehghankhold, M., Ataei, S. et al.* (2018). Impact of particle size and polydispersity index on the clinical applications of lipidic nanocarrier systems. *Pharmaceutics*. 10(2): E57. DOI: 10.3390/pharmaceutics10020057

Deyev, Lebedenko, 2017 – *Deyev, S.M., Lebedenko, E.N.* (2017). Targeted bifunctional proteins and hybrid nanoconstructs for cancer diagnostics and therapies. *Mol. Biol.* 51(6): 788-803.

Ding et al., 2015 – *Ding, J., Feng, M., Wang, F., et al.* (2015). Targeting effect of PEGylated liposomes modified with the Arg-Gly-Asp sequence on gastric cancer. *Oncol Rep*. 34(4): 1825-1834. DOI: 10.3892/or.2015.4142

Duan et al., 2015 – *Duan, H., Wang, D., Li, Y.* (2015). Green chemistry for nanoparticle synthesis. *Chem. Soc. Rev*. 44, 5778-5792. DOI: 10.1039/C4CS00363B

Feng et al., 2016 – *Feng, S.T., Li, H., Luo, Y. et al.* (2016). Molecular targeted magnetic resonance imaging of human colorectal carcinoma (LoVo) cells using novel superparamagnetic iron oxide-loaded nanovesicles: in vitro and in vivo studies. *Curr. Cancer Drug Targets*. 16(6): 551-560. DOI: 10.2174/1568009616666160603123616

Feng et al., 2018 – *Feng, B., Zhou, F., Hou, B. et al.* (2018). Binary cooperative prodrug nanoparticles improve immunotherapy by synergistically modulating immune tumor microenvironment. *Adv. Mater*. 30: 1803001. DOI: 10.1002/adma.201803001

Fernandes et al., 2015 – *Fernandes, E., Ferreira, J.A., Andreia, P. et al.* (2015). New trends in guided nanotherapies for digestive cancers: a systematic review. *J. Control. Release*. 209: 288-307. DOI: 10.1016/j.jconrel.2015.05.003

Gamper et al., 2019 – *Gamper, C., Spenlé, C., Boscá, S., et al.* (2019). Functionalized *Tobacco mosaic virus* coat protein monomers and oligomers as nanocarriers for anti-cancer peptides. Cancers (Basel). 11(10): 1609. DOI: 10.3390/cancers11101609

Garcia-Hevia et al., 2019 – *Garcia-Hevia, L., Banobre-Lopez, M., Gallo, J.* (2019). Recent progress on manganese-based nanostructures as responsive MRI contrast agents. *Chem.-Eur. J.* 25(2): 431-441. DOI: 10.1002/chem.201802851

Golden, Apetoh, 2015 – *Golden, E.B., Apetoh, L.* (2015). Radiotherapy and immunogenic cell death. *Sem. Radiat. Oncol.* 25(1): 11-17. DOI: 10.1016/j.semradonc.2014.07.005

Czapar, Steinmetz, 2017 – *Czapar, A.E., Steinmetz, N.F.* (2017). Plant viruses and bacteriophages for drug delivery in medicine and biotechnology. *Curr. Opin. Chem.* Biol. 38: 108-116. DOI: 10.1016/j.cbpa.2017.03.013

Guo et al., 2015 – *Guo, J., Fan, K.X., Xie, L.I. et al.* (2015). Effect and prognostic significance of the KAI1 gene in human gastric carcinoma. *Oncol. Lett*. 10(4): 2035-2042. DOI: 10.3892/ol.2015.3604

Horise et al., 2019 – *Horise, Y., Maeda, M., Konishi, Y. et al.* (2019). Sonodynamic therapy with anticancer micelles and high-intensity focused ultrasound in treatment of canine cancer. *Front. Pharmacol.* 10: 545. DOI: 10.3389/fphar.2019.00545

Hoshino et al., 2015 – *Hoshino, I., Maruyama, T., Fujito, H. et al.* (2015). Detection of peritoneal dissemination with near-infrared fluorescence laparoscopic imaging using a liposomal formulation of a synthesized indocyanine green liposomal derivative. *Anticancer Res*. 35(3): 1353-1359.

Hou et al., 2016 – *Hou, L., Feng, Q., Wang, Y. et al.* (2016). Multifunctional hyaluronic acid modified graphene oxide loaded with mitoxantrone for overcoming drug resistance in cancer. *Nanotechnology*. 27: 015701. DOI: 10.1088/0957-4484/27/1/015701

Hsu et al., 2016 – *Hsu, B.Y.W., Kirby, G., Tan, A., et al.* (2016). Relaxivity and toxicological properties of manganese oxide nanoparticles for MRI applications. *RSC Adv*. 6(51): 45462-45474. DOI: 10.1039/C6RA04421B

Huang et al., 2017 – *Huang, Z., Zhang, L., Zhu, D. et al.* (2017). A novel serum microRNA signature to screen esophageal squamous cell carcinoma. *Cancer Med.*, 6(1): 109-119. DOI: 10.1002/cam4.973

Huang et al., 2019 – *Huang, Y., Deng, X., Liang, J.* (2019). Review of the application of nanovesicles and the human interstitial fluid in gastrointestinal premalignant lesion detection, diagnosis, prognosis and therapy. *Int. J. Nanomedicine.* 14: 9469-9482. DOI: 10.2147/IJN.S208559

Huo et al., 2014 – *Huo, S., Jin, S., Ma, X. et al.* (2014). Ultrasmall gold nanoparticles as carriers for nucleus-based gene therapy due to size-dependent nuclear entry. *ACS Nano.* 8: 5852-5862. DOI: 10.1021/nn5008572

Jing et al., 2018 – *Jing, L., Qu, H., Wu, D. et al.* (2018). Platelet-camouflaged nanococktail: Simultaneous inhibition of drug-resistant tumor growth and metastasis via a cancer cells and tumor vasculature dual-targeting strategy. *Theranostics.* 8: 2683-2695.

Kalita et al., 2016 – *Kalita, V.I., Mamaev, A.I., Mamaeva, V.A., et al.* (2016). Structure and shear strength of implants with plasma coatings. *Inorg. Materials: Appl. Res.* 7(3): 376-387. DOI: 10.1134/S2075113316030102

Khaled et al., 2019 – *Khaled, H., Aziz, K., Sanders, K. et al.* (2019). Enhancing colorectal cancer radiation therapy efficacy using silver nanoprisms decorated with graphene as radiosensitizers. *Sci Rep.* 9: 17120. DOI: 10.1038/s41598-019-53706-0

Ko et al., 2019 – *Ko, Y.J., Kim, W.J., Kim, K., Kwon, I.C.* (2019). Advances in the strategies for designing receptor-targeted molecular imaging probes for cancer research. *J. Control. Release.* 305: 1-17. DOI: 10.1016/j.jconrel.2019.04.030

Kuai et al., 2016 – Kuai, R., Ochyl, L.J., Bahjat, K.S. et al. (2016). Designer vaccine nanodiscs for personalized cancer immunotherapy. *Nat. Mater.* 16: 489-496. DOI: 10.1038/nmat4822

Lapčík et al., 2019 – *Lapčík, L., Vašina, M., Lapčíková, B. et al.* (2019). Materials characterization of advanced fillers for composites engineering applications. *Nanotech. Rev.* 8(1): 503-512. DOI: 10.1515/ntrev-2019-0045

Lei et al., 2017 – *Lei, M., Fu, C., Cheng, X. et al.* (2017). Activated surface charge-reversal manganese oxide nanocubes with high surface-to-volume ratio for accurate magnetic resonance tumor imaging. *Adv. Funct. Mater.* 27(30): 1700978. DOI: 10.1002/adfm.201700978

Lenis-Rojas et al., 2017 – *Lenis-Rojas, O.A., Roma-Rodrigues, C., Fernandes, A.R., et al.* (2017). Dinuclear rull (bipy) 2 derivatives: structural, biological, and in vivo Zebrafish toxicity. *Evaluation. Inorg. Chem.* 56: 7127-7144. DOI: 10.1021/acs.inorgchem.7b00790

Li et al., 2017 – *Li, W.-Q., Wang, Z., Hao, S. et al.* (2017).. Mitochondria-targeting polydopamine nanoparticles to deliver Doxorubicin for overcoming drug resistance. *ACS Applied Materials Interfaces.* 9(20): 16793-16802. DOI: 10.1021/acsami.7b01540

Li et al., 2018a – *Li, P., Yao, Q., Lü, B. et al.* (2018). Visible light-induced supra-amphiphilic switch leads to transition from supramolecular nanosphere to nanovesicle activated by pillar[5]arene-based host-guest interaction. *Macromol Rapid Commun.* 39(20): e1800133. DOI: 10.1002/marc.201800133

Li et al., 2018b – *Li, X., Li, H., He, X., et al.* (2018). Spectrum- and time-resolved endogenous multiphoton signals reveal quantitative differentiation of premalignant and malignant gastric mucosa. *Biomed. Opt. Express.* 9(2): 453-471. DOI: 10.1364/BOE.9.000453

Li et al., 2019 – *Li, Y., Zhai, Y., Liu, W. et al.* (2019). Ultrasmall nanostructured drug-based pH-sensitive liposome for effective treatment of drug-resistant tumor. *J. Nanobiotechnology.* 17: 117. DOI: 10.1186/s12951-019-0550-7

Lian et al., 2017 – *Lian, W., Zhang, L., Yang, L., Chen, W.* (2017). AP-2alpha reverses vincristine-induced multidrug resistance of SGC7901 gastric cancer cells by inhibiting the Notch pathway. *Apoptosis.* 22: 933-941. DOI: 10.1007/s10495-017-1379-x

Lin et al., 2016 – *Lin, W.H., Yeh, S.H., Yeh, K.H. et al.* (2016). Hypoxia-activated cytotoxic agent tirapazamine enhances hepatic artery ligation-induced killing of liver tumor in HBx transgenic mice. *PNAS.* 113: 11937-11942. DOI: 10.1073/pnas.1613466113

Lin et al., 2018 – *Lin, L.Y., Yang, L., Zeng, Q. et al.* (2018). Tumor-originated exosomal lncUEGC1 as a circulating biomarker for early-stage gastric cancer. *Mol Cancer.* 17(1): 84. DOI: 10.1186/s12943-018-0834-9

Liu et al., 2017 – *Liu, T.Z., Zhang, D.W., Song, W.T., et al.* (2017). A poly(L-glutamic acid)-combretastatin A4 conjugate for solid tumor therapy: Markedly improved therapeutic efficiency through its low tissue penetration in solid tumor. *Acta Biomater.* 53: 179-189. DOI: 10.1016/j.actbio.2017.02.001

Lloyd et al., 2015 – *Lloyd, K.C., Meehan, T., Beaudet, A.* (2015). Precision medicine: Look to the mice. *Science.* 349: 390.

Ma et al., 2016 – *Ma, Z., Zhang, B.* (2016). Guedes da Silva M.F.C., et al. Synthesis, characterization, thermal properties and antiproliferative potential of copper (II) 4′-phenyl-terpyridine compounds. *Dalt. Trans.* 45: 5339-5355. DOI: 10.1039/C5DT02744F

Madamsetty et al., 2019 – *Madamsetty, V.S., Mukherjee, A., Mukherjee, S.* (2019). Recent trends of the bio-inspired nanoparticles in cancer theranostics. *Front Pharmacol.* 10: 1264. DOI: 10.3389/fphar.2019.01264

Marchio, Bussolino, 2018 – *Marchio, S., Bussolino, F.* (2018). Targeted nanomedicines for applications in preclinical cancer models. *Bull. Rus. State Med. Univ.* (6): 5-13.

Martins et al., 2016 – *Martins, M., Baptista, P.V., Mendo, A.S. et al.* (2016). In vitro and in vivo biological characterization of the anti-proliferative potential of a cyclic trinuclear organotin(IV) complex. *Mol. BioSyst.* 12: 1015-1023. DOI: 10.1039/C5MB00791G

Matsumura et al., 2015 – *Matsumura, T., Sugimachi, K., Iinuma, H., et al.* (2015). Exosomal microRNA in serum is a novel biomarker of recurrence in human colorectal cancer. *Br. J. Cancer.* 113(2): 275-281. DOI: 10.1038/bjc.2015.201

Mattheolabakis, Mikelis, 2019 – *Mattheolabakis, G., Mikelis, C.M.* (2019). Nanoparticle delivery and tumor vascular normalization: the chicken or the egg? *Front. Oncol.* 9: 1227. DOI: 10.3389/fonc.2019.01227

McMullen et al., 2017 – *McMullen, J.R.W., Selleck, M., Wall, N.R., et al.* (2017). Peritoneal carcinomatosis: limits of diagnosis and the case for liquid biopsy. *Oncotarget.* 8(26): 43481-43490. DOI: 10.18632/oncotarget.16480

Melerzanov et al., 2016 – *Melerzanov, A., Moskalev, A., Zharov, V.* (2016) Precision medicine and molecular *theranostics. Vrach (The Doctor).* (12): 11-14.

Miao et al., 2015 – *Miao, P., Wang, B., Chen, X. et al.* (2015). Tetrahedral DNA nanostructure-based microRNA biosensor coupled with catalytic recycling of the analyte. *ACS Appl. Mater. Interfaces.* 7: 6238-6243. DOI: 10.1021/acsami.5b01508

Millard et al., 2017 – *Millard, M., Yakavets, I., Zorin, V., et al.* (2017). Drug delivery to solid tumors: The predictive value of the multicellular tumor spheroid model for nanomedicine screening. *Int. J. Nanomed.* 12: 7993-8007. DOI: 10.2147/IJN.S146927

Mukherjee et al., 2019 – *Mukherjee, A., Waters, A.K., Kalyan, P. et al.* (2019). Lipid-polymer hybrid nanoparticles as a next-generation drug delivery platform: state of the art, emerging technologies, and perspectives. *Int. J. Nanomed.* 14, 1937-1952. DOI: 10.2147/IJN.S198353

Mullick Chowdhury et al., 2017 – *Mullick Chowdhury, S., Lee, T., Willmann, J.K.* (2017). Ultrasound-guided drug delivery in cancer. *Ultrasonography.* 36, 171-184. DOI: 10.14366/usg.17021

Muthuraj et al., 2016 – *Muthuraj, B., Mukherjee, S., Patra, C.R., Iyer, P.K.* (2016). Amplified fluorescence from polyfluorene nanoparticles with dual state emission and aggregation caused red shifted emission for live cell imaging and cancer theranostics. *ACS Appl. Mater. Interfaces.* 8: 32220-32229. DOI: 10.1021/acsami.6b11373

Nam et al., 2019 – *Nam, J., Son, S., Park, K.S. et al.* (2019). Cancer nanomedicine for combination cancer immunotherapy. *Nat. Rev. Mater.* 4: 398-494. DOI: 10.1038/s41578-019-0108-1

Neves et al., 2016 – *Neves, H.R., Bini, R.A., Barbosa, J.H.O. et al.* (2016). Dextran-coated antiferromagnetic MnO nanoparticles for a T-1-MRI contrast agent with high colloidal stability. *Part. Part. Syst. Char.* 33(3): 167-176. DOI: 10.1002/ppsc.201500251

Novochadov et al., 2016 – *Novochadov, V.V., Krylova, A.S., Anikeev, N.A., et al.* (2016). The functionalizing bioactive surface of screw titanium implants with chitosan: fabrication and surface features. *Eur. J. Mol. Biotech.* 4(4): 139-147. DOI: 10.13187/ejmb.2016.14.125

Özdemir et al., 2019 – *Özdemir, S., Çelik, B., Üner, M.* (2019). Chapter 15 – Properties and therapeutic potential of solid lipid nanoparticles and nanostructured lipid carriers as promising colloidal drug delivery systems. In: *Materials for Biomedical Engineering*, eds A.-M Holban., A.M. Grumezescu, eds. *Elsevier Istanbul:* 457-505.

Pabla, 2015 – *Pabla, B.* (2015). Colon cancer and the epidermal growth factor receptor: Current treatment paradigms, the importance of diet, and the role of chemoprevention. *World J. Clin. Oncol.* 6: 133. DOI: 10.5306/wjco.v6.i5.133

Pedrosa et al., 2019 – *Pedrosa, P., Corvo, M.L., Ferreira-Silva, M., et al.* (2019). Targeting cancer resistance via multifunctional gold nanoparticles. *Int. J. Mol. Sci.* 20(21): 5510. DOI: 10.3390/ijms20215510

Pitek et al., 2016 – *Pitek, A.S., Jameson, S.A., Veliz, F.A. et al.* (2016). Serum albumin 'camouflage' of plant virus based nanoparticles prevents their antibody recognition and enhances pharmacokinetics. *Biomaterials*. 89: 89-97. DOI: 10.1016/j.biomaterials.2016.02.032

Pouget et al., 2015 – *Pouget, J.P., Lozza, C., Deshayes, E. et al.* (2015). Introduction to radiobiology of targeted radionuclide therapy. *Front. Med.* 2: 12. DOI: 10.3389/fmed.2015.00012

Qu et al., 2014 – *Qu, M.H., Zeng, R.F., Fang, S., et al.* (2014). Liposome-based co-delivery of siRNA and docetaxel for the synergistic treatment of lung cancer. *Int. J. Pharm.* 474: 112-122. DOI: 10.1016/j.ijpharm.2014.08.019

Rentien et al., 2018 – *Rentien, A.L., Lévy, M., Copie-Bergman, C., et al.* (2018). Long-term course of precancerous lesions arising in patients with gastric MALT lymphoma. *Dig Liver Dis.* 50(2): 181-188. DOI: 10.1016/j.dld.2017.10.014

Riley et al., 2019 – *Riley R.S., June C.H., Langer R., Mitchell M.J.* (2019). Delivery technologies for cancer immunotherapy. *Nat. Rev. Drug Discov.* 18: 175-196. DOI: 10.1038/s41573-018-0006-z

Roma-Rodrigues et al., 2017 – *Roma-Rodrigues, C., Raposo L.R., Cabral R., et al.* (2017) Tumor microenvironment modulation via gold nanoparticles targeting malicious exosomes: implications for cancer diagnostics and therapy. *Int. J. Mol. Sci.* 18(1): e162. doi:10.3390/ijms18010162

Rosenblum et al., 2018 – *Rosenblum, D., Joshi, N., Tao, W. et al.* (2018). Progress and challenges towards targeted delivery of cancer therapeutics. *Nat. Commun.* 9, 1410-1410. DOI: 10.1038/s41467-018-03705-y

Sadegh Malvajerd et al., 2019 – *Sadegh Malvajerd, S., Azadi, A., Izadi, Z. et al.* (2019). Brain delivery of curcumin using solid lipid nanoparticles and nanostructured lipid carriers: preparation, optimization, and pharmacokinetic evaluation. *ACS Chem. Neurosci.* 10, 728-739. DOI: 10.1021/acschemneuro.8b00510

Saeed et al., 2019 – Saeed, M., Gao, J., Shi, Y., et al. (2019). Engineering nanoparticles to reprogram the tumor immune microenvironment for improved cancer immunotherapy. *Theranostics*. 9(26): 7981-8000. DOI: 10.7150/thno.37568

Selwan et al., 2016 – *Selwan, E.M., Finicle, B.T., Kim, S.M., Edinger, A.L.* (2016). Attacking the supply wagons to starve cancer cells to death. *FEBS Lett.* 590: 885-907. DOI: 10.1002/1873-3468.12121

Sharma et al., 2015 – *Sharma, G., Sharma, A.R., Nam, J. et al.* (2015). Nanoparticle based insulin delivery system: the next generation efficient therapy for Type 1 diabetes. *J. Nanobiotech.* 13: 74. DOI: 10.1186/s12951-015-0136-y

Sui et al., 2017 – *Sui, H., Zhao, J., Zhou, L. et al.* (2017). Tanshinone IIA inhibits beta-catenin/VEGF-mediated angiogenesis by targeting TGF-beta1 in normoxic and HIF-1alpha in hypoxic microenvironments in human colorectal cancer. *Cancer Lett.* 403: 86-97. DOI: 10.1016/j.canlet.2017.05.013

Sun et al., 2017 – *Sun, Z.P., Li, A.Q., Jia, W.H. et al.* (2017). MicroRNA expression profiling in exosomes derived from gastric cancer stem-like cells. *Oncotarget*. 8(55): 93839-93855. DOI: 10.18632/oncotarget.21288

Sun et al., 2018 – *Sun, B., Peng, J., Wang, S., et al.* (2018). Applications of stem cell-derived exosomes in tissue engineering and neurological diseases. *Rev Neurosci.* 29(5): 531-546. DOI: 10.1515/revneuro-2017-0059

Sokolov et al., 2017 – *Sokolov, I.L., Cherkasov, V.R., Tregubov, A.A.* (2017). Smart materials on the way to theranostic nanorobots: Molecular machines and nanomotors, advanced biosensors, and intelligent vehicles for drug delivery. *Biochim. Biophys. Acta*. S0304-4165(17)30035-1. DOI: 10.1016/j.bbagen.2017.01.027

Son et al., 2017 – *Son, S., Kim, N., You, D.G. et al.* (2017). Antitumor therapeutic application of self-assembled RNAi-AuNP nanoconstructs: Combination of VEGF-RNAi and photothermal ablation. *Theranostics*. 7: 9-22. DOI: 10.7150/thno.16042. eCollection 2017.

Sun et al., 2019 – *Sun, Q., Barz, M., De Geest, B.G. et al.* (2019). Nanomedicine and macroscale materials in immuno-oncology. *Chem. Soc. Rev.* 48: 351-381. DOI: 10.1039/c8cs00473k

Tagalakis et al., 2017 – *Tagalakis, A.D., Maeshima, R., Yu-Wai-Man, C., et al.* (2017). Peptide and nucleic acid-directed self-assembly of cationic nanovehicles through giant unilamellar vesicle modification: targetable nanocomplexes for in vivo nucleic acid delivery. *Acta Biomater.* 51: 351-362. DOI: 10.1016/j.actbio.2017.01.048

Tang et al., 2017 – *Tang, J., Ji, H., Ren, J. et al.* (2017). Solid lipid nanoparticles with TPGS and Brij 78: a co-delivery vehicle of curcumin and piperine for reversing P-glycoprotein-mediated multidrug resistance in vitro. *Oncol. Lett.* 13: 389-395. DOI: 10.3892/ol.2016.5421

Tang et al., 2018 – *Tang, L., Zheng, Y., Melo, M.B. et al.* (2018). Enhancing T cell therapy through TCR-signaling-responsive nanoparticle drug delivery. *Nat. Biotechnol.* 36: 707-716. DOI: 10.1038/nbt.4181

Tokuhisa et al., 2015 – *Tokuhisa, M., Ichikawa, Y., Kosaka, N. et al.* (2015). Exosomal miRNAs from peritoneum lavage fluid as potential prognostic biomarkers of peritoneal metastasis in gastric cancer. *PLoS One.* 10(7): e0130472. DOI: 10.1371/journal.pone.0130472

Tharkar et al., 2019 – *Tharkar, P., Varanasi, R., Wong, W.S.F. et al.* (2019). Nano-enhanced drug delivery and therapeutic ultrasound for cancer treatment and beyond. *Front. Bioeng. Biotechnol.* 7: 324. DOI: 10.3389/fbioe.2019.00324

Vodeneev et al., 2015 – *Vodeneev, V.A., Zvyagin, A.V., Shilyagina, N.Yu. et al.* (2015). Targeted radionuclide therapy: current status and prospects. Genes and Cells. 10(2): 23-29.

Wang, 2017 – *Wang, X.Y., Zhang, J.S., Wang, Y.T. et al.* (2016). Multi-responsive photothermal-chemotherapy with drug-loaded melanin-like nanoparticles for synergetic tumor ablation. *Biomaterials.* 81: 114-124. DOI: 10.1016/j.biomaterials.2015.11.037

Wang et al., 2014 – *Wang, B., Zhuang, X., Deng, Z.B. et al.* (2014). Targeted drug delivery to intestinal macrophages by bioactive nanovesicles released from grapefruit. *Mol. Ther.* 22(3): 522-534. DOI: 10.1038/mt.2013.190

Wang et al., 2017 – *Wang, L.S., Duncan, B., Tang, R. et al.* (2017). Gradient and patterned protein films stabilized via nanoimprint lithography for engineered interactions with cells. *ACS Appl. Mater. Interfaces.* 9: 42-46. DOI: 10.1021/acsami.6b13815

Wang et al., 2018 – *Wang, J., Liu, Y., Sun, W. et al.* (2018). Plasma exosomes as novel biomarker for the early diagnosis of gastric cancer. *Cancer Biomark.* 21(4): 805-812. DOI: 10.3233/CBM-170738

Wilhelm et al., 2016 – *Wilhelm, S., Tavares, A.J., Dai, Q. et al.* (2016). Analysis of nanoparticle delivery to tumours. *Nat. Rev. Mater.* 1: 16014. DOI: 10.1038/natrevmats.2016.14

Xhu et al., 2013 – *Zhu, L., Torchilin, V.P.* (2013). Stimulus-responsive nanopreparations for tumor targeting. *Integr. Biol.* 5, 96-107. DOI: 10.1039/c2ib20135f

Xia et al., 2016 – *Xia, Z., Wang, P., Liu, X. et al.* (2016). Tumor-penetrating peptide-modified DNA tetrahedron for targeting drug delivery. *Biochemistry.* 55: 1326-1331. DOI: 10.1021/acs.biochem.5b01181

Xiang et al., 2018 – *Xiang, Y., Li, N.L., Guo, L.J. et al.* (2018). Biocompatible and pH-sensitive MnO-loaded carbonaceous nanospheres (MnO@CNSs): a theranostic agent for magnetic resonance imaging-guided photothermal therapy. *Carbon.* 136: 113-124. DOI: 10.1016/j.carbon.2018.04.058

Yan et al., 2018 – *Yan, L., Dong, X., Gao, J. et al.* (2018). A novel rapid quantitative method reveals stathmin-1 as a promising marker for esophageal squamous cell carcinoma. *Cancer Med.* 7(5): 1802-1813. DOI: 10.1002/cam4.1449

Yang et al., 2018 – *Yang, Y., Lu, Y., Abbaraju, P.L. et al.* (2018). Stepwise degradable nanocarriers enabled cascade delivery for synergistic cancer therapy. *Adv. Funct. Mater.* 28: 1800706.

Yang et al., 2019 – *Yang, S., Tang, Z., Hu, C. et al.* (2019). Selectively potentiating hypoxia levels by Combretastatin A4 nanomedicine: toward highly enhanced hypoxia-activated prodrug Tirapazamine therapy for metastatic tumors. *Adv. Mater.*: e1805955.

Ye et al., 2018 – *Ye, Z., Zhang, T., He, W., et al.* (2018). Methotrexate-loaded extracellular vesicles functionalized with therapeutic and targeted peptides for the treatment of glioblastoma multiforme. *ACS Appl. Mater. Interfaces.* 10(15): 12341-12350. DOI: 10.1021/acsami.7b18135

You et al., 2016 – *You, Y., Wang, Z., Ran, H. et al.* (2016). Nanoparticle-enhanced synergistic HIFU ablation and transarterial chemoembolization for efficient cancer therapy. *Nanoscale*. 8: 4324-4339. DOI: 10.1039/C5NR08292G

Yu et al., 2019 – *Yu, S., Chen, Z., Zeng, X. et al.* (2019). Advances in nanomedicine for cancer starvation therapy. *Theranostics*. 9(26): 8026-8047. DOI: 10.7150/thno.38261

Zanganeh et al., 2016 – *Zanganeh, S., Hutter, G., Spitler, R. et al.* (2016). Iron oxide nanoparticles inhibit tumour growth by inducing pro-inflammatory macrophage polarization in tumour tissues. *Nat. Nanotechnol.* 11: 986-994. DOI: 10.1038/nnano.2016

Zhan et al., 2017 – *Zhan, Y.H., Shi, S.X., Ehlerding, E.B., et al.* (2017). Radiolabeled, antibody-conjugated manganese oxide nanoparticles for tumor vasculature targeted positron emission tomography and magnetic resonance imaging. *ACS Appl. Mater. Inter.* 9(44): 38304-38312. DOI: 10.1021/acsami.7b12216

Zhang et al., 2017 – *Zhang, C., Ni, D., Liu, Y., et al.* (2017). Magnesium silicide nanoparticles as a deoxygenation agent for cancer starvation therapy. *Nat. Nanotechnol.* 12: 378-386. DOI: 10.1038/nnano.2016.280

Zhang et al., 2018a – *Zhang, K., Du, X., Yu, K., et al.* (2018). Application of novel targeting nanoparticles contrast agent combined with contrast-enhanced computed tomography during screening for early-phase gastric carcinoma. *Exp. Ther. Med.* 15(1): 47-54. DOI: 10.3892/etm.2017.5388

Zhang et al., 2018b – *Zhang, P., Zhang, L., Qin, Z. et al.* (2018). Genetically engineered liposome-like nanovesicles as active targeted transport platform. *Adv. Mater.* 30: 7. DOI: 10.1002/adma.201705350

Zhang et al., 2018 – *Zhang, R., Feng, L., Dong, Z. et al.* (2018). Glucose & oxygen exhausting liposomes for combined cancer starvation and hypoxia-activated therapy. *Biomaterials*. 162: 123-131.

Zhang et al., 2019a – *Zhang, Y.R., Lin, R., Li, H.J. et al.* (2019). Strategies to improve tumor penetration of nanomedicines through nanoparticle design. *Wiley Interdiscip. Rev. Nanomed. Nanobiotechnol.* 11: e1519.10.1002/wnan.1519

Zhang et al., 2019b – *Zhang, E., Xing, R., Liu, S. et al.* (2019). Vascular targeted chitosan-derived nanoparticles as docetaxel carriers for gastric cancer therapy. *Int. J. Biol. Macromol.* 126: 662-672.

Zheng et al., 2014 – *Zheng, N.G., Mo, S.J., Li, J.P. et al.* (2014). Anti-CSC effects in human esophageal squamous cell carcinomas and Eca109/9706 cells induced by nanoliposomal quercetin alone or combined with CD 133 antiserum. *Asian Pac. J. Cancer Prev*. 15(20): 8679-8684. DOI: 10.7314/apjcp.2014.15.20.8679

Zhong et al. 2019 – *Zhong, Y., Su, T., Shi, Q. et al.* (2019). Co-administration of iRGD enhances tumor-targeted delivery and anti-tumor effects of Paclitaxel-loaded PLGA nanoparticles for colorectal cancer treatment. *Int. J. Nanomedicine*. 14: 8543-8560. DOI: 10.2147/IJN.S219820

Zhu et al., 2017 – *Zhu, G., Mei, L., Vishwasrao, H.D. et al.* (2017). Intertwining DNA-RNA nanocapsules loaded with tumor neoantigens as synergistic nanovaccines for cancer immunotherapy. *Nat. Commun.* 8: 1482. DOI: 10.1038/s41467-017-01386-7

Zhu et al., 2018 – *Zhu, Q., Heon, M., Zhao, Z. et al.* (2018). Microfluidic engineering of exosomes: editing cellular messages for precision therapeutics. *Lab Chip*. 18(12): 1690-1703. DOI: 10.1039/c8lc00246k

Published in the Slovak Republic
European Journal of Molecular Biotechnology
Has been issued since 2013.
E-ISSN: 2409-1332
2019, 7(2): 63-72

DOI: 10.13187/ejmb.2019.2.63
www.ejournal8.com

Contribution to the Toxicological Study of the Brown Alga Cystoseira Stricta by Shrimp Brine Test

Sofia Borsali [a, *], Rabah Chadli [a]

[a] Abdel Hamid Ibn Badiss University, Mostaganem, Algeria

Abstract

This study examines the eco-toxicological assessment of brown algae contamination in the western Mediterranean coast of Algeria at beach of Sidi Ladjal, Wilaya Mostaganem.

The toxicity of *Cystoseira stricta* forests has been estimated in Shrimp Brine (*Artemia salina*), LD_{50} lethality tests are widely used in research and applied toxicology; The responses to cyto-toxicity tests on algal extracts by solvents using a standardized method of Brine Shrimp are based on different concentrations. The LD_{50} values of the different extracts are obtained by different linear expressions. The results indicate that the raw extracts of the brown seaweed *Cystoseira stricta* samples from Sidi Ladjel beach are toxic to *Artemia salina,* These extracts gave different results for each concentration subjected to brine and the percentage of larval mortality increases with concentration. According to different Toxicity Assessment Criteria we were able to conclude that: The most toxic are those of chloroform and petroleum ether where ever Methanol and hexane extracts that are moderately toxic.

The study of the antioxidant power by the trapping of the radical DPPH, and the quantification of the total antioxidant capacity, reveals the presence of antioxidant properties for the studied extract; Also regarding the metal contamination, our alga has higher levels of zinc followed by copper and lead. All these results obtained are only a first steep in the search for biologically active natural substances from marine algae.

Keywords: antioxidant power, *Artemia salina,* beach sidi ladjal, *cystoseira stricta*, metal contamination, toxicity.

1. Introduction

Brown seaweeds are widespread because of their adaptability through reproduction and response to various ecological conditions.

This supposes that they secrete chemical defense substances, against the multiple dangers to which they are exposed (mobile predators, and invading micro-organisms).

The study of cyto-toxicity test responses on algal extracts by solvents was done using a standardized method of Brine Shrimp that is based on different concentrations.

This biological assay method using Artemia salina has been commonly used in eco-toxicological tests, it is sensitive, accurate and reliable for detecting toxic and bioactive compounds in plant extracts, but also the sample must be having exactly the same age and the same physiology (Parra et al., 2001; Lachumy et al., 2010).

Our goal is to detect the toxic or dangerous potential of our Cystoseira stricta algae sample by this Brine-Shrimp test, whose principle is a lethality assay of the practical system, to monitor the

* Corresponding author
E-mail addresses: sofiborsali@gmail.com (S. Borsali), chadlirabah@yahoo.fr (R. Chadli)

biological activities and the evaluation of the toxic potential. Brown algae contamination sampled at Sidi Ladjal Beach (Dahmani, 2014).

According to the study by P. Lavens, P. Sorgeloos who worked on the acetonic and hexanic extracts of the brown alga Cystoseira stricta harvested from the Algerian west coast (madrid beach), admits that it has a potency of antimicrobial activity that can possibly replace the less effective antibiotics and especially the antifungals where this species has shown a remarkable fungistatic effect during the test months (Lavens, Sorgeloos, 1996).

2. Materials and methods

The seaweed Cystoseira stricta sp was collected on 01/03/2017 at the beach of Khadra (Sidi Ladjal) willaya of Mostaganem in Algeria (see Figure 1-A), its botanical identification was carried out in situ (see Figure 01-B) and in the laboratory in order to be certain about our sample, then it is kept in a black plastic bag

A B

Fig. 1. A- Satellite view of the sampling site (Khadra commune). **B** – Algae Cystoseira stricta sp

Systematic position of the genus Cystoseira (source algaebase):

Field	Eukaryota
Reign	Chromista Cavalier-Smith
Branch	Heterokonta Cavalier-Smith
class	Phaeophyceae Kjellman
Order	Fucales Kylin
Family	Sargassaceae Kützing (incl Cystoseiraceae)
Genus	Cystoseira amentacea var.stricta C. Agardh

2.1. Extraction of the seaweed extract

Using the Soxhlet method and with four types of solvent, namely chloroform, methanol, petroleum ether and hexane The various characteristics (number of cycles, temperature and yield) were summarized in Table 1. 500 ml of each type of solvent are taken with 100 g of the algal sample, all the components are then filtered with Wattman Paper No. 1 filter. The extracts were then collected and concentrated using a rotary evaporator to finally calculate the yield of each extraction, the extracts collected are finally kept under low temperature until the moment of the test.

Table 1. The different characteristics of the soxhlet method

Types of solvents	Number of cycles	température	Yield
Chloroform	6	52	12,01%
Petroleum ether	7	60	0,36%
Méthanol	8	57	2,07%
Hexane	3	56	12,01%

2.2. Hatching of larvae

The cysts are imported by the aquaculture feed business Advenced solutions for animal rearing, the species of Artemia salina is of American origin from the salt lake of Utha (USA). In order to ensure

optimum cyst hatching, certain strict conditions must be respected P. Sorgeloos, namely: a temperature maintained between 25 and 28 °C and a salinity of 15 to 35 g/l with a pH at about 8.0 (Sorgeloos, 1986).

The cysts should be fed with an oxygen quantity of at least 2 mg/l, and a maximum cyst density not exceeding 2g/l to ensure a constant illumination of 1000 to 2000 lux.

The standard procedure employed is that of J. Dobbeileir, N. Adam, E. Bossuyt, E. Bruggrman, P. Sorgeloos, (Dobbeileir et al., 1980). It consists in incubating 250 mg of cysts in a cylindro-conical glass container containing 100 ml of filtered natural seawater (0.45 and 0.2 µm). The cysts should be kept in suspension by applying aeration to the bottom of the container (see Figure 2).

The temperature is maintained at 26°C, sometimes at 28°C using a thermostat, the young larvae are thus obtained after 24 hours and are obviously fed with yeast and milk powder (Benariba et al., 2013).

The collection of these young individuals is done with a plastic pipette for the study of the toxicity test.

Fig. 2. Breeding of Artemia salina

2.3. The lethal dose dose LD50 of Artemia salina

The tests were carried out in Petri dishes (see Figure 3), the extracts were diluted with 0.8 ml of dimethylsulfoxide (DMSO) at different concentrations (20 to 100 µg / ml-1) which filled with 39.2 ml of seawater, then 10 nauplii are added to each box.

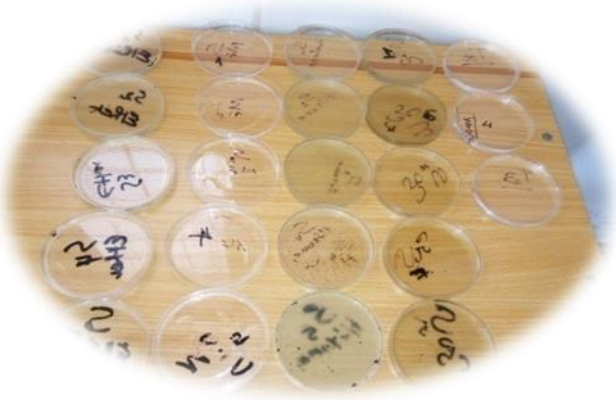

Fig. 3. Lethality test LD50

After 24 hours, we count the number of dead individuals in the test boxes and the control; beyond it is possible to define the lethal dose LD50.

In the case where the control contains dead larvae, the mortality percentage is corrected using the following formula:

% M = NLP / NLT * 100

With:

M: mortality percentage

NLP: number of dead larva in the presence of the product tested

NLT: number of dead larva in the presence of the control (solvent)

2.4. Evaluation of the antioxidant power :

The antioxidant activity of the extract of Cystoseira stricta sp was determined using the 1,1-diphenyl-2-picrylhydrazyl (DPPH) (Hoenig, 1978).

The absorbances measured at 517 nm are used to calculate the percentage inhibition of the DPPH radical, which is proportional to the anti-radical power of the sample.

• Preparation of DPPH at a concentration of 0.004 mg / ml in methanol,

• Preparation of extract in methanol at different concentrations (100, 200, 300, 400, 500 mg/ml);

• To 2 ml of the DPPH solution is added 0.014 mg for each extract at different concentrations;

• Preparation of white tube for each concentration: 50 ml of methanol and 0.014 of the corresponding extract;

• Preparation of negative tube control: 50 ml of methanol with 2ml of the DPPH solution,

• The white tube contains 2 ml of methanol,

• Incubation 30 min at room temperature and in the dark,

• Absorbance measurement at 517 nm

The results of the DPPH were expressed taking into account the average of three measurements obtained for the extract, the percentage reduction of the DPPH is calculated according to the following formula:

$$I\,\% = \frac{(\text{WHITE ABS}) - (\text{ABS EXTRACT})}{(\text{WHITE ABS})} \times 100$$

Knowing that :

DPPH (%): Percentage reduction of DPPH.

WHITE ABS: Absorption of white extract.

ABC EXTRACT: Extract Absorption

Extraction of heavy metals in marine plants

According to S.H. Hoenig, I. Kazap, J. Leibovici method which consists of wet digestion. Heavy metals (Cu, Pb and Zn) are extracted with aqua regia (sulphonitric solution – hydrogen peroxide). For that 1 ml of sulfuric acid, 3 ml of nitric acid, 3 ml of hydrogen peroxide at 30 volume, are added to 1g of the sample plants dried and crushed into fine particles (Hoenig, 1978).

The whole is heated at 75 ° C., until boiling for 15 minutes, after cooling the contents are filtered on filter paper at medium filtration speed in a 50 ml flask to its ml as required.

Automatically accompanied by a mineralization of whites, which consists of a regal water solution. It is from this test solution that flame atomic absorption spectrophotometry is performed.

a. Principle

It is an analytical method based on the exposure of the spectra of lines, allowing measure the metal elements. This method is based on the rule experimented by P. Clarkson, Y. Li, G. Richardson (Clarkson et al., 2004).

3. Results and discussion

Result of the extraction in different types of solvents according to the polarity and the number of cycles:

The result obtained in Figure 5 shows that the highest yields are those of Chloroform and Hexane with a level of 12.01 %, whereas Methanol and Ether of oil gives the lowest rates with respectively 2.07 % and 0.36 %.

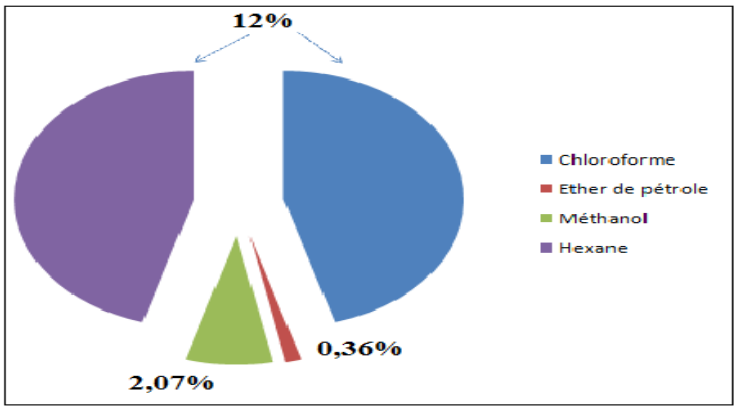

Fig. 4. Rates of return of different extracts

The calculation of the yield is done by the following equation:
R = (weight of extract / weight of dried seaweed) * 100
The products were tested at concentrations of 20, 40, 60, 80 and 100 µg / mL and the results obtained during these tests of toxicity of crude products in larvae of Artemia salina depending on the concentration and their Logarithms are summarized in Table 2 and illustrated in Figure 4.

Table 4. Result of Toxicity Activity

Cystoseira stricta (ug.ml-1) / Extrait	[c]	NLm	NLT	Nlc	%M	Ln[c]
Hexane	20 40 60 80 100	05 8 8.5 9.5 10	10 10 10 10 10	01 01 01 01 01	40 70 75 85 90	2.99 3.68 4.09 4.38 4.60
Petroleum ether	20 40 60 80 100	5 9 8.5 9.5 9.75	10 10 10 10 10	01 01 01 01 01	40 70 75 85 87.5	2.99 3.68 4.09 4.38 4.60
Chloroform	20 40 60 80 100	6 6.5 8 9.2 10	10 10 10 10 10	01 01 01 01 01	50 55 70 82 90	2.99 3.68 4.09 4.38 4.60
Méthanol	20 40 60 80 100	3.5 5 7.5 9 9.5	10 10 10 10 10	01 01 01 01 01	25 40 65 80 85	2.99 3.68 4.09 4.38 4.60

The results indicate that the raw extracts of the seaweed Cystoseira stricta samples from Sidi Ladjel beach are toxic to Artemia salina.

- The most toxic are those of chloroform and petroleum ether
- Methanol and hexane extracts are moderately toxic.

The extracts gave different results for each brine concentration and the percentage of larval mortality increases with concentration, which is clearly illustrated by the curves shown in Figure 5.

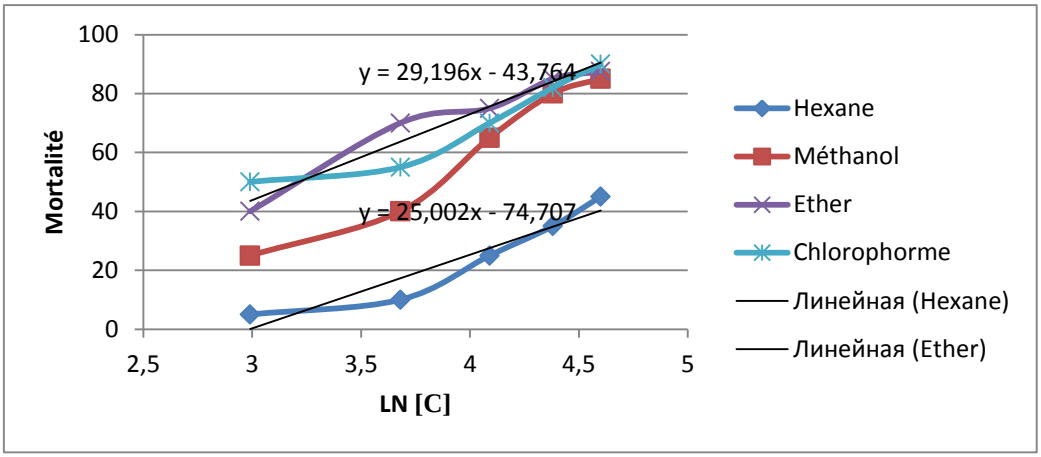

Fig. 5. Graph of the mortality at the different values of concentration of extracts by different types of solvents

Concentrations showed more than 80 % mortality of Artemia salina after 24 hours with ether, chloroform and methanol extracts (Figure 5).

These solvent extracts gave mortality rates of 10 % to 40 % for hexane, 25 % to 85 % for methanol, chloroform to give a mortality of 50 % to 90 % and finally the petroleum ether shows a rate of mortality rate ranging from 40 % to 90 %.

It can be seen from Figure 5 that the percentage mortality of Artemia salina increases after 24 hours of exposure to different concentrations of crude brown algae extracts, which was greater than 50 % for most components indicating that these extracts namely ether, methanol and chloroform are toxic.

It can be noted that:

These solvents have a selective effect and active ingredients extracted from the brown alga studied, for that the substance extracted from this alga has different effects on the larvae of Artemia salina, according to the types of solvents used during the extraction;

This variability of the biological activity results of brown algae extracts may depend on the chemical compound contents.

The toxicity criteria for the evaluation of Clarkson toxicity of plant extracts are classified as follows:

The toxicity of extracts based on this algae expressed in Dl50 is generally imposed on a valued comparison of P. Clarkson, Y. Li, G. Richardson Extracts with an LD50 greater than 1000 mg/ml are not toxic, the LD50 values of between 500 and 1000 µg/ml are weakly toxic and those with an LD50 of 100-500 µg/ml are then moderately toxic, while the extracts with an LD50 of 0-100 ug/ml are highly toxic (Clarkson et al., 2004).

Concerning our results, the values of the lethal dose "LD50" of the various solvent extracts obtained by the different linear expressions are displayed in Table 3 and illustrated by FIG.

Table 3. LD50 values of extracts of Cystoseira stricta sp

Species	Extrait	DL_{50} (µg/mL)
Cystoseira stricta Sp	Hexane	146.62
	Petroleum ether	15.36
	Chloroform	19.88
	Méthanol	39.64

According to the graph (Figure 6), the hexane extract exhibits a D150 cyto-toxic activity value of greater than 146.62 µg/ml which classifies it according to R. Merad, M. Reggabi, B. Alammir, S. Benali, R. Abetroun, M. Azzouz, D. Beaissa, as moderately toxic (Merad et al., 1991).

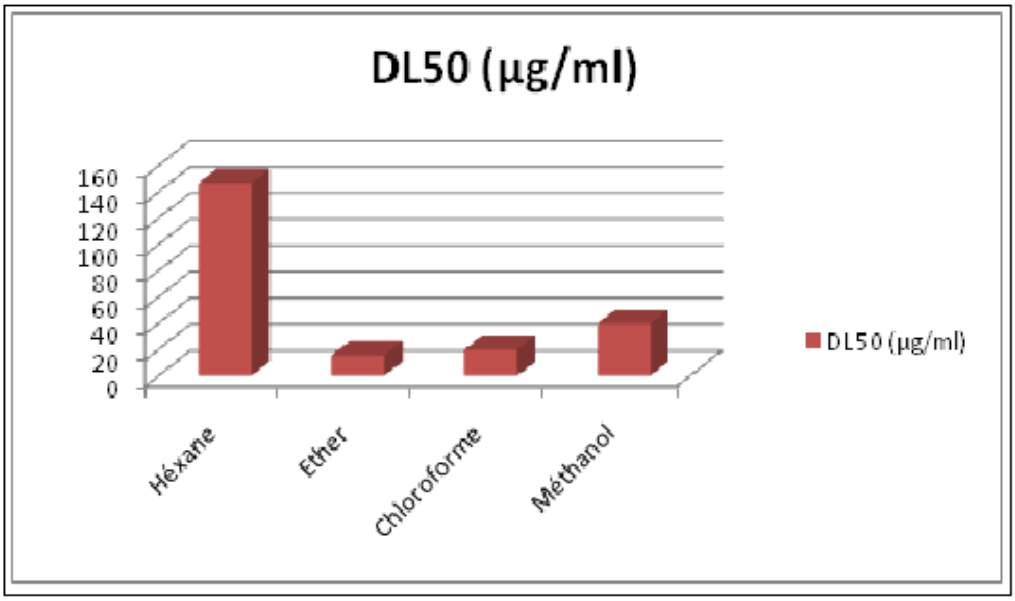

Fig. 6. Values of the lethal dose "LD50" of the different extracts

The hexane extract has a cyto-toxic activity value Dl50 greater than 146.62 µg/mL which classifies it according to M.H. Moshafi, F. Sharififar, G. Dehghan, A. Ameri as moderately toxic (Moshafi et al., 2009).

While other extracts of Cystoseira stricta are highly toxic to Artemia salina larvae with an LD50 of 15.36, 19.88 and 39.64 for ether, chloroform and methanol respectively.

In order to compare this toxicity noted with other products already tested, the results of other tests submitted to Artemia salina were used and summarized in Table 4.

Table 4. LD50 Results of Reference Products (Benkdad et al., 2011)

Product	DL_{50}(µg/mL)
Podophyllotoxin (alientary)	2.4
Digitalis (pharmaceutical)	77.2
Strychnine sulfate	515

These results show that our extracts are lower than strychnine sulfate (515 µg/mL) but are in the range of podophyllotoxin with 2.4 µg/mL and digitalis with 77.2 µg/mL.

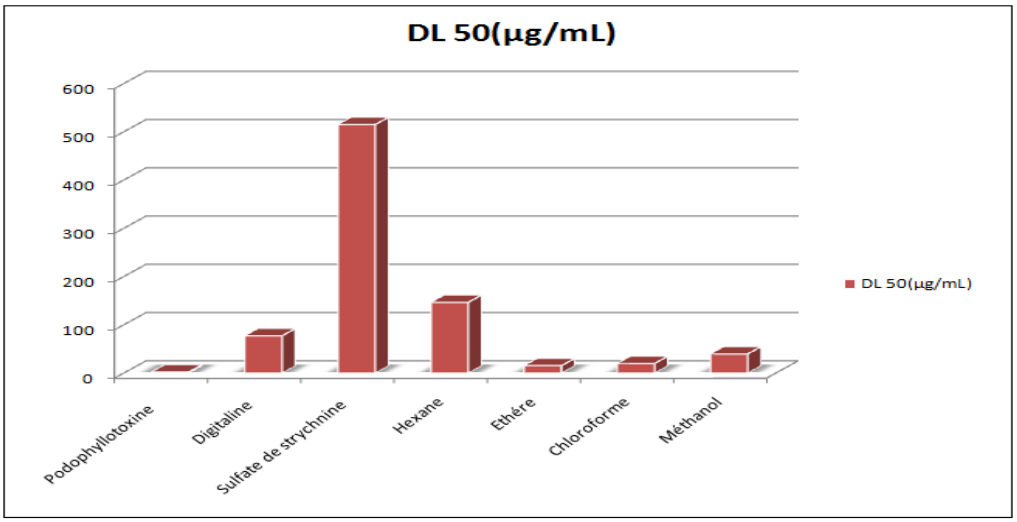

Fig. 7. Percent inhibition of DPPH by the extract of Cystoseira stricta sp.

Anti radical activity

The results of the anti-radical effect (antioxidant activity) of the extract of Cystoseira stricta sp are evaluated by tests based on the total antioxidant capacity and the trapping of the free radical DPPH that has been summarized in the Table 4 and represented by (Figure 5).

Table 4. The results of the anti-radical effect (antioxidant activity) of the extract of Cystoseira stricta sp are evaluated by tests based on the total antioxidant capacity and the trapping of the free radical DPPH

% of réduction of DPPH	61,14	50,93	28,15	15,11
Concentrations of the extract (mg/ml)	6,21	5,99	5,29	4,66

According to the results obtained there is an increase in anti-radical activity proportional to the increase in the concentration of the extract. At a low concentration of 4.66 mg/ml, the extracts have a low percentage of DPPH reduction estimated at 15.11 %. At moderately high concentrations, 6.21 mg/ml, the extract has higher percentages of DPPH reduction that vary up to 61.14 %.

From this result it is found that this high-dose extract (6.21 mg / ml) has an antiradical effect on DPPH.

Contamination by heavy metals

The analysis revealed the presence of xenobiotics (Cu, Pb and Zn) in the brown algae Cystoceira stricta (Table 6) shows that the most important contamination concerns relatively Zinc which is not considered as a toxic metal. However, a high concentration can cause physiological disturbances to the body.

Table 3. Average concentrations of heavy metals in µg/g dry weight in the brown seaweed Cystoceura stricta of Sidi Ladjal

Métals	Zinc (Zn)	Copper (Cu)	Lead (Pb)
Concentration found	187,589	109,648	97,0029

The comparison with the values of the literature allows us to note that the values obtained are close to those of polluted environments.

A. Kaimoussi, A. Mouzdahir, A. Saih found values between 6.96 and 66.8 µg/g in U. lactuca tissues, and between 16.21 and 147 µg/g in E. intestinalis tissues, arrived at a greater value, reaching a maximum limit of 337 µg/g dry weight, in U tissues. lactuca (Kaimoussi et al., 2004; Ho, 1988).

N. Favero, M.G. Frigo showed that algae accumulate Zn and Cu easily from seawater. But also according to the study of Benkdad et al. the metal contents in the tissues of the algae, mainly depending on the differences of the biological cycles and the conditions of the bioavailability of the metals (Favero, Frigo, 2002; Benkdad et al., 2011).

The comparison of the results obtained by our study with previous studies indicates the presence of high levels of zinc which is displayed with 187,589 µg/g. PS, followed by copper with 109.648 µg/g. PS and finally the lead that registers at a value of 97.0029 µg/g.

The concentrations of metals vary, not only among species of algae, but also within the same species from different sites.

That is due to abiotic or biotic factors, anthropogenic factors and distribution heterogeneous metals in the ecosystem. These variations are related to the age of the tissues, life cycle, ambient concentrations of metals other conditions environmental.

4. Conclusion

This study gave low LD50 values for the brown algae Cystoseira stricta sp obtained from the different extracts tested.

This toxic action is attributed to a cytogenetic and toxic compounds present in this alga, for this the study of the toxicity is essential in order to locate the limits of tolerance.

This study has shown in particular an abundance of this group of toxic compounds, whose main activity is antifungal, antimycotic, anti-inflammatory and anthelmintic is of particular interest in various pathologies.

As a result, the most toxic extract has the lowest LD50 and, by comparing the different lethal concentrations for the surfactants, it is quite possible to determine if the species is more sensitive and can to be affected by the pollution of its biotope.

References

Benariba et al., 2013 – Benariba, N, Djaziri, R, Bellakhdar, W. et al. (2013). Phytochemical screening and freeradical scavenging activity of Citrullus colo-cynthis seeds extracts. *Asian Pac J Trop Biomed*. 3:35-40.

Benkdad et al., 2011 – *Benkdad, A., Laissaoui, A., Tornero, M.V., Benmansour, M., Chakir, E., Garrido, I.M., Moreno, J.B.* (2011). Trace metals and radionuclides in macroalgae from moroccan coastal waters. *Environ monitassess*. 182: 317-324.

Clarkson et al., 2004 – *Clarkson, P., Li, Y., Richardson, G.* (2004). The market valuation of environmentalexpenditures by pulp and paper companies. *The Accounting Review*. 79, 329-353.

Dahmani, 2014 – *Dahmani, H*. (2014). Etude du pouvoir antimicrobien des extraits bruts de l'algue *Cystoceira stricta* de la cote ouest algérienne (plage de Madrid). Thèse de master en microbiologie. Université de Tlemcen. 60 p.

Dobbeileir et al., 1980 – *Dobbeileir, J., Adam, N., Bossuyt, E., Bruggrman, E., Sorgeloos, P.* (1980). New aspects of the use of inert diets for high culturing of brine shrimp: 165-174. In: The brine shrimp Artemia. Vol 3. Ecology, culturing use in aquaculture. Persoone, G., Sorgeloos, P., Roels, O., Jaspers, E. (Eds.) Universa Press Wetteren, Belgium, 456 p.

Favero, Frigo, 2002 – *Favero, N., Frigo, M.G.* (2002). Biomonitoring of metal availability in the southern basin of the lagoon of Venice (Italy) by means of macroalgae. Department of Biology, University of Padova, Padova, Italy.

Ho, 1988 – *Ho, J-S.* (1988). Phylogenetic analysis of the Eudactylinidae (Crustacea: Copepoda:Siphonostomatoida), with descriptions of two new genera. *Proceedings of the Biological Society of Washington*. 101: 317-339.

Hoenig, 1978 – *Hoenig, S.H., Kazap, I., Leibovici, J.* (1978). Suppression of Humoral Immune Response in Mice by Administration of High Molecular Levan Experientia, 34, 1362.

Kaimoussi et al., 2004 – *Kaimoussi, A., Mouzdahir, A., Saih, A.* (2004). Variations saisonnières des teneurs en métaux (Cd, Cu, Fe, Mn et Zn) chez l'algue Ulva lactuca prélevée au niveau du littoral de la ville d'El Jadida (Maroc). Comptes Rendus Biologies. 327, 361-369.

Lachumy et al., 2010 – *Lachumy, S.J.T., Sasidharan S., Sumathy V., Zuraini Z.* (2010). Pharmacological activity, phytochemical analysis and toxicity of methanol extract of Etlingera elatior (torch ginger) flowers. *Asian Pac J Trop Med.* 3: 769-774.

Lavens, Sorgeloos, 1996 – *Lavens, P., Sorgeloos, P.* (1996). Manual on the production and use of live food for aquaculture. FAO Tech. Pap. 361, 295.

Merad et al., 1991 – *Merad, R., Reggabi, M., Alammir, B., Benali, S., Abetroun, R., Azzouz, M., Beaissa, D.* (1991). Travaux pratiques de toxicologie. Coll. Le cours de pharmacie. *Off. Des desPubl. Univ. INESSM d'Alger*. 150 p.

Moshafi et al., 2009 – *Moshafi, M.H., Sharififar, F., Dehghan, G., Ameri, A.* (2009). Bioassay Screening of the Essential Oil and Various Extracts of Fruits of Heracleumper sicum Desf.and Rhizomes of Zingiber officinale Rosc. using Brine Shrimp Cytotoxicity Assay. *Iranian Journal of Pharmaceutical Research*. Vol 8, pp. 59-63.

Parra et al., 2001 – *Parra, A.L., Yhebra, R.S., Sardinas, I.G., Buela, L.I.* (2001). Comparative Study of the Assay of Artemia salina L. and the Estimate of the Medium Lethal Dose (LD50 Value) in Mice, to Determine Oral Acute Toxicity of Plant Extracts. *Phytomedicine.* 8: 395-400.

Sorgeloos, 1986 – *Sorgeloos, P.* (1986). Manual for the culture and use of brine shrimp Artemia in aquaculture. Belgian Administration for Development Cooperation and the FAO of the United Nations, Artemia Reference Center, Belgium, pp. 1-319.

Published in the Slovak Republic
European Journal of Molecular Biotechnology
Has been issued since 2013.
E-ISSN: 2409-1332
2019, 7(2): 73-85

DOI: 10.13187/ejmb.2019.2.73
www.ejournal8.com

Novel Simple Cyanine, Carbocyanine, and Dicarbocyanine Dyes: Synthesis, Characterization and Application on Polyester Fabric

Maha Mobark Gomaa [a, *]

[a] Aswan University, Aswan, Egypt

Abstract

Novel simple cyanine dyes, carbocyanine dyes and dicarbocyanine dyes derived from the nucleus 6-amino-3-methyl-1,2 diaza 4,13 dihydronaphthacene 5, 7, 12 trione (2) were prepared. The electronic visible absorption spectra of all the novel synthesized cyanine dyes were investigated in 95 % ethanol to evaluate their photosensitization characters and uses these dyes as photographic sensitizers in industry. The antimicrobial activity evaluation of mono, tri and pentamethine cyanine dyes against some bacterial and fungi strains(Escherichia coli, Staphylococcus aures, Aspergillus lavus and Candida albicans) was tested. The antimicrobial activity of the dyes usually increases when they give higher inhibition zone diameter against the tested bacterial and fungi strains. The dyeing process and fastness properities of the new synthesized cyanine dyes were examined on polyester fabric. Polyester is the hydrophobic fibres and usually dyed with cyanine dyes due to their high tinctorial strength and good fastness properties. The structural characterization of dyes carried out by elemental analysis, visible, mass spectroscopy, ^{1}H NMR and IR spectra.

Keywords: synthesis, cyanine dyes, visible spectra, antimicrobial activity, polyester fabric, methine cyanine dyes.

1. Introduction

Cyanine dyes (Shindy, 2017; Li et al., 1998; Yadav, 2005; Kabatc et al., 2012; Miki et al., 2017; Park et al., 2013; Keisar et al., 2017; Upadhyayula et al., 2015; Antonious, 1997; Sener et al.,2018; Hilal et al., 2007; Xiang et al., 2008; Ferreira et al., 2015; Li et al.,2012; Wada et al., 2015; Wang et al., 2017; He et al., 2017; Li et al., 2017) are important class of organic heterocyclic dyes. This is due to the excellent photochemical and photophysical properties, extraordinary appllications and uses of these dyes in a diverse and a board area, such as biochemistry, engineering, physics, biotechnology, biology, pharmacology and medicine. These dyes can be used in photoghraphy, analytical reagents over a wide pH media, in high energy laser and digital image storage, as indicator for solvent polarity, in biomedical and biological use as molecular probes and as fluorescent dyes for DNA visualization assays. In addition cyanine dyes (Sun et al., 2013; Sha et al., 2018; Christenson et al., 2014) used in high technique such as in optical recording materials. On the other side, cyanine dyes possess a wide range of bioactivities including antimicrobial efficiency, antibacterial agents, antioxidants, anticancer and antitumer agents (Power et al., 2009; Gomaa, 2014; Shindy et al., 2016; Fayez, 2009; Fayez et al., 2015; Badran et al., 2007; Mohareb et al., 2007; Vicini et al., 2002; Mishra et al., 2019; Yong et al., 2009; Rathish et al., 2012). The work in this paper aimed to synthesize novel methine cyanine dyes covers monomethine, trimethine and

* Corresponding author
E-mail addresses: mobarkmaha@yahoo.com (M. Mobark Gomaa)

pentamethine cyanine dyes to study their electronic transitions through investigating their visible absorption spectra in ethanolic solution to evaluate their photosensitization properties to be used as photographic sensitization in industry. The antimicrobial activities of monomethine, trimethine and pentamethine cyanine dyes were evaluated versus many species of both bacteria and fungi strains and showed promising results. The present study is an attempt to synthesis of novel methine cyanine dyes using for dyeing of polyester fabric to obtain dyed polyester fabric have good fastness properties. The polyester fabrics give high affinity for some prepared dyes.

2. Materials and methods

2.1. General

All melting points of the synthesized cyanine dyes measured by using Electrothermal 15v, 45w 1 A9100 melting point apparatus (Faculty of Science, Aswan University, Aswan, Egypt) and are uncorrected. Elemental analysis carried out at the Microanalytical Center by an automatic analyzer (Vario EL III Germany) (Cairo-Uni – versity). The IR (KBr) spectra measured with a FT-IR (4100 Jasco, Japan) (Cairo University). ^{1}H NMR spectra accomplished with Varian Gemini-300 MHz NMR spectrometer (Cairo University). The electronic absorption spectra carried out on visible spectrophotometer spectra 24 RS Labomed, INC. (Faculty of Science, Aswan University, Egypt). Mass spectroscopy recorded on Mass 1: GC2010 Shimadzu Spectrometer (Cairo University). Dyeing process examined on Infra dyeing machine in National Research Centre (Dokki, Giza, Egypt).

2.2. Synthesis

2.2.1. Synthesis of 6-amino-3-methyl-1,2 diaza 4,13 – dihydronaphthacene 5,7,12 trione (2)

This compound was synthesized according to reference described earlier (El-Kanzy et al., 2007).

2.2. 2. Synthesis of 6-amino 2,3 dimethyl 1,2 diaza 4,13-dihydronaphthacene 5, 7, 12 trione-2 ium iodide (3)

A pure sample of compound (2) was suspended in excess of ethyl (methyl) iodide and heated in a sealed tube at 140°C for 2 hrs. The sealed tube was cooled, opened and the product (3) was collected, washed with ether and crystallized from ethanol to give dark brown crystals (Table 1).

Table 1. Characterization of compounds (3–8c)

Comp. No.	Nature of products			Mol. Formula, (M. Wt)	Elemental analysis, % Calculated (Found)		
	Colour	Yield %	M.P., °C		C	H	N
3	Dark brown	90	160	$C_{18}H_{16}N_3O_3I$ (449)	48.10 (48.25)	3.56 (3.50)	9.35 (9.15)
4a	Brown	70	295	$C_{25}H_{23}N_4O_3I$ (554)	54.15 (54.00)	4.15 (4.13)	10.10 (10.20)
4b	Deep red	80	260	$C_{29}H_{25}N_4O_3I$ (604)	57.61 (57.68)	4.13 (4.22)	9.27 (9.40)
4c	Brownish red	75	240	$C_{29}H_{25}N_4O_3I$ (604)	57.61 (57.80)	4.13 (4.16)	9.27 (9.33)
5	Brown	70	210	$C_{23}H_{26}N_3O_5I$ (551)	50.09 (50.11)	4.71 (4.53)	7.62 (7.47)
6a	Red	65	280	$C_{27}H_{25}N_4O_3I$ (580)	55.86 (55.66)	4.31 (4.27)	9.65 (9.83)
6b	Violet	70	290	$C_{31}H_{27}N_4O_3I$ (630)	59.04 (59.23)	4.28 (4.26)	8.88 (8.73)
6c	Brownish red	67	260	$C_{27}H_{25}N_4O_3I$ (580)	55.86 (55.93)	4.31 (4.09)	9.65 (9.55)
7	Brown	80	200	$C_{21}H_{18}N_3O_4I$ (503)	50.09 (50.33)	3.57 (3.66)	8.34 (8.22)
8a	Deep red	77	260	$C_{29}H_{27}N_4O_3I$ (606)	57.42 (57.44)	4.45 (4.60)	9.24 (9.35)

8b	Deep violet	68	285	$C_{33}H_{29}N_4O_3I$ (656)	60.36 (60.50)	4.42 (4.33)	8.53 (8.41)
8c	Brownish red	75	250	$C_{29}H_{27}N_4O_3I$ (606)	57.42 (57.30)	4.45 (4.40)	9.24 (9.20)

2.2.3. Synthesis of monomethine cyanine dyes (4a-c)

A mixture of compound (3) (0.01mole) and iodoethane quaternary salts of either (pyridine, quinoline or isoquinoline) (0.01 mole) was refluxed for 7-8 hrs in ethanol (40 ml) containing piperidine (2-6 drops), filtered hot, concentrated and acidified with acetic acid. The precipitated products after dilution with water and ice filtered off and crystallized from ethanol. The data were recorded in Table 1.

2.2.4. Synthesis of intermediate compound (5)

1:1 molar ratios of the quaternary salt (3) and triethylorthoformate were refluxed in ethanol (30 ml) containing piperidine (3-6 drops) for 4 hrs., filtered hot to remove unreacted materials, concentrated to one half its initial volume, cooled, acidified, and precipitated by cold water. The brown precipitate was filtered, washed with water, dried and crystallized from ether. The data are registered in Table 1.

2.2.5. Synthesis of trimethine cyanine dyes (6a-c).

A mixture of the intermediate compound (5) (0.01 mol) and N-ethyl (2-picolinium, quinaldinium,4-picolinium) iodide quaternary salts (0.01 mol) heated under reflux in ethanol (35 ml) containing piperidine (3-9 drops) for 8hrs., filtered hot, concentrated, cooled, acidified with acid and precipitated by ice. The precipitates were filtered off, dried and crystallized from absolute ethanol. The data were tabulated in Table 1.

2.2.6. Synthesis of intermediate compound (7)

This intermediate compound (7) was prepared by refluxing compound (5) (0.01 mol) with acetaldehyde (0.01 mol) in ethanol (30 ml) and piperidine (2-6 drops) for 2-4 hrs., filtered hot, concentrated, cooled then precipitated by ice and water. The brown intermediate compound was crystallized from ethanol. The results are reported in Table 1.

2.2.7. Synthesis of pentamethine cyanine dyes (8a-c)

Equimolar ratios of the previously synthesized intermediate compound (7) (0.01mol) and N-ethyl (2-picolinium, quinaldinium, 4-picolinium) iodide quaternary salts (0.01) were dissolved in ethanol (40 ml) and piperidine (3-7 drops). The reaction mixture was refluxed for 9 hrs., filtered hot, concentrated, cooled , acidified with acid and precipitated by ice. The precipitates were filtered off, dried and crystallized from absolute ethanol. The data were tabulated in Table 1.

2.3. Antimicrobial studies

Antimicrobial activity of the tested samples (4a, 4b, 4c, 6a, 6b, 6c, 8a, 8b and 8c) was determined using a modified Kirby-Bauer disc diffusion method. Briefly, 100µl of the test bacteria/fungi were grown in 10 ml of fresh media until they reach a count of approximately 108 cells/ml for bacteria or 105 cells/ml for fungi.100µl of microbial suspension was spread on agar plates corresponding to the broth in which they were aintained. Isolated colonies of each organism that might be playing a pathogenic role should be selected from primary agar plates and tested for susceptibility by disc diffusion method. Disc diffusion method for filamentous fungi used to evaluate the susceptibilities of filamentous fungi to antifungal agent. Samples were dissolved in DMSO to give a final concentration (1 mg/ml). The agar used is Meuller-Hinton agar that is rigorously tested for composition and pH. Further the depth of the agar in the plate is a factor to be consider in the disc diffusion method. This method is well documented and standared zones of inhibition have been determined for susceptible and resistant values. Blank paper disks with a diameter of 8.0 mm were impregnated 10µ of tested concentration of the stock solutions. The biological activity for each substance was tested on surface – seeded nutrient agar medium with the prepared susceptible disc. Bacterial strains and the biological effect are shown in Table 4.

2.4. Fabric

Polyester fabric, bleached and mill-scoured were supplied by the company called El-Mahalla El-Kobra, Egypt. The fabrics always scoured at temperature 50 °C for 30 min, L:R(1:50), 2 g/L of Na_2CO_3 and 2 g /L of nonionic detergent solution (Hostapal; Clariant, Swiss). Then dried at room temperature after rinsed with cold water.

Dyeing Method

Dyeing process carried out by using distilled water while dyeing experiments required two step.Firstly, Polyester fabric dyed take place by using the prepared disperse dyes at pH 5 by adding acetic acid, liquor ratio at 1:50. Dye bath containes Matexil DA-N which (supplied by ICI Company, UK) as dispersing (1 ml/L) and 1 % of dye . The temperature start at 40 °C, then raised to 130 °C for about 60 min. using cold water in washing and reduction cleaning mad by both hydrosulphite (2g/L), sodium hydroxide (2g/L) at 60 0C for about 10 min. Then , treated the samples by acetic acid (1ml/L), cooled water and dried (Tarulata et al., 2011; Tarek et al., 2015).

2.5. Color Measurements of the dyed samples

Color Strength

Hunter Lab ultra Scan® PRO spectrophotometer use to determined the colorimetric analysis of dyes while the Kubelka Munk equation (Kubelka et al., 1931) used to determine colour strength value (K/S) as follow:

$$K/S = \frac{(1-R)^2}{2R} \qquad (1)$$

Where,

R = decimal fraction of the reflection of the dyed fabric,

K = absorption coefficient, and S = scattering coefficient

Fastness testing

The dyed samples subjected to washing, rubbing, light, sublimation test and perspiration according to the standard ISO methods, like ISO 105-X12 (1987), ISO 105-C04 (1989), ISO105-E04 (1989), ISO 105-B02 (1988) respectively.

3. Results and discussion

3.1. Synthesis

The polyheterocyclic starting compound namely 6-amino 2,3 dimethyl 1,2 diaza 4,13-dihydronaphthacene-5,7,12 trione-2 ium iodide (3) was synthesized by quaternization of compound (2) using an excess of iodomethane.The reaction of the compound (3) with an iodoethane quaternary salts of either pyridine, quinoline or isoquinoline in equimolar ratios in ethanol catalyzed by piperidine gave the 6-amino 2 methyl 1,2 diaza 4,13-dihydronaphthacene-5,7,12 trione 3[4(1)]monomethine cyanine (4a-c) Scheme (1), Table 1.

Treating on the newly synthesized monomethine dyes (4a-c) by conc. H_2SO_4 resulted in liberating iodine vapor on heating. This can be attributed to the liberation of hydrogen iodide and hydrogen molecule.

The reaction of the quaternary salt (3) with triethylorthoformate in equimolar ratio and in ethanol containing few mls of piperidine as a basic catalyst gave the corresponding intermediate compound (5) (Scheme 1).

The intermediate compound (5) reacted with equimolar ratios of N-ethyl(2-picolinium, quinaldinium, 4-picolinium) iodide quaternary salts in ethanol and piperidine to give 6-amino 2 methyl 1,2 diaza 4,13-dihydronaphthacene-5,7,12 trione 3[2(4)] trimethine cyanine dyes(6a-c) (Scheme 1). Treatment on the previous trimethine cyanine dyes (6a-c) by conc. H_2SO_4 liberating iodine vapor. This back to elimination two molecules of ethanol and hydrogen iodide molecule.

Finally, reaction of equimolar ratio of intermediate compound (5) with acetaldehyde in ethanol and piperidine yielded compound (7). The later compound (7) undergoes condensation reaction with equimolar ratios of N-ethyl(2-picolinium, quinaldinium, 4-picolinium) iodide quaternary salts in ethanol and piperidine to give 6-amino 2 methyl 1,2 diaza 4,13-dihydronaphthacene-5,7,12 trione 3[2(4)]petamethine cyanine dyes (8a-c). (Scheme 1). The structure of the dyes were identified by elemental analysis, visible spectra Tables 1, 2, IR, ^{1}H NMR and Mass spectroscopic (Table 3).

3.2. Spectral behavior in 95 % ethanol solution:

Dyes (4a-c), (6a-c), and (8a-c) are highly coloured compounds in their ethanolic solution ranging from deep red to deep violet. The electronic absorption spectrum features (λ_{max} and ε_{max} values) of the newly synthesized mono cyanine dyes (4a-c), tri cyanine dyes (6a-c) and penta methine cyanine dyes (8a-c) were examined in 95 % ethanol solution and the results are summarized in Table 2.

The Uv-Visible absorption spectrum of the monomethine cyanine dyes (4a-c) in 95 % ethanol shows bands in the visible region 405-520 nm. These bands underwent displacements to give red(or blue) shifts with increasing (or decreasing) depending upon the nature of the quaternary residue(A), extention of π-delocalization and their linkage position. So, the dye (4a), A=1-ethyl pyridinium-4-yl salt showed λ_{max} at 405,445 nm. Substitution A = 1-ethyl pyridinium-4-yl salt in dye (4a) by A = 1-ethyl quinolinium-4-yl salt in dye (4b) caused a bathochromic shift of λ_{max} = 75 nm, so compound (4b), exhibited λ_{max} = 520 nm. This back to the more extensive π-delocalization and conjugation within the extra phenyl ring in quinolinium ring in dye (4b) (Table 2) (Ahmed et al., 2018; Gomaa et al., 2012; Shindy et al., 2019; Shindy, 2018; Shindy et al., 2017; Shindy et al., 2015; Soriano et al., 2015; Shindy et al., 2018).

It is also interesting to note that the visible absorption maximum of dye(4b), A = 1-ethyl quinolinium-4-yl salt is red – shifted to dye (4c), A = 2-ethyl isoquinolinium-1-yl so dye (4c) showed λ_{max}= 500 nm. This is due to the increasing π-delocalization within 4-yl salt in dye (4b) if compared with 1-yl salt in dye (4c) (Table 2).

Morever, the Uv-visible absorption spectrum of the trimethine cyanine dyes (6a-c) discloses bands in the visible region 360-600 nm. Their intensity and positions are influenced by the nature of the heterocyclic quaternary residue (A), extention of π-delocalization and their linkage position. So, the absorption spectra of dye 6a, A = 1-ethyl pyridinium -2-yl salt showed λ_{max} = 360, 505 nm. Substituting of A = 1-ethyl pyridinium-2-yl salt in dye (6a) by A = 1-ethyl quinolinium -2-yl salt in dye (6b) resulted in red- shifted of λ_{max} = 10 nm with increasing the number of absorption bands, (6b λ_{max} = 370, 450, 505 and 600 nm). This is due to the decreasing π-delocalization in dye (6a) than analogous (6b).

Additionally, changing the linkage position from 2-yl salt in trimethine cyanine dye (6a), A= 1-ethyl pyridinium -2- yl salt to 4-yl salt in trimethine cyanine dye (6c), A = 1-ethyl pyridinium 4-yl salt showed a remarkable bathochromic shift of λ_{max}= 10 nm if compared with compound (6a), (6c, λ_{max} = 365, 415,515 nm). This illustrated according to the increasing of the extension conjugation of 4-linkage pyridine moiety in dye (6c) better than 2-linkage analogous in dye (6a) (Table 2).

Finally, the Uv-visible absorption spectrum of pentamethine cyanine dyes (8a-c) displays bands in the visible region 530-690 nm. Their molar absorptivity of bands and positions are effected by the nature of quaternary salt residue (A) and their linkage position. So, substituting A = 1-ethyl pyridinium-2-yl salt in pentamethine cyanine dye (8a) by A = 1-ethyl quinolinium-2-yl salt in pentamethine cyanine dye (8b) causes red shifted by 30 nm and increasing the number of bands. This back to the increasing π-delocalization and conjugation in quinaldinium dye (8b) compared to α-picolinium dye (8a) (Table 2). Changing the linkage position from 2-yl salt in pentamethine dye (8a) to 4-yl salt in pentamethine dye (8c) produced red shifted by 10 nm. This can be explained in the light of increasing conjugation in the γ-picolinium dye (8c) (Table 2).

Comparing the Uv-visible absorption spectrum of trimethine cyanine dyes(6a-c) with those of the pentamethine cyanine dyes (8a-c) showed that the latter dyes are red shifted dyes compared with the former dyes. This is due to the increasing number of methine groups in pentamethine cyanine dyes which increasing conjugation. It is also notice that trimethine cyanine dyes (6a-c) showed absorption bands and their molar extinction coefficients, their positions of these bands are highly effected if compared with monomethine cyanine dyes (4a-c) (Table 2).

Table 2. The electronic absorption spectra of new synthesized cyanine dyes (4a-c), (6a-c) and (8a-c) in 95 % EtOH

Compound	**λ_{max}, nm (ε_{max}mol^{-1}, cm^{-1})**		
Monomethine cyanine dyes (4a-c)	4a 405(19500) 445(15000)Sh.	4b 520(17500)	4c 500(22000)
Trimethine cyanine dyes (6a-c)	6a 360(22000) 505(20000)	6b 370(22000) 450(14000) 505(12000)Sh. 600(12500)	6c 365(22500) 415(16000) 515(20000)
Pentamethine cyanine dyes (8a-c)	8a 530(20000) 670(5500)Sh.	8b 560(14500) 670(2500)Sh. 690(2500).	8c 450(19500) 680(11000)

Table 3. IR and ^{1}H NMR (Mass) spectral data of the prepared compounds

Comp. No.	**IR Spectrum (KBr, cm-1)**	**^{1}H NMR Spectrum (DMSO, δ); & (Mass data)**
3	1387 (C-N), 1451 (C=N), 1593 (C=C), 1652 (quinone ring), 2940 (quaternary salt), 3434 (NH_2).	0.82-1.08 (S, 3H, CH_3, N-methyl iodide), 2.00-2.50(S, 2H, NH_2), 3.17 (S, 2H, CH_2), 3.50 (S, 3H, CH_3), 4.10 (S, 1H, quinone), 7.40-8.40 (m, 5H, 4Ar-H+NH).
4b	1369 (C-N), 1451 (C=N) 1666 (quinone ring), 2924 (quaternary salt), 3423(NH_2).	0.80-2.00 (m, 9H, CH_3,CH_3 of N-quinolinium, CH_2, CH), 2.50 (S, 2H, NH_2), 3.31 (S, 2H, CH_2 of N-quinolinium), 7.00-8.50 (12H, 10Ar-H+NH+ = CH).
5	1263 (C-O ether), 1379 (C-N), 1360-1447 (C=N), 1590 (C=C), 1625 (quinone ring) 2936 (quaternary salt), 3424 (NH_2).	1.15-1.20 (t, 6H,2 CH_3 of diethoxyethyl), 1.25-1.90 (m, 4H, CH_3 of methyl iodide+ CH of diethoxyethyl), 2.50 (S, 2H, NH_2), 2.70 (S,2H,CH_2), 3.00 (S ,4H ,2CH_2 of diethoxy ethyl), 3.40 (m, 2H, CH_2 of diethoxyethyl), 3.90-4.00(S, 1H, quinone), 6.90-8.60 (m, 5H, 4Ar-H +NH). M+: 551
6a	1375 (C-N), 1492 (C=N), 1622 (C=C), 2920, 2858 (quaternary salt), 3432(NH_2).	0.80-2.00 (m, 9H, CH_3,CH_3 of, N-pyridinium, CH_2, CH), 2.50 (S,2H,NH_2), 3.43 (S ,2H, CH_2 of N-pyridinium), 7.20-8.50 (m, 12H, 8Ar-H+NH+ = CH).
7,8b	1371, 1339(C-N), 1441, 1443 (C=N), 1630, 1621 (C=C), 1763(C=O) aldehydic for compound (7). 2925, 2924 (quaternary salt), 3424, 3422 (NH_2).	(M+1): 504 For compound (7) (8b): 1.17-2.20 (m,9H,CH_3,CH_3 of N-quinolinium, CH_2, CH), 2.50 (S, 2H, NH_2), 3.33 (S, 2H, CH_2 of N-quinolinium), 7.45-8.32 (m, 16H, 10Ar-H+NH+ = CH).

3.3. Antimicrobial activity

The antibacterial activities and antifungal activities of all the newly synthesized quinone cyanine dyes 4a, 4b, 4c, 6a, 6b, 6c, 8a, 8b, and 8c were tested against some bacterial strains (Escherichia coli and Staphylococcus aureus) and fungi strains (Aspergillus flavus and Candida albicans) (Table 4).When a filter paper disc impregnated with a tested chemical is placed on agar the chemical will diffuse from the disc into the agar. This diffusion will place the chemical in the agar only around the disc. The solubility of the chemical and its molecular size will determine the size of the area of chemical infiltration around the disc. If an organism is placed on the agar it will not grow in the area around the disc if it is susceptible to the chemical. This area of no growth around the disc is known as a [Zone of inhibition] or [Clear zone]. The data obtained are expressed as size (mm) of inhibition zone. Diameter of the inhibition zone were high (22-18 mm), moderate (17-12 mm), low (11-1 mm), no response(-) (Ballatore et al., 2012; King et al.,2010; El-Mashad et al.,2012; Mohamed et al., 2014). Studying the antimicrobial(antibacterial, antifungal)activity evaluation against some bacterial and fungi strains have a great practical value in cyanine dyes because of the uses and applications of these dyes as bactericidal and fungicidal in pharmaceutical industry. In this study, all the newly synthesized dyes are biologically active against bacteria this is due to the presence of quinone ring with its high potency. Dyes (4a-c) possess highest potency as antimicrobial activity if compared with the others showed moderate to low (Table 4). Generally, decreasing carbon content of the tested dyes (4a-c) if compared with (6a-c, 8a-c) increased the activity against bacterial strains. This could be correlated to the hydrophilic and hydrophopic structural equilibria of the tested dyes. Comparing the antibacterial activity of the monomethine cyanine dye (4a), trimethine cyanine dye(6a) and pentamethine cyanine dye (8a) by their analogous (4b), (6b) and (8b) resulted in that the latter dyes (4b, 6b, 8b) have higher inhibition zone diameter than the former dyes (4a, 6a, 8a). This is due to the increasing π-delocalization and conjugation in the quinoline ring system in (4b, 6b, 8b). Morever, the antimicrobial activity of the trimethine cyanine dye (6c) and pentamethine cyanine dye (8c) showed higher inhibition zone diameter than analogous (6a) and (8a). This attributed to the extention of π-delocalization in the former dyes (6c, 8c) which contains γ-picoline. Conversly, all the prepared cyanine dyes are biologically inactive against fungi except (4b) showed moderate fungicidal activity only on Candida albicans (Table 4). From Table 4 we can conclude that: all the tested dyes can be used as antibacterial agents against bacterial strains (Escherichia coli and Staphylococcus aureus) while dye (4b) only can be used as fungicidal against (Candida albicans). Finally: the antimicrobial activity of dyes depending upon the type of bacterial and fungi strains, number of methine groups, type of quaternary salt residue (A) and linkage position.

3.4. Color strength

ΔE, b, a, L and color strength K/S values of the polyester fabrics dyed by using disperse dyes are recorded in Table 5. The dying process carried out at pH 4.5, L. R 1:50, at 130 ^{o}C, and 1 % (w.o.f) for 60 min. The CIE (L*, a*, b*) system was employed to determine the color coordinates, where the value of (b*) range from yellow (positive) to blue (negative), (a*) range from green (negative) to red (positive), and (L*) denote to lightness or darkness (0-100). From Table 5 we conclude that the dyed polyester fabric with high L* value (62.35-75.58), a* value (2.75-8.17), and b* value (1.75-16.43) for dyed the polyester fabric. The value of K/S refer to the amount of dye which absorbed on the the fiber. Table 5 shows that dyes 4b and 8b exhibit the highest value of K/S and the polyester fabrics give high affinity for some prepared dyes.

Table 4. Biological activity of some newly synthesized compounds

Sample		Inhibition zone diameter (mm/mg sample)			
		Escherichia coli **(G^-)**	***Staphylococcus aureus*** **(G^+)**	***Aspergillus flavus*** **(Fungus)**	***Candida albicans*** **(Fungus)**
Control: DMSO		0.0	0.0	0.0	0.0
Standar	**Ampicillin antibacterial agent**	22	18	--	--
	Amphotericin B antifungal agent	--	--	16	19
4a		14	18	0.0	0.0
4b		16	17	0.0	12
4c		14	18	0.0	0.0
6a		10	11	0.0	0.0
6b		13	14	0.0	0.0
6c		12	13	0.0	0.0
8a		12	13	0.0	0.0
8b		14	16	0.0	0.0
8c		13	16	0.0	0.0

Table 5. Color strength K/S, L, a, b, ΔE value of polyester fabrics dyed by disperse dyes

Samples	K/S	L	a	b	ΔE
4 b	2.63	63.40	3.71	7.91	21.53
6 a	1.84	75.58	6.87	9.19	14.03
6 b	2.12	71.45	8.17	16.43	22.01
6 c	2.00	72.50	6.49	9.59	15.91
8 a	1.96	71.58	5.12	8.48	15.35
8 b	2.37	62.35	2.75	1.75	20.84

Table 6. Fastness properties of polyester fabrics dyed by disperse dyes

Dyes	Washing fastness			Rubbing fastness		Perspiration fastness						Sublimation		Light fastness
						Acidic			Alkaline					
	Alt.	St.*	St.**	Dry	Wet	Alt.	St.*	St.**	Alt.	St.*	St.**	210	180	
4b	4-5	4-5	4-5	4-5	4-5	4-5	4-5	4-5	4-5	4-5	4-5	4-5	4-5	3-4
6a	4-5	4-5	4-5	4-5	4-5	4-5	4-5	4-5	4-5	4-5	4-5	4-5	4-5	4
6b	4-5	4-5	4-5	4-5	4-5	4-5	4-5	4-5	4-5	4-5	4-5	4	4-5	4
6c	4-5	4-5	4-5	4-5	4-5	4-5	4-5	4-5	4-5	4-5	4-5	4	4-5	4
8a	4-5	4-5	4-5	4-5	4-5	4-5	4-5	4-5	4-5	4-5	4-5	4-5	4-5	4
8b	4-5	4-5	4-5	4-5	4-5	4-5	4-5	4-5	4-5	4-5	4-5	4-5	4-5	3-4

St.* Staining on cotton
St. ** Staining on wool
Alt. Alteration in colour

3.5. Fastness properties

Most polyester fabric which dyed by using quinone cyanine dyes were examined towards light, sublimation, rubbing, perspiration and washing and showed promising results. The results are recorded in Table 6. From Table 6 we could conclude that the light fastness properities were good (3-4) while (washing, fastness, dry and wet crocking, both acidic and alkaline perspiration) test gave a very good (4-5).

4. Conclusion

From all the previous discussed results we summarized that:

1. The (bathochromic, hypsochromic) shifts, number of bands and intensity of bands for the new prepared quinone cyanine dyes depending upon:

a- The nature of quaternary salt residue(pyridinium dye < quinolinium dye in monomethine cyanine dyes, picolinium dyes < quinaldinium dyes in the trimethine and pentamethine cyanine dyes).

b- Linkage position(isoquinolinium dye < quinolinium dye in monomethine cyanine dyes , α-picolinium dyes < γ – picolinium dyes in trimethine and pentameth -ine cyanine dyes).

c- The number of methine units in the order of: (pentamethine cyanine dyes > trimethine cyanine dyes > monomethine cyanine dyes).

2. The intensity of the colours of (mono, tri, and penta)methine cyanine dyes (4a-c, 6a-c, 8a-c) are discussed according to the presence of two mesomeric structures (A) and (B) producing a delocalized positive charges over the conjugated system of the quinone cyanine dyes. Scheme (2).

3. The quinone dyes (4a-c, 6a-c, 8a-c) can be used:

a- As photoghraphic sensitizers in industry due to their spectral properities.

b- As antimicrobial agents against some(fungal and bacterial) strains due to their biological activity and promising results. Antimicrobial activity depending upon: i-Types of dyes [penta, tri, mono], ii – Nature of quaternary salt residue (A) [quinolinium, pyridinium, quinaldinium and/or picolinium salt residue], iii-Linkage positions [γ-picolinium, α-picolinium, isoquinolinium and/or quinolinium] and kinds of bacterial and fungi strains.

4. The dyeing process and fastness properities of the synthesized quinone cyanine dyes were examined on polyester fabric. The polyester fabrics give high affinity for some prepared quinone dyes.

5. Acknowledgements

Sincere appreciation and gratitude acknowledgement to all members of the Chemistry Department in Aswan University for their help and support.

References

Ahmed et al., 2018 – *Koraiem, Ahmed I., El-Shafei, Ahmed, Abdellah, Islam M., Fathy F. Abdel Latif, Reda M. Abd El-Aal* (2018). Theoretical and experimental spectro- scopic investigation of new polymethine donor- π- acceptor cyanine dyes: synthesis, photophysical and TDDFT studies. *J. Mol. Struct*. 1173: 406-416. DOI: https://doi.org/10.1016 /j.molstruc.2018,07.021

Antonious, 1997 – *Antonious, M.S.* (1997). Solvent polarity indicator: flexible styryl pyridinium and quinolinium fluorescence probes for medium free-volume. *Spectrochimica Acta part A: Molecular and biomolecular spectroscopy*. 53(11): 317-323. DOI: https://doi.org/10.1016/ S1386-1425(96)01788-X

Badran et al., 2007 – *Badran, M.M., Moneer, A.A., Refaat, H.M., El-Malah, A.A.* (2007). Synthesis and antimicrobial activity of novel quinoxaline derivatives. *J. Chin. Chin.Chem. Soc.* 54(2): 469-478. DOI: https://doi.org/10.1002/jccs.200700066

Ballatore et al., 2012 – *Ballatore, C., Crowe, A., Piscitelli, F., James, M.* (2012). Aminothienopyridazine inhibitors of tau aggregation:evaluation of structure activity relationship leads to selection of candidates with desirable in vivo properties. *Bioorg. Med. Chem.* 20: 4451. DOI: https:/doi.org/10.1016/j.bmc.2012.5.027

Christenson et al., 2014 – *Christenson, C.W., Saini, A., Valle, B., Shan, J., Singer, K.D.* (2014). Nonlinear fluorescence modulation of an organic dye for optical data storage. *J. Opt. Soc. Am. B*. 31(3): 637-641. DOI: https://doi.org/10.1364/JOSAB.31.000 637

El-Kanzy et al., 2007 – *El-Kanzi, N.A.A., Khalafallah, A.K., Younis, M.* (2007). Effect of iodine on the antimicrobial activity of new spiro and isolated B-lactame thiazolidinone derivatives. *Phosphorous, Sulfur and silicon and the related elements*. 182(5): 1163-1181. DOI: https://doi.org/10.1080/10426500601149929

El-Mashed et al., 2012 – *El-Mashad, N., Foad, M.F., Soudy, N., Salem, D.A.* (2012). Susceptibility tests of oropharyngeal candida alicans from Egyptian patients to fluconazole determined by three methods. *Braz. J. Microbiol.* 43: 266-273. DOI:10.15 90/S1517-838220120001000031

Fayez et al., 2015 – *Eissa, Fayez M., Abdelghany, A.R.* (2015). New 1,3,4-oxadi-azino isoquinoline methine cyanine dyes: synthesis, photosensitivity and antimicrobial activity. *J. of heterocyclic chemistry*. 53(2). DOI: https://doi.org/10.1002/j het.2428

Fayez, 2009 – *Eissa, Fayez M.* (2009). Preparation, antimicrobial activity and absorption spectra of pyrazolo-oxadiazine cyanine dyes. *J. Chin. Chem. Soc.* 56: 843-849. DOI: https://doi.org/10.1002/jccs.200900125

Ferreira et al., 2015 – *Ferreira, D.P., Conceicao, D.S., Prostota, Y., Santos, P.F., Ferreira, L.F.V.* (2015). Fluorescent"rhodamine-like" hemicyanines derived from the 6-(N,N-diethylamino)-1,2,3,4-tetrahydroxanthylium system. *Dyes and Pigments*. 112: 73-80. DOI: https://doi.org/10.1016/dyepig.2014.06.021

Gomaa et al., 2012 – *Gomaa, M.M., El-Deen, N.S., El-Kanzi, N.A.* (2012). Benzo [g] quinoline heterocyclic derivative as a typical precursor in the synthesis of new class of cyanine-like dyes. *Eur. J. Chem*. 3(4): 461-467. DOI: 10.5155/eurjchem.3.4.461-467,699

Gomaa, 2014 – *Gomaa, M.M.* (2014). Oxonium heterocyclic quinone in the syn- thesis of some cyanine dyes and their antimicrobial activity. *Eur. J. Chem.* 5(3): 463-468. DOI: http://dx.doi.org/10.5155/eurjchem.5.3.643-469,973

He et al., 2017 – *He, L., Yang, X., Xu, K., Kong, X., Lin, W.* (2017). A multi-signal fluorescent probe for simultaneously distinguishing and sequentially sensing cysteine/homocysteine, glutathione, and hydrogen sulfide in living cell. *Chem. Sci.* 8: 6257-6265. DOI: https://doi.org/10.1039/c7sc00423k

Hilal et al., 2007 – *Hilal, H., Taylor, J.* (2007). Determination of the stoichiometry DNA-dye interaction and application to the study of a bis-cyanine dye-DNA complex. *Dyes and Pigments*. 75: 483-490. DOI: https://doi.org/10.1016/j.dyepig.2006.6.032

Kabatc et al., 2011 – *Kabatc, J., Bajorek, Agnieszka, Dobosz, Robert* (2011). Bichromophoric hemicyanine dyes as fluorescence probes applied for monitoring of the photochemically initiated polymerization. *J. Mol. Structure*. 985(1): 95-104. DOI: https://doi.org/10.1016/jmolstruc.2010.10.027

Keisar et al., 2014 – *Keisar, O.R., Finfer, E.K., Ferber, S., Finaro, R., Shabat, D.* (2014). Synthesis and use of Qcy7-derived modular probes for the detection and imaging of biologically relevant analytes. *Nature Protocols*. 9(1): 27-36. DOI: 10.1038/nprot.2013.166

King et al., 2010 – *King, P., Lomovskaya, O., Griffith, D., Burns, J., Dudley, M*. (2010). In vitro pharmacodynamics of levofloxacin and other aerosolized antibiotics under multiple conditions relevant to chronic pulmonary infection in cystic fibrosis. *Antimicrob. Agents Ch*. 54: 143-148. DOI: 10.1128/AAC.00248-09

Kubelka et al., 1931 – *Kubelka, N.A., Munk, F.Z.* (1931). *Tech. Phys*. 12: 593.

Li et al., 1998 – *Li, Q., Lin, G.L, Peng, B-X, LI, Z.-X* (1998). Synthesis, characterization and photographic properties of some new styryl cyanine dyes. *Dyes and Pigments*. 38: 211-218. DOI: https://doi.org/10.1016/S0143-7208(97)00088-0

Li et al., 2012 – *Li, Z., Sun, S., Liu, F., Pang, Y., Fan, J., Song, F., Pang, X*. (2012). Large fluorescence enhancement of a hemicyanine by supramolecular interaction with cucurbit[6]Uril and its application as resettable logic gates. *Dyes and Pigments*. 93(1-3): 1401-1407. DOI: 10.1016/jdyepig.2011.10.005

Li et al., 2017 – *Li, C., Tebo, A., Gautier, A*. (2017). Fluorogenic labeling strategies for biological imaging. *Int.J. Mol. Sci*. 18: 1473. DOI: https://doi.org/10.3390/ijms 18071473

Miki et al., 2017 – *Miki, K., Kojima, K., Oride, K., Harada, H.A., Ohe, Morinibu, K*. (2017). pH-Responsive near-infrared fluorescent cyanine dyes for molecular imaging based on pH sensing. *Chem. Comm*. 53: 7792-7795. DOI: https://doi.org/10.1039/c7cc03035e

Mishra et al., 2019 – *Mishra, V.R., Ghanavatkar, C.W., Sekar, N*.(2019). UV pro- tective heterocyclic disperse azo dyes: spectral properties, dyeing potent antibacterial activity on dyed fabric and comparative computational study. *Spectrochimica Acta part A:Molecular and Biomolecular spectroscopy,*223:117353.https:doi.org/10.1016/j.saa. 2019.117353.

Mohamed et al., 2014 – *Mohamed, M.A. and Ibrahim, O.B*. (2014). Study the chemical composition and biological outcomes resulting from the interaction of the hormone adrenaline with heavy elements: Infrared, Raman, electronic, H^1NMR, XRD and SEM studies. *J. Mol. Struct*. 1056: 13-24. DOI: https://doi.org/10.1016/j.molstruc.201310.019

Mohareb et al., 2007 – *Mohareb, R.M., Ho, J.Z., Alfarouk, F.O*. (2007). Synthesis of thiophenes, azoles and azines with potential biological activity by employing the versatile heterocyclic precursor N-benzoycyano acetylhydrazine. *J. Chin. Chem. Soc*. 54: 1053-1066. DOI: https://doi.org/10.1002/ jccs.200700152

Park et al., 2013 – *Park, J., Kim, D., Lee, K., Kim,Y*. (2013). Reactive cyanine fluo- rescence dyes indicating pH perturbation of biomolecules. *Bull. Kor. Chem. Soc*. 34(1): 1-4. DOI: https://doi .org/10.5012/bkcs.2013.34.1.287

Power et al., 2009 – *Powar, M.J., Burungle, A.B., Karale, B.K*. (2009). Synthesis and antimicrobial activity of spiro [chromeno[3,3-d] [1,2,3] thiadiazole- 4,1' cyclo- hexane , spiro [chromeno] - [4,3-d][1,2,3]selenadiazole - 4,1 '- cyclohexane and spiro [chromon-2,1-cyclohexane]4-one-5-spiro-4-acetyl-2(acetylamino)-Δ2-1,3,4-thiadiazolines compounds. *Arkivoc*. 9: 97-107. DOI: https://doi.org/10.3998/ark.5550190.0010.do8

Rathish et al., 2012 – *Rathish, I., Kalim, J., Shamim, A., Sameena, B., Alam, M., Akhter, M., Pillai, K., Ovais, S. and Samim, M*. (2012). Synthesis and evaluatin of anti-cancer activity of some novel 6-aryl-2(p-sulfamyl phenyl)-pyridazin-3(2H)-ones. *Eur. J. Med. Chem*. 49: 304-309. DOI: 10.1016/J.eJmech.2012-01.026

Sener et al., 2018 – *Sener, N., Mohammed, H.J.A., Yerlikaya, S., Celik Altunoglu, Y., Gur, M., Baloglu, M.C, Sener, I*. (2018). Anticancer, antimicrobial, and DNA protection analysis of novel 2,4-dihydroxyquinoline dyes. *Dyes and Pigments*. 157: 11-19. DOI: https://doi.org/ 10.1016/j.dyepig.2018.04.040

Sha et al., 2018 – *Sha, X.L., Niu, J.Y., Sun, R., Xu, Y.J., Ge, J.F*. (2018). Synthesis and optical properties of cyanine dyes with an aromatic azonia skeleton. *Org. Chem*. 5: 555-560. DOI: https://doi.org/10.1039/C7QO00889A

Shindy et al., 2015 – *Shindy, H.A., Gomaa, M.M., Harb, N.A*. (2015). Synthesis, structure/spectra correlation and chromism studies of some novel monomethine and bis-monomethine cyanine dyes. *Eur.Rev.Chem. Res*. 4(2): 126-140. DOI: 10.13187/ercr. 2015.4.126

Shindy et al., 2016 – *Shindy, H.A., Khalafallah, A.K., Gomaa, M.M.,Eed, A.H*. (2016). Novel hemicyanine and aza-hemicyanine dyes: synthesis, spectral investigation and antimicrobial evaluation. *Eur. J. Mol. Biotechnol*. 13(3): 94-103. DOI: 10.13187 /ejmb.2016.13.94

Shindy et al., 2017 – *Shindy, H.A., Khalafallah, A.K., Gomaa, M.M., Eed, A.H.* (2017). Synthesis, spectral sensitization, solvatochromic and halochromic evaluation of new monomethine and trimethine cyanine dyes. *Eur. J. Mol. Biotechnol.* 5(1): 30-42. DOI:10.13187/ejmb.2017.1.30

Shindy et al., 2018 – *Shindy, H.A., EL-Maghraphy, M.A., Gomaa, M.M., Harb, N.A.* (2018). Synthesis, electronic transitions and antimicrobial activity evaluation of novel monomethine and trimethine cyanine dyes. *Eur. J. Mol. Biotechnol.* 6(2): 83-95. DOI: 10.13187/ejmb.2018.2.83

Shindy et al., 2019 – *Shindy, H.A., EL-Maghraphy, M.A. ,Goma, M.M, Harb, N.A.* (2019). Polynuclear heterocyclic monomethine and trimethine cyanine dyes :synthesis and various absorption spectra studies. *Eur. J. Mol. Biotechnol.* 7(1): 25-39. DOI: 10.131 87/ejmb.2019.1. 25.

Shindy, 2017 – *Shindy, H.A.* (2017). Fundamentals in the chemistry of cyanine dyes. *Dyes and Pigments*. 145: 505-513. DOI: https://doi.org/10.1016/j.dyepig.2017.06.029

Shindy, 2018 – *Shindy, H.A.* (2018). Structure and solvent effects on the electronic transitions of some novel furo/pyrazle cyanine dyes. *Dyes Pigments*. 149: 783-788. DOI: https://doi.org/10.1016/j.dyepig.2017.11.055

Soriano et al., 2015 – *Soriano, E., Holder, C., Levitz, A., Henary, M.* (2015). Benzo [c,d]indolium containing monomethine cyanine dyes: synthesis and photophysical properties. *Molecules*. 21(1): 23-37. DOI: https:/doi.org/10.3390/molecules.21010023

Sun et al., 2013 – *Sun, R., Yan, B., Ge, J., Xu, Q., Li, N., Wu, X., Song, Y., Lu, J.* (2013). Third-order nonlinear optical properties of unsymmetric pentamethine cyanine dyes possessing benzoxazolyl and benzothiazolyl groups. *Dyes and Pigments*. 96: 189-195. DOI: https://doi.org/ 1016/j.dyepig.2012.07.007

Tarek et al., 2015 – *Tarek, Aysha, Mervat, El-Sedik, Hamada, M. Mashaly, Morsy, El-Apasery, Oldřich, Machalickya, Radim, Hrdinaa* (2015). Synthesis, characterization, and applications of isoindigo/pechmann dye heteroanalogue hybrid dyes on polyester fabric. *Coloration Technol.* 131: 1-9. DOI:10.1111/cote.12161

Tarulata et al., 2011 – *Tarulata, B. Shah, Ravindran, S. Shiny, Ritu, B, Dixit, Bharat C. Dixit* (2011). Synthesis and dyeing properties of new disazo disperse dyes for polyester and nylon fabrics. *Journal of Saudi Chemical Society*. 1-9. DOI: 10.1016/j.jscs.2011.11.022

Upadhyayula et al., 2015 – *Upadhyayula, S., Nunez, V., Espinoza, E.M., Larsen, J. M., Bao, D., Shi, D., Mac, J.T., Anvari, B. and Vullev, V.* (2015). Photo induced dyna- mics of a cyanine dye : parallel pathways of nonradiative deactivation involving multiple excited state twisted transients. *Chem. Sci.* 6: 2237-2251.DOI: 10.1039/c5sc90020d

Vicini et al., 2002 – *Vicini, P., Zani, F., Cozzini, P., Doytchinova, I.* (2002). Hydra-zones of 1,2-benzisothiazole hydrazines: synthesis, antimicrobial activity and QSAR investigation. *Eur. J. Med. Chem.*, 37:553. DOI: https://doi.org/10.1016/S0223-5234(02)01378-8

Wada et al., 2015 – *Wada, H., Hyun, H., Vargas, C., Gravier, J., Park, G., Gioux, S., Frangioni, J.V., Henary, M., Choi, H.S.* (2015). Pancreas-Targeted NIR fluorophores for dual channel-guided Abdominal surgery. *Theranostics*. 5: 1-11. DOI:10.7150/THNO.10259

Wang et al., 2017 – *Wang Y., Zhu M., Jiang E., Hua R., Na R., Li Q.X.* (2017). A Simple and rapid turn on ESIPT fluorescent probe for colorimetric and ratiometric detection of biothiols in living cells. *Sci.Rep.* 7: 1-9. DOI: https://doi.org/10.1038/s41598-017-03901-8

Xiang-Han et al., 2008 – *Xiang-Han, Z., Lan-Ying, W., Zhi-Xiang,N., Shi-Huan,T., Zu-Xun, Z.* (2008). Microwave-assisted solvent-free synthesis and spectral properties of some dimethine cyanine dyes as fluorescent dyes for DNA detection. *Dyes and Pigments*. 79: 205-209. DOI: 10.1016/j.dyepig.2008.02.010

Yadav, 2005 – *Yadav, H.O.* (2005). Relation between the thermal activation energy of conduction and the first excited singlet state energy-a case of photo-conducting. *Thin solid film*. 477(S 1-2): 222-226.

Yong et al., 2009 – *Yong, Li, Zheng-Yin, Yang, Ming-Fang, Wang* (2009). Synthesis, characterization, DNA binding properties and antioxidant activity of Ln(III)complex with hesperetin-4-one (benzoyl) hydrazone. *Eur. J. Med. Chem.* 44(11): 4585-95. DOI: https://doi.org/ 10.1016/j.ejmech.2009.06.027

Appendix

(4a-c): A = 1-ethyl pyridinium-4-yl salt (a),
A = 1-ethyl quinolinium-4-yl salt (b),
A = 2-ethyl isoquinolinium-1-yl-salt (c).
(6a-c)& (8a-c): A = 1-ethyl pyridinium-2-yl salt (a),
A = 1-ethyl quinolinium-2-yl salt (b),
A = 1-ethyl pyridinium-4-yl-salt (c).

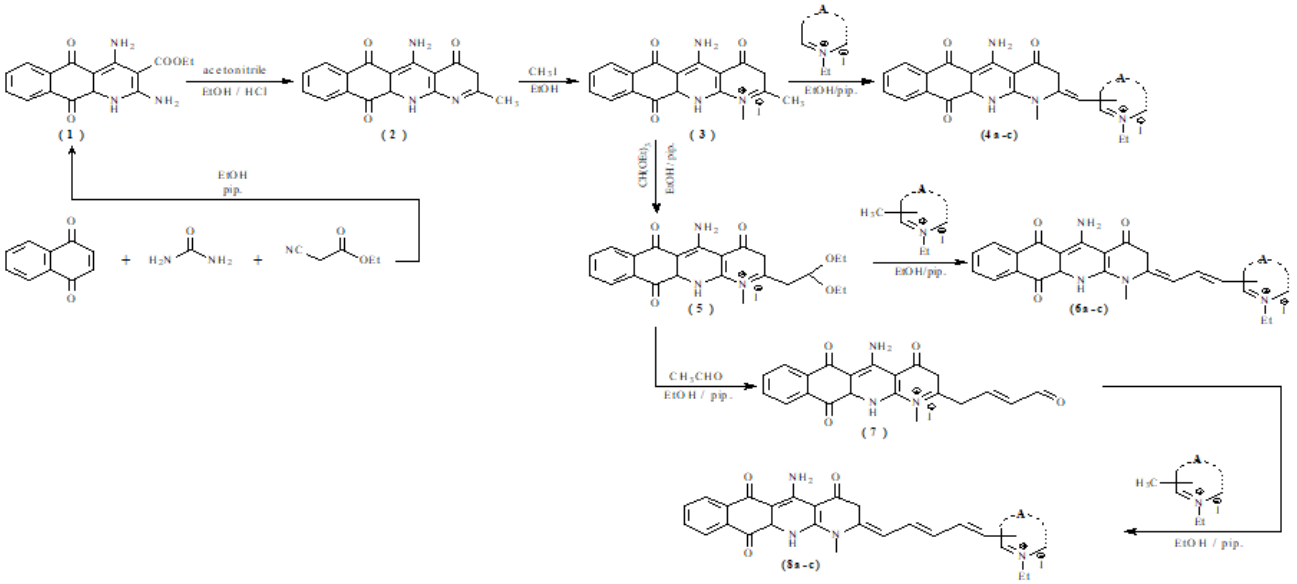

Scheme (1). Synthesis strategy of the prepared compounds (3), (4a-c), (5), (6a-c), (7) and (8a-c)

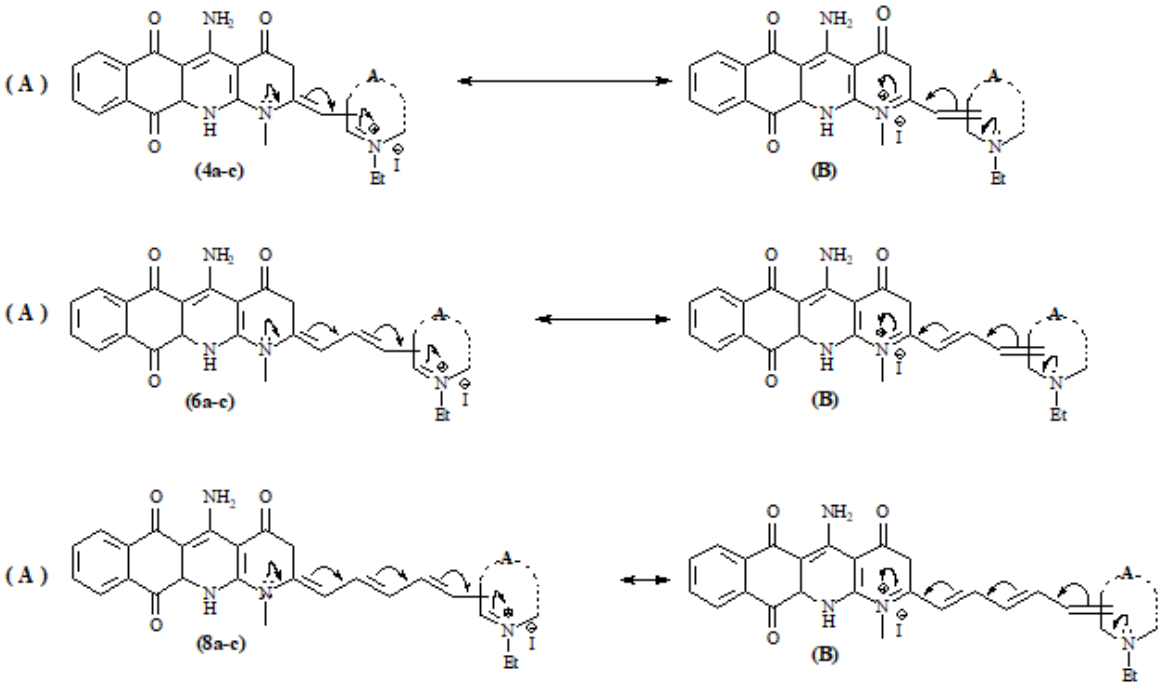

Scheme (2). Colour intensity and the electronic charge transfer pathways illustration of the synthesized monomethine cyanine dyes (4a-c), trimethine cyanine dyes (6a-c) and pentamethine cyanine dyes (8a-c)

Published in the Slovak Republic
European Journal of Molecular Biotechnology
Has been issued since 2013.
E-ISSN: 2409-1332
2019, 7(2): 86-90

DOI: 10.13187/ejmb.2019.2.86
www.ejournal8.com

Spectral Analyses of Water ADVA. Biophysical, Biochemical and Biological Effects

Ignat Ignatov [a, *]

[a] Scientific Research Center of Medical Biophysics (SRCMB), Sofia, Bulgaria

Abstract

Studies were performed with water ADVA. The analyses have been conducted with Nonequilibrium Energy Spectrum (NES) and Differential Nonequilibrium Energy Spectrum (DNES) methods (Antonov, 1995; Ignatov, 1998). Increasing of DNES spectrum of water ADVA according to the control sample was observed. The NES and DNES spectrum were in the range (-0.08 – -0.14 eV) (8.9 –15.5 μm) (645–1129 cm^{-1}).

The parameters of the following local extremums were studied:

E=-0.1112 eV)(λ=11.15 μm)(ṽ=897 cm^{-1}) is the local extremum for stimulating effect on nervous system and improvement of nervous conductivity.

E=-0.1212 eV (λ=10.23 μm)(ṽ=978 cm^{-1}) is the local extremum for anti inflammatory effect.

E= -0.1387 eV)(λ=8.95 μm)(ṽ=1117 cm^{-1}) is the local extremum for inhibition of development of tumor cells of molecular level.

Keywords: Water ADVA, NES, DNES, biophysical, biochemical and biological effects.

1. Introduction

The research is conducted using spectral methods NES and DNES (Antonov, 1995; Ignatov, 1998). The methods NES and DNES show the parameters of electromagnetic hydrogen bonds of O–H…O–H groups of water molecules. For this purpose the model of W. Luck is used, which consider water as an associated liquid, consisted of O–H…O–H groups (Luck et al., 1980). The major part of these groups is designated by the energy of hydrogen bonds (-E), while the others are free (E = 0).

The spectral analyses with methods NES and DNES are conducted with control sample of tap water from Stara Zagora region, Bulgaria and water ADVA. The water ADVA was made with process of electromagnetic activation and cleaning with system of bio security.

2. Materials and Methods

2.1. NES and DNES Spectral Analyses

The device for DNES spectral analysis based on an optical principle was designed by A. Antonov. For this, a hermetic camera for evaporation of water drops under stable temperature (+22–24 °C) conditions was used. The water drops were placed on a water-proof transparent pad, which consisted of thin maylar folio and a glass plate. The light was monochromatic with filter for yellow color with wavelength at λ = 580±7 nm. The device measures the angle of evaporation of water drops from 72.3° to 0°. The DNES-spectrum was measured in the range of -0.08– -0.1387 eV or λ = 8.9–13.8 μm using a specially designed computer program. The main estimation criterion in

* Corresponding author
E-mail addresses: mbioph@dir.bg (I. Ignatov)

these studies was the average energy ($\Delta E_{H...O}$) of hydrogen O...H-bonds among H_2O molecules in water samplles.

2.2. Statistical analyses with methods of Student and Fisher

The studies of tap water from Stara Zagora region, Bulgaria and ADVA water were performed each month,

The results were calculated with statistical methods of Student and Fisher.

3. Results and discussion

3.1. Parameters of NES and DNES spectrums of ADVA water

The spectrum analysis is conducted with tap water from Stara Zagora region, Bulgaria and ADVA water. The energy spectrum of water is characterized by a non-equilibrium process of water droplets evaporation; therefore, the term non-equilibrium spectrum (NES) of water is used.

The difference *Δf(E) = f (samples of water) – f (control sample of water)*– is called the "differential non-equilibrium energy spectrum of water" (DNES). The Figure 1 shows that on the X-axis are depicted three scales. The energies of hydrogen bonds among H_2O molecules are calculated in electronvolts (eV). On the Y-axis is depicted the function of distribution of H_2O molecules according to energies f(E), measured in reciprocal electronvolts unit eV^{-1}. The local extremums of water samples are detected at E = -0.1112 eV, E = -0.1212 eV and E = -0.1387 eV. The value measured at E = -0.1212 eV is characteristic for anti-inflammatory effect (Ignatov et al., 2014). The value measured at E = -0.1112 eV is characteristic for the presence of Ca^{2+} ions in water (Antonov, 1995). The value measured at E = -0.1387 eV is characteristic for inhibiting the growth of tumor cells (Ignatov, Mosin, 2012). Experiments conducted by Antonov with cancer cells of mice in water demonstrated a reduction of this local extremum to a negative value in DNES spectra.

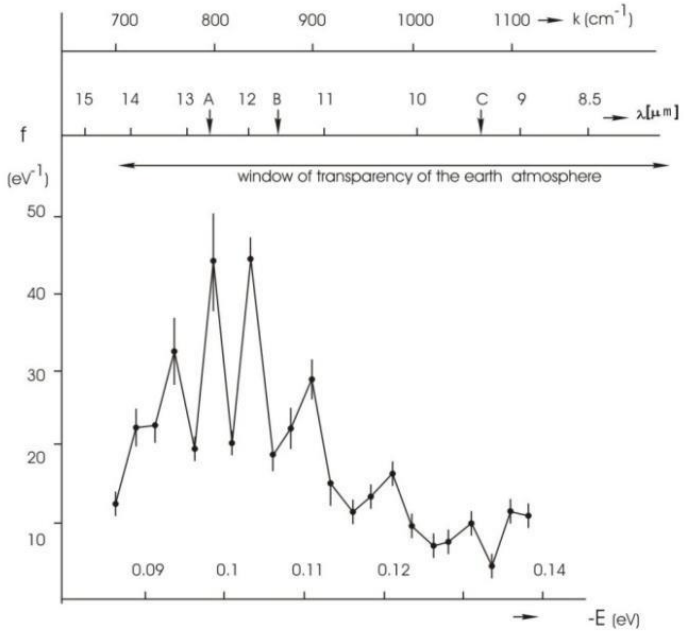

Fig. 1. The NES-spectrum of deionized water (chemical purity – 99.99 %; pH – 6,0–7,5; electric conductivity – 10 μS/cm): the horizontal axis shows the energy of the H...O hydrogen bonds in the associates (– E (eV)); the vertical axis – the energy distribution function – f (eV^{-1}); *k* – the vibration frequency of the H–O–H atoms (cm^{-1}); λ – wavelength (μm)

The following results of the effects of ADVA water with NES and DNES methods are obtained:

The difference of DNES spectra between ADVA water and Control Sample of Tap water is ΔE = (-0.1207 eV)- (-0.1127 eV)= -8.0±1,1 meV.

The difference is essential and shows biophysical and biochemical effects of molecular and cell level.

The result is essential for increasing of average value of hydrogen bonds among water molecules in water ADVA with result ΔE = -8.0±1,1 meV according tap water.

3.2. The mathematical models of ADVA water

The mathematical model of ADVA water gives valuable information for the possible number of hydrogen bonds as percent of H_2O molecules with different values of distribution of energies (Table 1 and Figure 2). These distributions are basically connected with the restructuring of H_2O molecules having the same energies.

The average energy ($E_{H...O}$) of hydrogen H...O- bonds among H_2O molecules of the samples of ADVA water and Tap water (Control Sample):

–The result of NES for ADVA water is E = -0.1207 eV;

–The result of NES for Tap water (Control Sample) is E = -0.1127 eV eV.

The Table 1 and Figure 2 show the mathematical Models of ADVA water and Tap water (Control Sample).

Table 1. Mathematical Models of ADVA water and Tap water (Control Sample)

-E(eV) x-axis	Water ADVA (%((-E_{value}) */ (-$E_{total\ value}$)**	Control Sample Tap water (%((-E_{value}) */ (-$E_{total\ value}$)**	-E(eV) x-axis	Water ADVA (%((-E_{value}) */ (-$E_{total\ value}$)**	Control Sample Tap water (%((-E_{value}) */ (-$E_{total\ value}$)**
0.0937	0	15.3	0.1187	0	0
0.0962	0	5.1	0.1212	**16.8**[2]	**5.1**[2]
0.0987	4.2	5.1	0.1237	0	0
0.1012	0	5.1	0.1262	16.8	5.1
0.1037	0	5.1	0.1287	12.6	5.1
0.1062	4.2	10.2	0.1312	4.2	5.1
0.1087	4.2	0	0.1337	4.2	5.1
0.1112	**16.8**[1]	**5.1**[1]	0.1362	0	0
0.1137	0	5.1	0.1387	**7.6**[3]	**8.2**[3]
0.1162	8.4	10.2	–	–	–

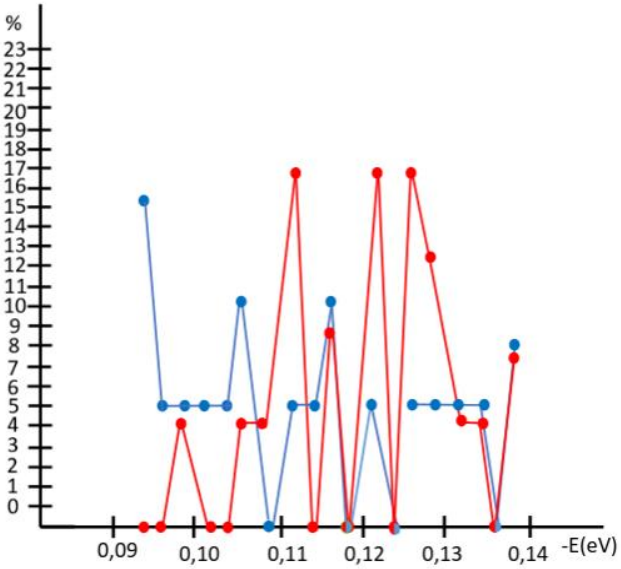

Fig. 2. Mathematical Models of water ADVA (red color) and Tap water (blue color)

Notes:

E=-0.1112 eV is the local extremum for stimulating effect on nervous system and improvement of nervous conductivity.

E=-0.1212 eV is the local extremum for anti inflammatory effect.

E= -0.1387 eV is the local extremum for inhibition of development of tumor cells of molecular level.

* ($-E_{value}$) stands for the value of hydrogen bonds energy for one parameter of (-E).

** ($-E_{total\ value}$) stands for the total value of hydrogen bonds energy.

Table 1 and Figure 2 shows the distribution (%, ($-E_{value}$)/($-E_{total\ value}$) of H_2O molecules of Water ADVA and Tap water (control sample) respectively.

E=-0.1112 eV is the local extremum for stimulating effect on nervous system and improvement of nervous conductivity. The effect of Water ADVA is 16.8 % and for Control sample is 5.1 %

E=-0.1212 eV is the local extremum for anti inflammatory effect. The effect of Water ADVA is 16.8 % and for Control sample is 5.1 %

4. Conclusion

The results are shown restructuring of water molecules in configurations of clusters, which have influence successful on human health of molecular and cell level. The biophysical and biochemical effects are base for biological effects.

Non-equilibrium energy spectrum (NES) and Differential non-equilibrium energy spectrum (DNES) of water ADVA have shown effects on nervous system and conductivity of nervous tissue. There have anti inflammatory effects. These effects together with big alteration of energy of hydrogen bonds have led to detox and anti aging effects.

References

Alberts et al., 1994 – *Alberts, B. et al.* (1994). Molecular Biology of the Cell 3rd ed.

Antonov, 1995 – *Antonov, A.* (1995). Research of the Non-equilibrium Processes in the Area in Allocated Systems. Dissertation thesis for degree "Doctor of Physical Sciences", Blagoevgrad, Sofia.

Antonov, Galabova, 1992 – *Antonov, A., Galabova, T.* (1992). Ext. Abstr. *The 6th National Conference of Biomedical Physics and Engeneering*, 60.

Bachir, Pogorelov, 2018 – *Bachir, V.M., Pogorelov, A.G.* (2018). Universal Electrochemical Technology for Environmental Protection, *International Journal of Pharmaceutical Research & Allied Sciences*, 7(1): 41-57.

Chaplin, 2011 – *Chaplin, M.* (2011). The Water Molecule, Liquid Water, Hydrogen Bonds and Water Networks / in: Water The Forgotten Biological Molecule, D.Le Bihan & H.Fukuyama (eds.), Singapore: Pan Stanford Publishing Pte. Ltd.

Choi, Jordan, 2010 – *Choi T.N., Jordan K.D.* (2010). Application of the SCC-DFTB Method to $H^+(H_2O)_6$, $H^+(H_2O)_{21}$, and $H^+(H_2O)_{22}$. *J. Phys. Chem. B*, 114: 6932-6936.

Gluhchev et al., 2015 – *Gluhchev, G., Ignatov, I., Karadzhov, S., Miloshev, G., Ivanov, N., Mosin, O.V.* (2015). Electrochemically Activited Water. Biophysical and Biological Effects of Anolyte and Catholyte as Types of Water. *Journal of Medicine, Physiology and Biophysics*. 10: 1-17.

Hoeijmakers, 2009 – *Hoeijmakers, J.H.* (2009). DNA Damage, Aging, and Cancer. *The New England Journal of Medicine*. 361(15): 1475-85.

Ignatov et al., 2014 – *Ignatov, I., Mosin, O. V., Velikov, B., Bauer, E. Tyminski, G.* (2014) Longevity Factors and Mountain Water as Factor. Research in Mountain and Fields Areas in Bulgaria. *Civil and Environmental Research*. 30 (4): 51-60.

Ignatov et al., 2019 – *Ignatov, I., Toshkova, R., Gluhchev, G., Drossinakis, Ch.* (2019). Results of Blood Serum from Cancer Treated Hamsters with Infrared Thermal Field and Electromagnetic Fields. *Journal of Health, Medicine and Nursing*. 58: 101-112.

Ignatov, 2011 – *Ignatov, I.* (2011). Entropy and Time in Living Organisms. *Euromedica, Hanover*. 60-62.

Ignatov, Mosin, 2013 – *Ignatov, I., Mosin, O.V.* (2013). Possible Processes for Origin of Life and Living Matter with modeling of Physiological Processes of Bacterium Bacillus Subtilis in Heavy Water as Model System. *Journal of Natural Sciences Research*. 3(9): 65-76.

Ignatov, Mosin, 2013 – *Ignatov, I., Mosin, O.V.* (2013). Modeling of Possible Processes for Origin of Life and Living Matter in Hot Mineral and Seawater with Deuterium. *Journal of Environment and Earth Science*. 3 (14): 103-118.

Ignatov, Mosin, 2013 – *Ignatov, I., Mosin, O.V.* (2013). Structural Mathematical Models Describing Water Clusters. *Journal of Mathematical Theory and Modeling*. 3(11): 72-87.

Ignatov et al., 2013 – *Ignatov, I., Toshkova, R., Gluhchev, G., Zvetkova, E.* (2019). Results with IR Spectroscopy of CortiNon+ on the Development of Experimental Graffi Tumor on Hamsters. *European Reviews of Chemical Research*. 6 (2): 61-67.

Ignatov, 2020 – *Ignatov, I.* (2020). Health Status as Result of Analyses of Parameters of Hydrogen Bonds Among Water Molecules in Human Body. Entropy in Living Organisms. *Journal of Medicine, Physiology and Biophysics*. 64: 14-20.

Kirkpatrick, 2009 – *Kirkpatrick, R.D.* (2009). The Mechanism of Antimicrobial Action of Electro-chemically Activated (ECA) Water and its Healthcare Applications. Doctoral Thesis, University of Pretoria.

Lata et al., 2016 – *Lata, S. et al.* (2016). Anti bacterial Effectiveness of Electro-Chemically Activated (ECA) Water as a Root Canal Irrigant – An In-vitro Comparative Study. *Journal of Clinical and Diagnostic Research*. 10 (10): 138-142.

Liu et al., 1996 – *Liu K., Cruzan J.D., Saykally R.J.* (1996). Water Clasters. *Science Magazine*. 271 (5251): 929-933.

Luck et al., 1980 – *Luck, W., Schiöberg, D., Ulrich, S.* (1980). Infared Iinvestigation of Water Structure in Desalination Membranes. *J. Chem. Soc. Faraday Trans.*, 2(76), 136-147.

Petrushanko, Lobyshev, 2001 – *Petrushanko, I. Ju., Lobyshev, V.I.* (2001). Non-equlibrium State of Electrochemically Activated Water and its Biological Activity. *Biofizika,* 46(3): 389-401.

Shu et al., 2020 – *Shu, Li., Jegatheesan, L., Jegatheesan, V., Chun, Q.L.* (2020). The Structure of Water. *Fluid Phase Equilibria*, 511.

Stoner et al., 1982 – *Stoner, G.E., Cahen, G.L.Jr., Sachyani, M., Gileadi, E.* (1982). The Mechanism of Low Frequency a.c. Electrochemical Disinfection, *Bioelectrochemistry and Bioenergetics*, 9 (3): 229–24.

Sykes, 2007 – *Sykes, M.* (2007). Simulations of RNA Base Pairs in a Nanodroplet Reveal Solvation-Dependent Stability. *PNAS*. 104 (30): 12336-12340.

Toshkova et al., 2019 – *Toshkova, R., Ignatov, I., Zvetkova, E., Gluhchev, G.* (2019). Effects of Catholyte Water on the Development of Experimental Graffi Tumor on Hamsters. *European Journal of Medicine*. 7(1): 45-56.

Toshkova et al., 2019 – *Toshkova, R., Ignatov, I., Zvetkova, E., Gluhchev, G.* (2019). Effects of Catholyte Water on the Development of Experimental Graffi Tumor on Hamsters. *Cells & Cellular Life Sciences Journal*. 4(1): 000140.

Toshkova et al., 2019 – *Toshkova, R., Ignatov, I., Zvetkova, E., Gluhchev, G.* (2019). Bioinfluence with Infrared Thermal and Electromagnetic Fields as a Therapeutic Approach of Hamsters with Experimental *Graffi* Myeloid Tumor. *Journal of Natural Sciences Research*. 9(4): 1-11.

Published in the Slovak Republic
European Journal of Molecular Biotechnology
Has been issued since 2013.
E-ISSN: 2409-1332
2019, 7(2): 91-99

DOI: 10.13187/ejmb.2019.2.91
www.ejournal8.com

The Use of the Parr Function Would Include the Reactivity of the Carbenes with β-himachalene

Z. Jalil [a], M. El idrissi [b, *], A. Barhoumi [b], A. Zeroual [b], M. Mbarki [a], A. Tounsi [c]

[a] Sultan Moulay Slimane University, Béni-Mellal-23000, Morocco
[b] Chouaïb Doukkali University, El Jadida, Morocco
[c] Moulay Slimane University, Mghila, Béni Mellal, Morocco

Abstract

Cyclopropanes are molecules of great importance since they are present in several biologically active molecules in addition to being powerful intermediates in the synthesis of complex molecules. During this work, we have étudiéla régio-selectivity of the reactions of cycloaddition [1+2] of the carbènes and ß-himachalènepar the method D.F.T at the level of the base(basis) 6-31 (d), one using a new descriptor of the régio-selectivity it is the function(office) of Parr, we notice according to this study that the attack of a mole of carbènes is preferentially made at the level of the connection C6=C7 of ß-himachalène of in both possibilities of carbènes (nucléophile or électrophile). We also notice that the interaction enters orbital borders of reactives (ß-himachalène-carbènes) is made in a facial way, we also notice that the differences of électrophile Δω (Between carbènes: { CH(CH3), :CCl(Ph), :CH(Ph), :CCl(CH3), :CHF, :CF(Ph), :CF(Cl), :CF2, :C(Ph)2, :CH2, :CHCl, :CCl2, et :C(Br)2} and β-himachalene)varies from 0.162 eV to 3.408 eV; This shows that all reactions studied have a polar character, unlike reactions using alkoxycarbenes and silane-carbene {:ccl(OCH3), CF(OCH3), :C(OCH3)2, :C(OH)2 and:CH(SiH3). } have a non-polar character because Δω is less than 1 (Δω<1).

Keywords: cycloaddition [1+2], D.F.T, carbenes, nucleophilic power, electrophilic power, polar character, regioselectivity.

1. Introduction

Carbenes are defined as neutral species with divalent carbon with only six electrons of valence. They have long been considered to be very reactive and difficult to isolate transient species (Figure 1). These compounds are highly reactive, usually known to be unstable and have a very limited lifespan. (Cheng et al., 2004; de Frémont et al., 2009, Vignolle et al., 2006). For example, dimethyl carbene (Pezacki et al., 1999; Ford, et al., 1998) and dichlorocarbene (Chateauneuf et al., 1990) have, respectively, a half-life of the order of nanosecond and microsecond while dimethoxycarbene has a half-life of 2 milliseconds (Moss et al., 1988). This difference in the reactivity of dialkoxycarbenes is largely due to the interaction between n-oxygen electrons and the carbon orbital of carbene, increasing the energy of the pπ' carbene molecular orbital and ΔE value(pπ'-σ'). (Figure 1). These interactions thus give dialkoxycarbenes a nucleophilic character (Rondan et al., 1980).

* Corresponding author
E-mail addresses: idrissi_82@hotmail.fr (M. El idrissi)

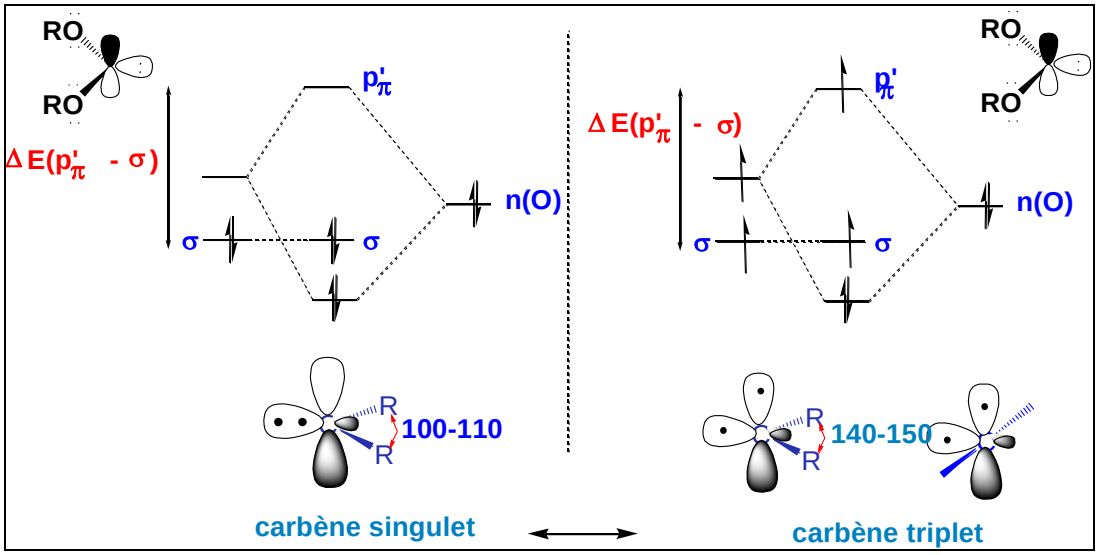

Fig. 1. Molecular orbital borders of a singlet and triplet dialkoxycarbenes

Computational methods

The equilibrium geometries were optimized at the calculation level B3LYP/6-31G(d) (Lee et al., 1988; Becke et al., 1993; Rassolov et al., 2001) using the Gaussian 09 (Schlegel et al., 1994), program using the Berny algorithm (Frisch et al., 2009). The transition states, corresponding to the two modes of alpha and bita epoxidation, were located at B3LYP/6-31G(d). Their existence has been confirmed by the presence of one and only imaginary frequency in the Hessian matrix. The maximum transfer of charges ΔNmax that will allow us to define the electrophilic power of a system defined by: $\Delta N_{max} = -\frac{\mu}{\eta}$. The global nucleophilia index ω is defined by the expression (Parr et al., 1999) $\omega = \frac{\mu^2}{2\eta}$ with μ the electronic chemical potential $\mu = \left(\frac{\varepsilon_{HOMO}+\varepsilon_{LUMO}}{2}\right)$ and electronic hardness $\eta = (\varepsilon_{LUMO} - \varepsilon_{HOMO})$ (Parr, Yang, 1989).

Domingo et al (Domingo et al., 2002) proposed that if a molecule is weakly electrophilic, then it is systematically strongly nucleophilic only true for simple molecules. For high nucleophilia values low values of ionization potentials and vice versa. Used the energies (HOMO) obtained by the Kohn-Sham method (Kohn et al., 1965). The empirical (relative) nucleophilia (N) index is defined as follows (L. R. Domingo et al., 2002): $N = \left(E_{HOMO(Nu)} - E_{HOMO(TCE)}\right)$.

Nucleophilic is traced to tetra cyano ethylene (TCE) because TCE has the lowest HOMO energy value in the organic molecules series. The local electrophilic index and the local nucleophilic index were evaluated using the following expressions (Domingo et al., 2013; Gleiter et al., 1968): $\omega_k = \omega.P^+$ and $N_k = N.P^-$ such as P^+ and P- are the functions of electrophilic and nucleophilic Parr respectively (Hoffmann et al, 1968; Mendez et al., 2011), are obtained from the Mulliken atomic density analysis of the anion and the neutral molecule cation.

2. Results and discussion

Simplistically, the fundamental state of a carbene can be determined by comparing the values of ΔE(pπ'-σ') to electronic and steric repulsion energies. In the event that the value of ΔE(pπ'-σ') to the orbital pπ' to obtain the triplet state becomes more important than the electronic and steric repulsion energies related to the singulet state. A singular fundamental state is then observed. It has been suggested in the past that an existing carbene in the fundamental state singulet had a value of ΔE(pπ'-σ') greater than 2 eV (46 kcal/mol) while a triplet carbene had a value of ΔE(pp-σ') less than 1.5 ev (35 kcal/mol) (Kassaee et al., 2011; Hirai et al., 2009). These trends were confirmed by Mendez in a theoretical study of the electronic structure of a variety of carbenes. (Geise, Hadad, 2000) the latter has established that the value of ΔE_{ST} (by convention, a negative value of ΔE_{ST} implies a singulet state lower in energy than the triplet state). In the case of dimethoxycarbene, an ΔE_{ST} of -53.0 kcal/mol was calculated (Table 1). In 2011 Kassaee reported similar TSE values of -57 and -55 kcal/mol (Domingo et al., 2008; Domingo et al., 2002).

Table 1. ΔEST values calculated for the different carbenes

	Carbene	ΔEST(Kcal/mol)
1	CH(SiH3)	23,3
2	CH2	13,7
3	CH(CH3)	7,9
4	CCl(Ph)	-4,6
5	CHCl	-2,2
6	CH(Ph)	7,1
7	CCl(CH3)	-4,9
8	CHF	-12,1
9	CF(Ph)	-13,3
10	CCl2	-16,6
11	CF(Cl)	-33,4
12	CCl(OCH3)	-36,0
13	CF(OCH3)	-51,8
14	CF2	-52,1
15	C(OCH3)2	-53,0
16	C(OH)2	-54,5

Prediction of relative reactivity of reagents and polarity of cycloaddition reactions

The polar character of AD reactions can be obtained from the difference in the overall electrophiles of the reagents. This difference was used to determine the polar character of this type of reaction. Indeed, recent studies of AD reactions have shown that DFT-derived reactivity indices are an effective tool for establishing the polar/non-polar character of cycloaddition reactions (El Idrissi et al., 2014). The calculated values of the overall reactivity indices, namely the electronic chemical potential μ, global hardness η, global electrophilic ω, global nucleophilia N and the overall maximum load transfer ΔNmax for reagents are given in Table 2.

Table 2. HOMO/LUMO energies, electronic chemical potential μ, global hardness η, global electrophilia ω, global nucleophilia N and maximum overall load transfer/Nmax of carbenes 1-18 and β-himachalene

Reactifs	carbene	HOMO	LUMO	μ	η	ω	N	ΔNmax
1	CH(SiH3)	-6,179	-1,006	-3,592	5,173	1,247	3,353	0,694
2		-6,625	-3,303	-4,964	3,322	3,708	2,907	1,494
3	CH2	-5,695	-2,076	-3,885	3,619	2,085	3,837	1,073
4		-5,747	-2,925	-4,336	2,822	3,331	3,785	1,536
5	CH(CH3)	-6,708	-3,292	-5	3,416	3,659	2,824	1,463
6	CCl(Ph)	-5,181	-2,666	-3,923	2,515	3,060	4,351	1,559
7	CHCl	-6,206	-2,557	-4,381	3,649	2,630	3,326	1,200
8		-6,623	-2,557	-4,59	4,066	2,590	2,909	1,128
9	CH(Ph)	-5,774	-2,457	-4,115	3,317	2,553	3,758	1,240
10	CCl(CH3)	-7,357	-3,551	-5,454	3,806	3,907	2,175	1,433
11	CHF	-7,771	-2,998	-5,384	4,773	3,037	1,761	1,128
12	CF(Ph)	-6,669	-1,496	-4,082	5,173	1,610	2,863	0,789
13		-6,775	-0,767	-3,771	6,008	1,183	2,757	0,627
14	CCl2	-8,088	-2,111	-5,099	5,977	2,175	1,444	0,853
15	CF(Cl)	-5,806	-0,008	-2,907	5,798	0,728	3,726	0,501
16		-6,443	-0,137	-3,29	6,306	0,858	3,089	0,521
17	CCl(OCH)	-7,061	-3,600	-5,330	3,461	4,104	2,471	1,540
18	CF(OCH3)	-5,533	-3,045	-4,289	2,488	3,696	3,999	1,723
	CF2							

	C(OCH3)2 C(OH)2 C(Br)2 C(Ph)2							
19	β-himacha-ène	-5,692	0,693	-2,499	6,488	0,696	3,999	0,385

In the case of the reaction (1) between β-himachalene and CH(SiH3) carbenes, the electronic chemical potential of β-himachalene (μ = -2.499 u.a) is higher than that of CH(SiH3) carbenes (μ = -3.592 u.a); this indicates that the transfer of electrons will take place from β-himachalene to the CH(SiH3) carbenes. On the other hand, the overall electrophilic index of β-himachalene (ω = 0.696 ev) is lower than that of carbene C(Ph)2(ω = 1,247 eV) and therefore CH(SiH3) carbenes behave like an electrophilic, while β-himachalenese behaves like a nucleophile. It is noted that the overall nucleophilia indices also show that carbene CH(SiH3)(N = 3.353eV) is less nucleophilic than β-himachalene (N = 3.427eV). In addition, ΔNmax, which represents the maximum load ratio that can be acquired by a system of its environment, is maximum for CH(SiH3)(0,694) and minimum for β-himachalene (0,385).

For the reaction (2) between β-himachalene and CH2 carbenes, the electronic chemical potential of β-himachalene (μ = -2.499 u.a) is higher than that of CH2 carbenes (μ = -4.964 u.a); this indicates that the transfer of electrons will take place from β-himachalene to CH2 carbens. On the other hand, the overall electrophilic index of β-himachalene (ω = 0.696 eV) is lower than that of carbene CH2(ω= 3.708 eV) and therefore carbene CH2 behaves like an electrophilic, while β-himachalene behaves like a nucleophile. It is noted that the overall nucleophilia indices also show that CH2 (N = 2.907 eV) is less nucleophilic than β-himachalene (N = 3.427 eV). In addition, ΔNmax, which represents the maximum load ratio that can be acquired by a system of its environment, is maximum for CH(SiH3)(0,694) and minimum for β-himachalene (0,385).

For the reaction (2) between β-himachalene and CH2 carbenes, the electronic chemical potential of β-himachalene (μ = -2.499 u.a) is higher than that of CH2 carbenes (μ = -4.964 u.a); this indicates that the transfer of electrons will take place from β-himachalene to CH2 carbens. On the other hand, the overall electrophilic index of β-himachalene (ω = 0.696 ev) is lower than that of carbene CH2(ω = 3.708 eV) and therefore carbene CH2 behaves like an electrophilic, while β-himachalene behaves like a nucleophile. It is noted that the overall nucleophilia indices also show that CH2 (N = 2.907 eV) is less nucleophilic than β-himachalene (N = 3.427 eV). In addition, ΔNmax, which represents the maximum load ratio that a system of its environment can acquire, is maximum for CH2(1,494) and minimum for β-himachalene (0,385). It is noted that the same remarks are observed during the reaction of β-himachalene with other carbenes {CH(CH3), CCl(Ph), CHCl, CH(Ph), CCl(CH3), CHF, CF(Ph), CCl2, CF(Cl), CCl(OCH3), CF(OCH3), CF2, C(OCH3)2, C(OH)2, C(Br)2 and C(Ph)2}.

In order to show the donor (nucleophilic) or acceptor (electrophilic) character of the two reagents and the polar character of the reactions, we calculated the HOMO/LUMO energy gaps of the reagents and the differences in electrophilia (Table 3).

Table 2 also shows that the $|E_{HOMO}^{\beta-himachalene} - E_{Lumo}^{carbene}|$ are lower than écarts $|E_{HOMO}^{Carbene} - E_{Lumo}^{\beta-Himachalene}|$ for 18 reactions.

In conclusion, for the 18 reactions studied, carbenes behave like electrophiles (electron acceptors) and β-himachalene behaves like nucleophiles (electron donors).

Table 2 also shows that electrophilic differences, varies from 0.162 eV to 3.408 eV; showing that all reactions studied have a polar character except reactions where alkoxycarbenes and silane-carbene are used {:CCl(OCH3), :CF(OCH3), :C(OCH3)2, :C(OH)2 and :CH(SiH3)} have a non-polar character because . is less than 1 (Δω < 1) (El Idrissi et al., 2014).

Table 3. Difference between the two possible combinations HOMO/LUMO and Δω (eV)

Reactions	Carbenes	$\lvert E_{HOMO}^{Carbene} - E_{Lumo}^{\beta-Himachalène} \rvert$	$\lvert E_{HOMO}^{\beta-himachalène} - E_{Lumo}^{carbene} \rvert$	Δω(eV)
1	:CH(SiH3)	6,872	4,6859	0,551
2	:CH2	7,318	2,388	3,012
3	:CH(CH3)	6,388	3,615	1,389
4	:CCl(Ph)	6,440	2,766	2,635
5	:CHCl	7,401	2,399	2,963
6	:CH(Ph)	5,874	3,025	2,364
7	:CCl(CH3)	6,899	3,134	1,934
8	:CHF	7,316	3,134	1,894
9	:CF(Ph)	6,467	3,234	1,857
10	:CCl2	8,050	2,140	3,211
11	:CF(Cl)	8,464	2,693	2,341
12	:CCl(OCH3)	7,362	4,195	0,914
13	:CF(OCH3)	7,468	4,924	0,487
14	:CF2	8,781	3,580	1,479
15	:C(OCH3)2	6,499	5,683	0,032
16	:C(OH)2	7,136	5,554	0,162
17	:C(Br)2	7,754	2,091	3,408
18	:C(Ph)2	6,226	2,646	3,000

According to écarts $\lvert E_{HOMO}^{\beta-himachalene} - E_{Lumo}^{carbene} \rvert$ and $\lvert E_{HOMO}^{Carbene} - E_{Lumo}^{\beta-Himachalene} \rvert$ and Δω mentions in Table 2 it can be concluded that:

- The values of Δω for reactions 13-15 (experimental data not available) are lower than those of previous reactions 1-12 (experimental data available). Therefore, reactions 13-15 predicted to be more scinetically disadvantaged compared to reactions 1-12;

- The gaps (HOMO/LUMO) for β-himachalene reactions with the following carbenes: :CH(SiH3), :CCl(OCH3), :CF(OCH3),:C(OCH3)2, and :C(OH)2. are greater than those of the β-himachalene reactions with the following carbenes: :CH(CH3), :CCl(Ph), :CH(Ph), :CCl(CH3), :CHF, :CF(Ph), :CF(Cl),:CF2, :C(Ph)2, :CH2, :CHCl, :CCl2, et :C(Br)2. which shows that the reactions of β-himachalene with the following carbenes: CH(SiH3), :CCl(OCH3), :CF(OCH3),:C(OCH3)2, et :C(OH)2. are more kinetically difficult compared to the reactions of β-himachalene with the following carbenes: CH(CH3), :CCl(Ph), :CH(Ph), :CCl(CH3), :CHF, :CF(Ph), :CF(Cl),:CF2, :C(Ph)2, :CH2, :CHCl, :CCl2, and :C(Br)2 as already predicted with the values of Δω.

Prediction of the region-chemoselectivity of the cycloaddition reactions studied

The best descriptors for studying local reactivity and regioselectivity of a cycloaddition reaction are local electrophilia and local nucleophilia. In a polar cycloaddition reaction between two replacement reagents. The interaction at two most favourable centres will take place between the most electrophilic centre characterized by the highest value of the local electrophilia index ω_k in the electrophilia, and the most nucleophilic center characterized by the highest value of the N_k local nucleophilia index in the nucleophilia. The local electrophilic powers and local nucleophilic power for 18 carbenes and atoms C2, C3, C6 and C7 of β-himachalene calculated with the function of Parr (Spin Atomic Density) are given in Table 4.

Table 4. Local electrophilic and nucleophilic power for the 18 carbenes and β-himachalene obtained by a Parr function calculus (atoms C2, C3, C6 and C7 of β-himachalene)

Carbenes	Reactifs	P^+	P^-	ω_k	N_k
1	CH(SiH3)	0,953	0,95	1,188	3,185
2	CH2	1,092	0,989	4,049	2,875
3	CH(CH3)	1,044	0,925	2,176	3,549
4	CCl(Ph)	1,01	0,535	3,364	2,024
5	CHCl	1,014	0,84	3,710	2,372
6	CH(Ph)	1,135	0,545	3,473	2,371
7	CCl(CH3)	0,963	0,783	2,532	2,604
8	CHF	0,983	0,84	2,545	2,443
9	CF(Ph)	0,98	0,533	2,501	2,003
10	CCl2	0,974	0,674	3,805	1,465
11	CF(Cl)	0,914	0,691	2,775	1,216
12	CCl(OCH3)	0,894	0,703	1,439	2,012
13	CF(OCH3)	0,873	0,737	1,032	2,031
14	CF2	0,899	0,769	1,955	1,110
15	C(OCH3)2	0,85	0,723	0,618	2,693
16	C(OH)2	0,916	0,932	0,785	2,878
17	C(Br)2	0,66	0,638	2,708	1,576
18	C(Ph)2	1,087	0,606	4,017	2,423
β-himacha-ène	C2	0,08	0,14	0,05	0,47
	C3	0,13	0,09	0,09	0,30
	C6	0,27	0,25	0,18	0,85
	C7	0,28	0,27	0,19	0,92

Static evidence of local electrophilia ωk and Nk local nucleophilia are reliable descriptors for the prediction of the interaction electrophilia-nucleophilia most favoured for the formation of a chemical bond between two atoms. The values of local electrophilia ωk for carbenes and Nk local nucleophilia for atoms C2, C3, C6 and C7 of β-himachalene, calculated with the function Parr (Spin Atomic Density) are reported in Table 4. The results show that the most favoured interaction will take place between the carbon atom of the carbene (having the highest value of ωk) and the atoms C6 and C7 of the β-himachalene (having the highest value of Nk). Therefore, the experimentally observed regioselectivity is correctly predicted by the Parr functions.

For carbenics 15 and 16 the electrophilic power decreases, which indicates that carbenic C(OCH3)2(ω = 0.728 eV) is the least electrophilic system of this series. Therefore, Carbenes 15 and 16 can play the role of a nucleophile, so two approaches can be classified:

Interactions between β-himachalene HOMO and carbenes LUMO Figure 2.

The electrophilic attack of carbenes on β-himachalene takes place on the C6=C7 bond and allows to form cyclopropane, a study shows that the reaction of an equivalent of dichlorocarbene with an equivalent of β-himachalene is highly regio-selective, the interaction is between β-himachalene HOMO and carbene LUMO in a facial way (Figure 2).

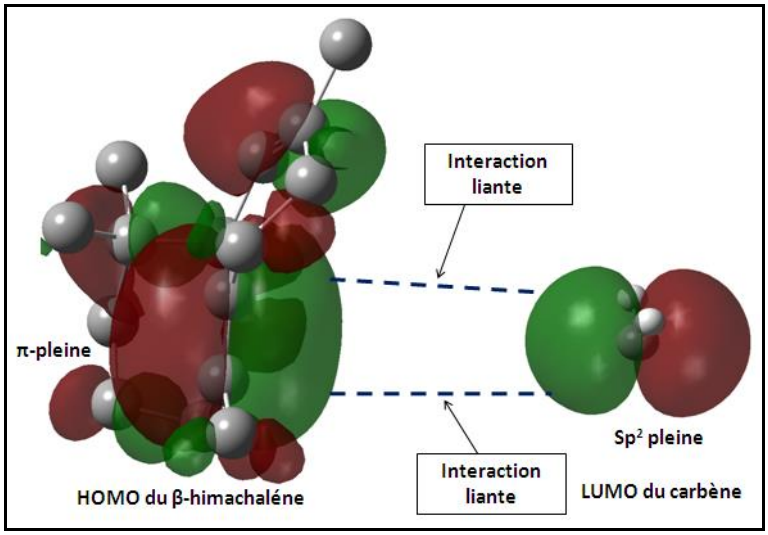

Fig. 2. Optimized structures and HOMO densities of β-himachalene and LUMO carbene density calculated by the B3 lyp/6-31 G(d) method

Interactions between β-himachalene LUMO and carbene HOMO Figure 3.

The nucleophilic attack of the carbene (nucleophilic power of the carbenes is greater than the nucleophilic power of the β-himachalene) takes place at the level of the C6=C7 link because the local electrophilic power of the sites C6 and C7 is at the site of the sites C2 and C3, and the interaction between the Homo orbital of the carbene and Lumo of the β-himachalene and we find that the attack is facial (Figure 3).

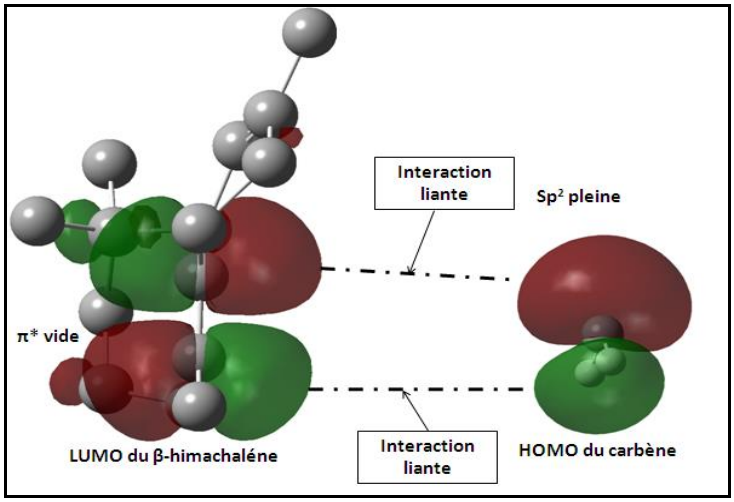

Fig. 3. Optimized structures and densities of β-himachalene and HOMO carbene density calculated by the B3 lyp/6-31 G(d) method

As mentioned above, the interaction between the orbital boundaries of the reagents is done in a facial way, one reagents approach each other the groupings substituted to the carbenes rotates out of the formed cyclopropanation to minimize steric congestion.

5. Conclusion

The regioselectivities of β-himachalenein cycloaddition reactions [1+2] have been studied using the index of local nucleophilia recently proposed by Domingo, P. Pérez and J. A. Sáez (Parr functions). Our results show that the experimental regioselectivities are correctly reproduced with this empirical index which proves to be more reliable than the net loads. Indeed, the index of local

nucleophilia predicts that the double link C6=C7 is more reactive than the link C2=C3 in both cases where β-himachalene plays the role of an electrophile or a nucleophile.

The difference in electrophilia between β-himachaleneand carbenes makes it possible to classify these cycloaddition reactions into two categories: non-polar reactions where the following carbenes are used: (:CH(SiH3), CCl(OCH3), :CF(OCH3), C(OCH3)2, :C(OH)2).

Polar reactions if the following carbenes are used: (:CH2, :CH(CH3), :CCl(Ph),:CHCl, :CH(Ph), :CCl(CH3),:CHF, :CF(Ph), , CCl2, :CF(Cl),:CF2,:C(Ph)2).

References

Becke et al., 1993 – *Becke, Axel D.* (1993). A new mixing of Hartree-Fock and local density-functional theories. *J. Chem. Phys.* Vol. 98, pp. 1372-1377.

Chateauneuf et al., 1990 – *Chateauneuf J.E., Johnson, R.P., Kirchnoff, M.M.* (1990). *J. Am. Chem. Soc.* 112: 3217-3218.

Cheng et al., 2004 – *Cheng, Y. Meth-Cohn, O.* (2004). Heterocycles Derived from Heteroatom-Substituted Carbenes. *Chem. Rev.* 104: 2507-2530.

de Frémont et al., 2009 – *de Frémont, P., Marion, N., Nolan, S.P.* (2009). Carbenes: Synthesis, properties, and organometallic chemistry. *Coord. Chem. Rev.* 253: 862-892.

Domingo et al., 2002 – *Aurell, M.J., Perez, P., Contreras, R.* (2002). Quantitative Characterization of the Global Electrophilicity Power of Common Diene/Dienophile Pairs in Diels-Alder Reactions. *Tetrahedron.* Vol. 58, pp. 4417-4423.

Domingo et al., 2002 – *Aurell, M.J., Pérez, P., Contreras, R.* (2002). Quantitative characterization of the local electrophilicity of organic molecules. Understanding the regioselectivity on Diels–Alder reactions. *A.J. Phys. Chem.* Vol. 106, pp. 6871-6875.

Domingo et al., 2008 – *Chamorro, E., Perez, P.* (2008). Understanding the reactivity of captodative ethylenes in polar cycloaddition reactions. A theoretical study. *J. Org. Chem.* 73 : 4615.

Domingo et al., 2013 – *Domingo, L.R., Pérez, P., Sáez, J.A.* (2013). Understanding the local reactivity in polar organic reactions through electrophilic and nucleophilic Parr functions. *RSC Adv.* 3: 1486.

El Idrissi et al., 2014 – *Zeroual, A., Benharref, A. El Hajbi, A. (*2014). Theoretical study of regioselectivity and stereoselectivity of condensation of β-himachalene with dichlorocarbene using density functional theory (DFT). *International Journal of Innovation and Applied Studies*. Vol. 5, pp. 120-130.

Ford et al., 1998 – *Ford, F., Yuzama, T., Platz, M.S., Matzinger, S., Fülscher, M.* (1998). *J. Am. Chem. Soc.* 120: 4430-4438.

Frisch et al., 2009 – *Frisch, M.J.* (2009). Gaussian, Inc., Wallingford CT.

Geise, Hadad, 2000 – *Geise M., Hadad, C.M.* (2000). Computational Study of the Electronic Structure of Substituted Phenylcarbene in the Gas Phas. *J. Org. Chem.* 65: 8348-8356.

Gleiter et al., 1968 – *Gleiter R., Hoffmann, R.* (1968). *J. Am. Chem. Soc.* 90: 5457-5460.

Hirai et al., 2009 – *Itoh, T. Tomioka, H.* (2009). *Chem. Rev.* 109: 3275-3332.

Hoffmann et al., 1968 – *Hoffmann, R.* (1968). Triethylene and addition of methylene to ethylene. *J. Am. Chem. Soc.* 90: 1475-1485.

Kassaee et al., 2011 – *Kassaee, M.Z., Ghambarian, M., Shakib, F.A., Momeni, M.R.* (2011). Carbenes with reduced heteroatom stabilization: a computational approach. *J. Phys. Org. Chem.* 24: 351-359.

Kohn et al., 1965 – *Kohn, W., Sham, L.* (1965). Self-Consistent Equations Including Exchange and Correlation Effects. *J. Phys. Rev.* 140: 1133-1338.

Lee et al., 1988 – *Lee, C.T., Yang, W.T., Parr, R.G.* (1988). Density-Functional Exchange-Energy Approximation with Correct Asymptotic Behavior. *Phys. Rev. B.* Vol. 37, pp. 785-789.

Mendez et al., 2011 – *Mendez F., Garcia-Garibay, M.A.* (2011). A hard–soft acid–base and DFT analysis of singlet–triplet gaps and the addition of singlet carbenes to alkenes. *J. Org. Chem.*, 64: 7061-7066.

Moss et al., 1988 – *Moss, R.A, Wlostowski, M., Shen, S., Krogh-Jespersen, K., Matro, A.* (1988). Dimethoxycarbene: direct observation of an archetypal nucleophilic carbine. *Journal of the American Chemical Society*. 110 (13): 4443-4444.

Parr et al., 1999 – *Parr, R.G., von Szentpaly, L., Liu, S.* (1999). Electrophilicity index. *J. Am. Chem. Soc.* 121, 1922-1924.

Parr, Yang, 1989 – *Parr, R., Yang, W.* (1989). Density Functional Theory of Atoms and Molecules; Oxford University Press: New York.

Pezacki et al., 1999 – *Pezacki, J., Couture, P., Dunn, J.A., Warkentin, J., Wood, P.D., Lusztyk, J., Ford, F., Platz, M.S.* (1999). *J. Org. Chem.* 64: 4456-4464.

Rassolov et al., 2001 – *Rassolov, V.A., Ratner, M.A., Pople, J.A., Redfern, P.C., Curtiss, L.A.* (2001).“6-31G* Basis Set for Third-Row Atoms. *J. Comp. Chem.* Vol. 22, pp. 976-984.

Rondan et al., 1980 – *Rondan, N.G., Houk, K.N., Moss, R.A.* (1980). *J. Am. Chem. Soc.* 102: 1770-1776.

Schlegel et al., 1994 – *Schlegel, H.B. et al.* (1994). Geometry Optimization on Potential Energy Surface. In: D.R. Yarkony (Ed.), Modern Electronic Structure Theory, World Scientific, Singapore.

Vignolle et al., 2006 – *Cattoën, X., Bourissou, D.* (2006). Stable Noncyclic Singlet Carbenes. *Chem. Rev.* 109: 3333-3384.

Published in the Slovak Republic
European Journal of Molecular Biotechnology
Has been issued since 2013.
E-ISSN: 2409-1332
2019, 7(2): 100-108

DOI: 10.13187/ejmb.2019.2.100
www.ejournal8.com

Composition for Targeted Plant Root Treatment in Drylands: Justification of Components and Concentrations for Field Tests

Valery V. Novochadov [a, *], Elena A. Ivantsova [a], Nikolay V. Onistratenko [a], Pavel A. Krylov [a]

[a] Volgograd State University, Russian Federation

Abstract

The study deals with the problem of combating the growth of undesirable vegetation on the borders of agroecosystems and in unrecoverable areas (intrusions) within these systems. The immediate objective of the study was to reduce the growth of dominant and subdominant species in arid plant communities on the example of *Artemisia lerchiana*.

To solve this problem, we used an approach based on the impact on the irremediable or difficultly eliminated herbaceous areas using plant root treatment in the early vegetative phase. To do this, we developed an aqueous suspension of the original variable composition, which provided delivery to the plant roots, based on 1 kg of surface soil layer: 20-40 mg of copper ions and/or 1-2 mg of zinc ions (1); 8-20 mg of citric and/or succinic acid, permissible in the form of sodium or potassium salts (2); and 10-20 mg of chitosan (3).

As a result, a complex biogenic effect of the received suspension on the soil microbiota and plants was achieved. The improved inhibiting the plant growth and reducing the projective coverage (only for zinc ions or combination copper with chitosan in high concentrations), are the experimental basis for subsequent field tests. For this study we developed a working algorithm for the selection of components and its concentration, based on mathematical modeling of different responses of plant communities to variations in the composition of the suspension for plant root treatment.

Keywords: arid plant communities, undesirable vegetation, plant traits, copper, zinc, chitosan, plant biotechnology, plant root treatment, *Artemisia lerchiana*.

1. Introduction

The approaches to observation and control of ruderal vegetation using mechanical methods, if necessary, in combination with various herbicides and their compositions are well-known from the literature (Monaco et al., 2008; Kraehmer et al. 2014). These works present in detail some technical devices for mechanical soil treatment (Tu et al., 2001; Monaco et al., 2008) and technologies of their application depending on the type of soil, main crop, season, nature and degree of contamination of the agroecosystem and surrounding area. We may find a lot of developed algorithms for calculating the concentrations of active substances in herbicide compositions depending on the dominant types of undesirable vegetation (Tu et al., 2001; Ani et al., 2018), protocols of their application, including the use of the sprayer shape, the angles of solution direction to the plants, and the speed of movement along the processing area (Zimdahl, 2017).

* Corresponding author
E-mail addresses: novochadov.valeriy@volsu.ru (V.V. Novochadov)

Thus, although research and innovation activity in this direction does not weaken due to the emergence of new agricultural technologies and the presence of plant invasions, the fundamental approaches to this issue can be considered well-established.

At the same time, there are often situations that represent unrecoverable areas of undesirable vegetation penetrating the territory of managed agroecosystems, the so-called technogenic intrusions. As a usual characteristic, it is shown for intrusions to have reduced species composition, direct or indirect negative impact on the adjoining agroecosystem contributing the violation of consort links in it.

It was shown that agroecosystem demonstrates the decrease in the projective coverage, biological productivity of arable crops in the contact zone with the intrusion. These plots form a special microrelief, changing moisture conditions and transfer of pollutants with subsequent accumulation in the system 'soil – plant' (Ivantsova et al., 2017; Ivantsova, Novochadov, 2019).

Such areas in the area of power lines, gas and oil pipelines, etc. can invade significantly deep into the territory of agroecosystem, and the use of classical methods of combating undesirable vegetation here is limited both by agricultural protocols, and ecology.

There is, therefore, an objective need to find and develop new methods of combating undesirable vegetation on the territory of technogenic intrusions, on one hand providing for the preservation of a certain part of this ecosystem (ecological aspect), on the other hand being strongly aimed to reduce the negative impact of vegetation on the adjoining agroecosystem (production aspect). For obvious reasons, these technical solutions must be adapted to modern agricultural technologies, labor-intensive, and economically feasible.

In this area, we know a way to combat weeds by forming a seed mixture of different plant types, so that the new herbaceous cover completely suppressed the growth of weeds in the surrounding area. The combined crop mix helped to increase the full employment of ecological niches and, consequently, reduced the diversity and density of weed plants (Hossain et al., 2012; El-Sayed et al., 2014). The disadvantage of this method is that it is not quite suitable for solving the problem of man-made intrusions. In addition, the soil needs to be pre-machined, and use of this method is almost impossible in intrusion territory.

Velisevich et al. (2010) described a method of protection against undesirable vegetation, including treatment with herbicides by contact spraying, followed by removal of the plant mass by mechanical means. The main drawback of this approach is the same, because we have no possibility to carry out mechanical tillage in areas bordering the agroecosystem. In addition, the herbicide application may be limited by the main production process.

Currently, there is information about the use of fertilizers based on polymer matrices containing polycarboxylic acids or polysaccharides (Danilova, 2016; Sarkar et al., 2018). Their use is an effective way to retain the liquid and redistribute of trace elements or microorganisms both on the plants and in the soil. Such polymers can contribute to changing the species composition of intrusions and become a component of technologies to combat undesirable vegetation.

Based on the above, the immediate task of the study was to overcome the negative impact of irremediable or difficultly eliminated grass vegetations on the adjoining agroecosystems. In order to solve this problem, we used an approach based on the impact on weeds in these areas by means of plant root treatment in the early vegetative phase.

2. Material and methods

To select the components of the suspension for root treatment, we used a forecast based on a mathematical model that was compiled earlier and tested on the results of our own observations (Ivantsova et al., 2018).

As follows from these studies, control effects should not actively affect the agroecosystem (1); they should be achieved by introducing an additional component, not by reducing the existing one (2); they should not have herbicidal effect (3). The formula of the introduced compound should not contain more than three components, since in this case the costs increase significantly, and it is impossible to reliably predict the result (4). We refused to introduce microorganisms due to the difficulties of dosage and increasing labor intensity at all stages of the technology.

As a result, the main components in the suspension formula for plant root treatment, which allows for minimal impact on the plant communities of intrusion to sufficiently reduce their negative impact on the adjoining agroecosystem, were a trace element (copper or zinc),

a metabolite stimulating the soil microbiota (citric or succinic acid), and a polymer for moisture protection and activation of micromycetes (chitosan).

Table 1 illustrates the preliminary justification for the required amounts of individual substances to be applied to the soil.

Table 1. Calculation of the required number of suspension components for plant root treatment (all values are expressed in mg/kg of dry soil)

Suspension component	Range of values in soil intrusion	Decision rule based on a mathematical model (Ivantsova et al., 2018)	Interval of checked values for root treatment
Chitosan	–	Ensure the presence of at least 100 mg/kg in the surface layer of the soil (up to 5 mm). Dose of chitosan should increase as the metal dose increases.	5.0 – 40.0
Copper	12.0 – 45.0	The increase of concentration by 30-100 % is effective. The effect is less, the greater metal concentration in soil	10.0 – 80.0
Zinc	2.0 – 7.0		0.5 – 4.0
Succinic acid	Not defined	Application of up to 2.5 mg/kg for every 10 % of the expected projective coverage is effective	8.0 – 20.0
Citric acid			

As a result, twenty working formulas of suspension were prepared for the test. In the first group, the chitosan was introduced into the soil at doses from 0.05 to 4.0 mg/kg together with citric acid. The suspensions in the second group were a combination of citric acid and copper in concentrations that ensure the introduction of a trace element into the soil from 10.0 to 80.0 mg/kg. The third group tested a similar composition, varying in zinc in amounts from 0.5 to 4.0 mg/kg of soil. The fourth group was represented by suspensions including copper, citric acid and chitosan, the fifth group varied in zinc content, respectively.

Table 2 details the compositions of individual suspensions, which will be referred to in the text in the future. For example, subgroup IV-A denotes a suspension that provides 10.0 mg/kg of copper, 10.0 mg/kg of citric acid, and 0.05 mg/kg of chitosan to the soil.

Table 2. Calculated increments of substance concentrations (mg/kg of dry soil) after plant root treatment using test suspensions

Group*	Subgroup			
	A	B	C	D
I	Chitosan 0.05	Chitosan 0.1	Chitosan 0.2	Chitosan 0.4
II	Cu 10.0	Cu 20.0	Cu 40.0	Cu 80.0
III	Zn 0.5	Zn 1.0	Zn 2.0	Zn 4.0
IV	Cu 10.0 + Chitosan 0.05	Cu 20.0 + Chitosan 0.1	Cu 40.0 + Chitosan 0.2	Cu 80.0 + Chitosan 0.4
V	Zn 0.5 + Chitosan 0.05	Zn 1.0 + Chitosan 0.1	Zn 2.0 + Chitosan 0.2	Zn 4.0 + Chitosan 0.4

* – in all cases, citric acid is present at a concentration that provides 10 mg/kg of this substance to the soil.

As the object for testing, we chose the plant *Artemisia lerchiana* (Web.), as well-studied, having the necessary cultural properties and found us earlier as a dominant or subdominant in more than 70 % of the intrusions in arid zone.

To obtain plants in the early vegetative phase, we placed ehe native soil from intrusions in the pots, two plants were placed by root planting in each one, cut off to 3-4 root buds. After 2 weeks, the root treatment was performed, randomly forming 2 cases (four plants) in each subgroup. To form the control group, we exclude root treatment in two cases. Considering the number of plants and the number of buds that produced shoots, the average number of measured objects in each sample was from 10 to 15, which was enough for their representativeness.

Inspection and photo documentation of plants we performed immediately before the plant root treatment and 30 days after it (Figure 1).

The main indicators characterizing the effect of substances received in the soil were the average increase in the length of new shoots (mm) and the average projective coverage (%) in each subgroup.

A

B

C

Fig. 1. Digitized images of growing *Artemisia lerchiana* for morphometry. A. Side view for measuring the shoot height. B. Top view for measuring projective coverage. C. Binarization of the previous image, cleaning from artifacts and noises, performed by ImageJ, before automatic determination of projective coverage value

The measurements were performed using the capabilities of the free access program ImageJ (NIH, USA), and MS Excel (Microsoft, USA) was used for subsequent processing and visualization of the results. Since the normal distribution hypothesis was rejected, non-parametric criteria were used: the distribution was expressed as the median and the interquartile range (Me [Q1 ÷ Q3]), and the Kruskal-Wallis test was used to compare samples ($p < 0.01$).

3. Results and discussion

Table 3 shows the results of measurements of the average shoot height and the projective coverage after application of suspensions depending on their different composition

In group I, where we included only chitosan and citric acid in the suspension formula, as the concentration of chitosan increased, the negative effect on the growth of shoots increased. The effect was detected starting from a dose of 0.1 mg/kg of soil. At the same time, we did not find any significant effect in relation to the projective coverage.

In group II, we tested the effect of copper in combination with citric acid and obtained similar results. A dose-dependent negative effect on the growth of shoots was detected, starting from the addition of 20.0 mg/kg of copper to the soil. No effect was found with respect to the projective coverage.

Completely different changes we registered due to testing zinc together with citric acid (group III). This suspension significantly slowed down the growth of shoots and caused the formation of foliage with a low projective coverage. The effects of zinc did not depend on the administered dose of the trace element.

In group IV, where we tested the co-action of copper and chitosan, a distinct effect on both analyzed indicators was detected in subgroups IV-C and IV-D, that is, when adding 40.0 mg/kg of trace element and 0.2 mg/kg of chitosan to the soil or more.

Table 3. Changes in growth and development after plant root treatment of *Artemisia lerchiana* with suspensions of different composition

Group/Subgroup	Indicators, Me [Q1 ÷ Q3]	
	Average growth of shoot length, mm	Average projective cover, %
Control	1183 [1020 ÷ 1285]	84.2 [75.9 ÷ 89.1]
Chitosan and citric acid		
I-A	1109 [961 ÷ 1243]	82.0 [70.5 ÷ 87.4]
I-B	796 [675 ÷ 910] *	77.3 [66.1 ÷ 83.8]
I-C	644 [558 ÷ 736] *	74.5 [64.8 ÷ 77.3]
I-D	302 [259 ÷ 334] *	77.0 [65.5 ÷ 82.6]
Copper and citric acid		
II-A	1057 [894 ÷ 1218]	83.5 [72.2 ÷ 88.8]
II-B	841 [717 ÷ 965] *	80.7 [69.7 ÷ 85.0]
II-C	696 [601 ÷ 805] *	81.4 [70.0 ÷ 87.4]
II-D	638 [550 ÷ 726] *	76.0 [65.5 ÷ 78.9]
Zinc and citric acid		
III-A	445 [383 ÷ 512] *	67.2 [60.1 ÷ 73.2] *
III-B	497 [429 ÷ 570] *	68.5 [61.3 ÷ 75.0] *
III-C	436 [375 ÷ 501] *	63.0 [57.8 ÷ 70.9] *
III-D	400 [344 ÷ 464] *	62.7 [55.6 ÷ 68.7] *
Copper, chitosan and citric acid		
IV-A	1215 [1033 ÷ 1395]	80.0 [69.1 ÷ 86.6]
IV-B	977 [840 ÷ 1128]	73.5 [62.3 ÷ 79.0]
IV-C	323 [281 ÷ 370] *	70.2 [61.0 ÷ 76.8] *
IV-D	304 [265 ÷ 354] *	67.8 [59.5 ÷ 74.9] *
Zinc, chitosan and citric acid		
V-A	895 [763 ÷ 1028]	65.3 [59.0 ÷ 71.2] *
V-B	502 [430 ÷ 577] *	61.8 [56.1 ÷ 68.5] *
V-C	800 [684 ÷ 927] *	56.0 [49.7 ÷ 63.0] *
V-D	711 [615 ÷ 822] *	55.4 [49.4 ÷ 61.9] *

* – significant differences with values in the control group

Group V was represented by samples that received together zinc, chitosan and citric acid. In this case, we identified the maximum negative changes from the growth of shoots and projective coverage. The changes in the growth of the shoot length dominated at low doses of the introduced substances, the effects on the projective coverage dominated at higher ones.

The effect of trace elements on plant communities can only partially be reduced to direct metabolic consequences of their penetration into plant cells, where metals are included in the complex proteins with regulatory, transport, and enzymatic properties (Singh, Parihar, 2015; He et al., 2016; Novochadov et al., 2018). Equally important events occur directly in the soil, where metals, including copper and zinc, can significantly change the growth rate and metabolic activity of microorganisms. The microbiota provides a complex of protective and trophic processes, based on stimulation of oxidation, deposition, complexation, transport and conjugation. As a result, this leads to changes in the growth and development of plants, as well as their sensitivity to environmental influences (Ma et al., 2016; Meena et al., 2017; Kertész et al., 2017; Bargaz et al., 2018).

The root treatment options used by us provided, after natural alignment of the resulting concentration and pH gradients, the content of mobile trace elements exceeding from 30 % to 100 % above the initial concentrations. It is the combined effects of these metals in the suspension on the soil microbiota and plants that explain the results obtained for inhibiting the growth and development of the model plant (*Artemisia lerchiana*).

Regarding chitosan, the use of polymers for soil treatment has been shown to be effective due to the ability to thus provide water retention and trace elements near plant roots (Danilova, 2016; Sarkar et al., 2018). Chitosan after entering the soil becomes insoluble and forms a three-dimensional matrix structure. Perhaps such deposits serve as a matrix for the growth of soil microfungi, which use these polymers as the main source of carbon. The organic acids received as part of the suspension, which exist in these conditions in the form of soluble and bioavailable anions, support all the above processes. This, in our opinion, achieves a complex biogenic effect of the received suspension on the soil microbiota and plants, resulting in an increase in the contribution of microfungi to the transformation of humus, mobilization of soil trace elements, intensification of vegetative processes in plants with subsequent depletion of consort bonds in the system 'soil – plant microbiota'.

The direct composition for plant root treatment can be selected empirically, which requires information about the content of mobile forms of copper and zinc in the soil, the species composition of plant community, its projective coating, and the influence on the adjoining agroecosystem. If we have a low influence on agroecosystem, the use of any actions is not advisable. For direct field testing, we have developed a working algorithm that uses only the soil concentrations of copper and zinc, as well as the influence of the intrusion on the adjoining agroecosystem for the selection of suspension components and their dosage (Figure 2).

It is known that plant communities living in more severe and stressful habitat conditions are less susceptible to invasion by alien species, compared with similar ones in more temperate habitats. This is due to limited reproduction, low rates of population movement, while the plant communities have enough resistance to invasive impacts (Zefferman, 2015; Hudson et al., 2017).

Both restriction of distribution and resistance to invasion can simultaneously contribute to the low aggressiveness of plant communities themselves in harsh habitats in relation to surrounding territories (Liu et al., 2014; Uroy et al., 2019).

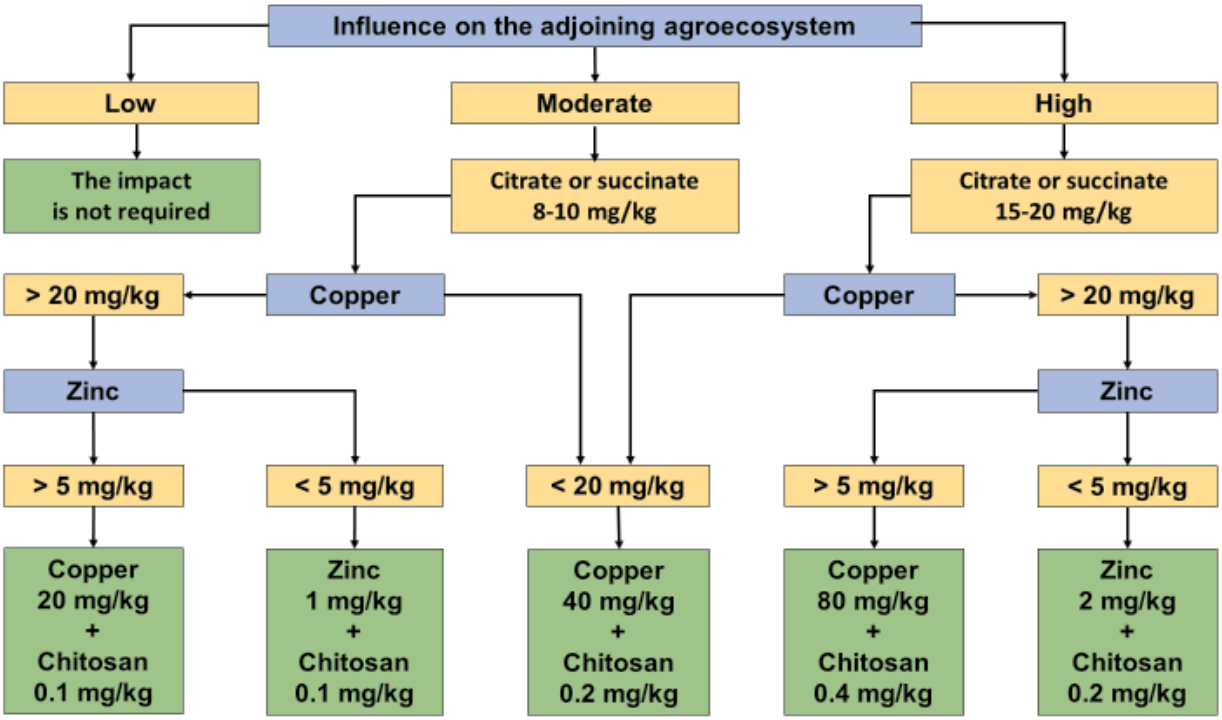

Fig. 2. A working algorithm for field testing the effectiveness of the developed suspensions to reduce the negative impact of undesirable plant communities on the adjoining agroecosystem

We associate the potential effectiveness of the developed suspensions in their application in real land use conditions with the emerging stress conditions in relation to plants that are dominant and subdominant in arid plant communities.

4. Conclusion

This study has shown the effectiveness of new suspensions for plant root treatment as a tool to reduce the growth of dominant and subdominant species in arid plant communities on the example of *Artemisia lerchiana*. To do this, we developed an aqueous suspension of the original variable composition, which provided delivery to the roots of plants, based on 1 kg of surface soil layer: 20-40 mg of copper ions and/or 1-2 mg of zinc ions (1); 8-20 mg of citric and/or succinic acid, permissible in the form of sodium or potassium salts (2); and 10-20 mg of chitosan (3).

As a result, a complex biogenic effect of the received suspension on the soil microbiota and plants was achieved. The improved inhibiting the plant growth and reducing the projective coverage (only for zinc ions or combination copper with chitosan in high concentrations), are the experimental basis for subsequent field tests. For this study we developed a working algorithm for the selection of components and their concentration, based on mathematical modeling of different responses of plant communities to variations in the composition of the suspension for plant root treatment.

5. Acknowledgments

The publication was supported by the Ministry of Education and Science of the Russian Federation on the theme 'Development of ecologically-oriented biotechnologies for the optimization of arid agrobiocenoses in the South of Russia based on the achievements of physicochemical biology and bioinformatics' (Project no. 40.7534.2017/8.9).

References

Ani et al., 2018 – *Ani, O., Onu, O., Okoro, G., Uguru, M.* (2018). Overview of Biological Methods of Weed Control, Biological Approaches for Controlling Weeds. *Ramalingam Radhakrishnan, IntechOpen*. DOI: 10.5772/intechopen.76219. [Electronic resource]. URL:

https://www.intechopen.com/books/biological-approaches-for-controlling-weeds/overview-of-biological-methods-of-weed-control

Bargaz et al., 2018 – *Bargaz, A., Lyamlouli, K., Chtouki, M. et. al.* (2018). Soil microbial resources for improving fertilizers efficiency in an integrated plant nutrient management system. *Frontiers in Microbiology*. 9, 1606. DOI: 10.3389/fmicb.2018.01606

Danilova, 2016 – *Danilova, T.N.* (2016). Regulation of water regime in sod-podzolic soil and plant water availability with water-absorbent polymer. *Agrophysics*. (1): 8-16.

El-Sayed et al., 2014 – *El-Sayed, W.S., Akhkha, A., El-Naggar, M.Y. et al.* (2014). In vitro antagonistic activity, plant growth promoting traits and phylogenetic affiliation of rhizobacteria associated with wild plants grown in arid soil. *Front. Microbiol.* 5: 651. DOI: 10.3389/fmicb.2014.00651

He et al., 2016 – *He, M.Z., Dijkstra, F.A., Zhang, K. et al.* (2016). Influence of life form, taxonomy, climate, and soil properties on shoot and root concentrations of 11 elements in herbaceous plants in a temperate desert. *Plant and Soil*. 398 (102): 339-350. DOI: 10.1007/s11104-015-2669-0

Hossain et al., 2012 – *Hossain, A., Lozovskaya, M.V., Teixeira da Silva, J.A., Zvolinsky, V.P.* (2012). High temperature combined with drought affect rainfed spring wheat and barley in South-Eastern Russia: I. Phenology and growth. *Saudi J. Biol. Sci.* 19(4): 473-487. DOI: 10.1016/j.sjbs.2012.07.005

Hudson et al., 2016 – *Hudson, L.N., Newbold, T., Contu, S. et al.* (2016). The database of the PREDICTS (Projecting Responses of Ecological Diversity in Changing Terrestrial Systems) project. *Ecol. Evol.* 7(1): 145-188. DOI: 10.1002/ece3.2579

Ivantsova et al., 2017 – *Ivantsova, E.A., Novochadov, V.V., Onistratenko, N.V., Postnova, M.V.* (2017). Ecological aspects of phytosanitary optimization of arid agrobiocenoses in South Russia. *Bulgarian J. Agric. Sci.* 23(5): 834-842.

Ivantsova et al., 2018 – *Ivantsova, E.A., Onistratenko, N.V., German, N.V. et al.* (2018). Targered changes in the natural and semi-artifical arid phytocenoses in the contact zone with the agrocenoses: a system control model-based approach. *Eur. J. Mol. Biotech.* 6 (1): 53-60. DOI: 10.13187/ejmb.2018.1.53

Ivantsova, Novochadov, 2019 – *Ivantsova, E.A., Novochadov, V.V.* (2019). The nature of interaction between components of the anthropogenically transformed ecosystems in southern Russia. *Proceedings of Nizhnevolzhskiy Agrouniversity Complex: Science and Higher Vocational Education*. (3): 79-86. DOI: 10.32786/2071-9485-2019-03-9

Kertész et al., 2017 – *Kertész, M., Aszalós, R., Lengyel, A., Ónodi, G.* (2017). Synergistic effects of the components of global change: Increased vegetation dynamics in open, forest-steppe grasslands driven by wildfires and year-to-year precipitation differences. *PLoS One*. 12(11): e0188260. DOI: 10.1371/journal.pone.0188260

Kraehmer et al., 2014 – *Kraehmer, H., van Almsick, A., Beffa, R. et al.* (2014). Herbicides as weed control agents: state of the art: II. Recent achievements. *Plant physiology*. 166(3): 1132-1148. DOI: 10.1104/pp.114.241992

Liu et al., 2014 – *Liu, H., Zhang, D., Yang, X. et al.* (2014). Seed dispersal and germination traits of 70 plant species inhabiting the Gurbantunggut desert in Northwest China. *Sci. World J.* e346405. DOI: 10.1155/2014/346405

Ma et al., 2016 – *Ma, Y., Oliveira, R.S., Freitas, H., Zhang, C.* (2016). Biochemical and molecular mechanisms of plant-microbe-metal interactions: relevance for phytoremediation. *Front. Plant Sci.* 7: e918. DOI: 10.3389/fpls.2016.00918

Meena et al., 2017 – *Meena, K.K., Sorty, A.M., Bitla, U.M. et. al.* (2017). Abiotic stress responses and microbe-mediated mitigation in plants: the omics strategies. *Front. Plant Sci.* 8: 172. DOI: 10.3389/fpls.2017.00172

Monaco et al., 2008 – *Monaco, T.J., Weller, S.C., Ashton, F.M.* (2008). Weed Science: Principles and Practices, 4th ed. Wiley-Blackwell, 700 p.

Novochadov et al., 2018 – *Novochadov, V.V., Krylov, P.A., Tikhonova, A.A.* (2018) Manganese- and Zinc-containing metalloproteins have a value in the species composition of semi-artificial arid phytocenoses in the contact zone with the agrocenoses. *Eur. J. Mol. Biotech.* 6(2): 76-82. DOI: 10.13187/ejmb.2018.2.76

Sarkar et al., 2018 – *Sarkar, D.J., Barman, M., Bera, T. et al.* (2018). Agriculture: polymers in crop production mulch and fertilizer. In book: Encyclopedia of Polymer Applications. *CRC Press, Taylor & Francis Group*. DOI: 10.1201/9781351019422-140000083

Singh, Parihar, 2015 – *Singh, S., Parihar, P.* (2015). Heavy metal tolerance in plants: role of transcriptomics, proteomics, metabolomics, and ionomics. *Front. Plant Sci.* (6): 1143. DOI: 10.3389/fpls.2015.01143

Tu et al., 2001 – *Tu, M., Hurd, C., Randall, J.M. and The Nature Conservancy* (2001). Weed Control Methods Handbook: Tools & Techniques for Use in Natural Areas. *All U.S. Government Documents (Utah Regional Depository)*. Paper 533.

Uroy et al., 2019 – *Uroy, L., Mony, C., Ernoult, A.* (2019). Additive effects of connectivity provided by different habitat types drive plant assembly. *Sci. Rep.* 9: e13952. DOI: 10.1038/s41598-019-50184-2

Velisevich et al., 2010 – *Velisevich, S.N., Vorob'ev, V.N., Davydov, V.V.* (2010). Method of cleaning of alienated territories from unwanted vegetation. RU 2405293 C9. 10.12.2010.

Zefferman et al., 2015 – *Zefferman, E., Stevens, J.T., Charles, G.K. et al.* (2015). Plant communities in harsh sites are less invaded: a summary of observations and proposed explanations. *AoB Plants*. 7(1): plv056. DOI: 10.1093/aobpla/plv056.

Zimdahl, 2017 – *Zimdahl, R. (ed.)* (2017). Integrated Weed Management for Sustainable Agriculture. Burleigh Dodds Science Publishing Ltd.

Published in the Slovak Republic
European Journal of Molecular Biotechnology
Has been issued since 2013.
E-ISSN: 2409-1332
2019, 7(2): 109-122

DOI: 10.13187/ejmb.2019.2.109
www.ejournal8.com

Different Methods in the Synthesis of Polyheterocyclic Cyanine Dyes: A Review

H. A. Shindy [a, *]

[a] Department of Chemistry, Faculty of Science, Aswan University, Aswan 81528, Egypt

Abstract

In this paper review different methods in the synthesis of polyheterocyclic cyanine dyes have been reviewed. In this paper review detailed synthesis steps for the synthesis of some polyheterocyclic cyanine dyes were represented via equations. The synthesis covers polyheterocyclic monomethine cyanine dyes (simple cyanine dyes), dimethine cyanine dyes, trimethine cyanine dyes (carbocyanine dyes), tetramethine cyanine dyes, pentamethine cyanine dyes (dicarbocyanine dyes), aza-methine cyanine dyes, hemicyanine dyes (styryl cyanine dyes), merocyanine dyes (acyclic merocyanine dyes and cyclic merocyanine dyes). Besides, in the introduction section of this paper review some light is focused on the some recent applications of cyanine dyes. This review paper is very readable, informative, and useful for synthetic dye chemists, researchers and students who looks for the different methods in the synthesis and preparation of various classes of polyheterocyclic cyanine dyes. In addition, this paper review can be used and/or will be most valuable as a thesis and/or as a note book for student lectures, particularly for the post graduate students and researchers in the field of heterocyclic and/or cyanine dyes chemistry. This specific type of collective review in the different methods in the synthesis of only polyheterocyclic cyanine dyes has been paid little attention and is lacking in the chemistry literature.

Keywords: Cyanine dyes, synthesis, polyheterocyclic cyanine dyes, different classes of cyanine dyes, uses of cyanine dyes, applications of cyanine dyes, properties of cyanine dyes.

1. Introduction

Many and many attention and have been paid to the chemistry of cyanine dyes (Shindy, 2016; Shindy, 2017; Shindy, 2018; Shindy, 2018a; Shindy, 2012; Shindy et al., 2018; Shindy, 2019; Shindy et. al., 2019; Shindy et. al., 2019a; Shindy et. al., 2017; Komljenovic et al., 2016; Zhang et al., 2016; Solomon et al., 2014; Keisar et al., 2014; Yi et al., 2014; Hyun et al., 2015; Njiojob et al., 2015; Wada et al., 2015; Sun et al, 2013; Zhao et al., 2013). This is strong evidence and/or a certificate for the great importance of these large class of heterocyclic dyes in the modern science and advanced technology. Cyanine dyes have been used in photography for more than 100 years to sensitize silver halide efficiently upon the absorption of light (Hamer, 1964). So, cyanine dyes can be used to sensitize nanocrystalline TiO_2 in solar cells. The high extinction coefficients of cyanine dyes can make them absorb enough light and the absorption spectra of cyanine dyes can be tuned easily in the whole spectrum by tailoring their structures. Therefore it is of great interest to study their sensitization for nanocrystalline TiO_2 (or other semiconductors) solar cells. In addition, extensive synthetic procedures for generating cyanine dyes of diverse molecular structure were developed so far (Mishra et al., 2000; Wang et al., 2003; Wang et al., 2003a) This is because cyanine dyes (polymethine dyes) have found various applications as photographic sensitizers for both color and non-color (black and white) films and as textile dyes. They are also useful as

* Corresponding author
E-mail addresses: hashindy2@hotmail.com (H.A. Shindy)

photosensitizers in blue green light and as analytical reagent over a wide pH medium. In addition cyanine dyes (hemicyanine dyes) can be used as fluorescence probes in biochemistry and biophysical area (Ephardt, Fromhers, 1989). They are also commonly applied to lasers (Zhao et al., 1996), electronics (Gromov et al., 1992) and non-linear optics (He et al., 1995).

2. Results

Different Methods in the Synthesis of Polyheterocyclic Cyanine Dyes

Phenoxazine bis dimethine cyanine dye were synthesized via reaction of bis oxazole dimethine cyanine dye containing a free aldehyde group with 2-methyl-5-acetyloxazolo[4,5-b]phenoxazine-3-methiodide (Osman et al., 1978), Scheme 1.

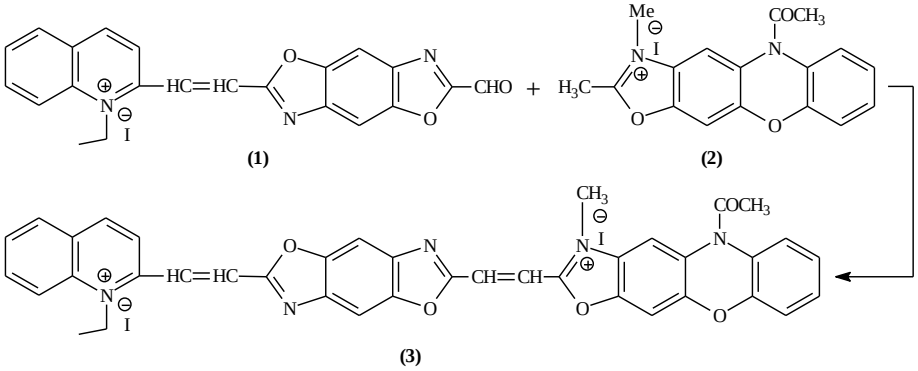

Fig. 1. Scheme 1

A number of aza-cyanine dyes by the use of N-bridgehead heterocyclic indolizinium ylide were prepared (Koraiem et al., 2006), Scheme 2.

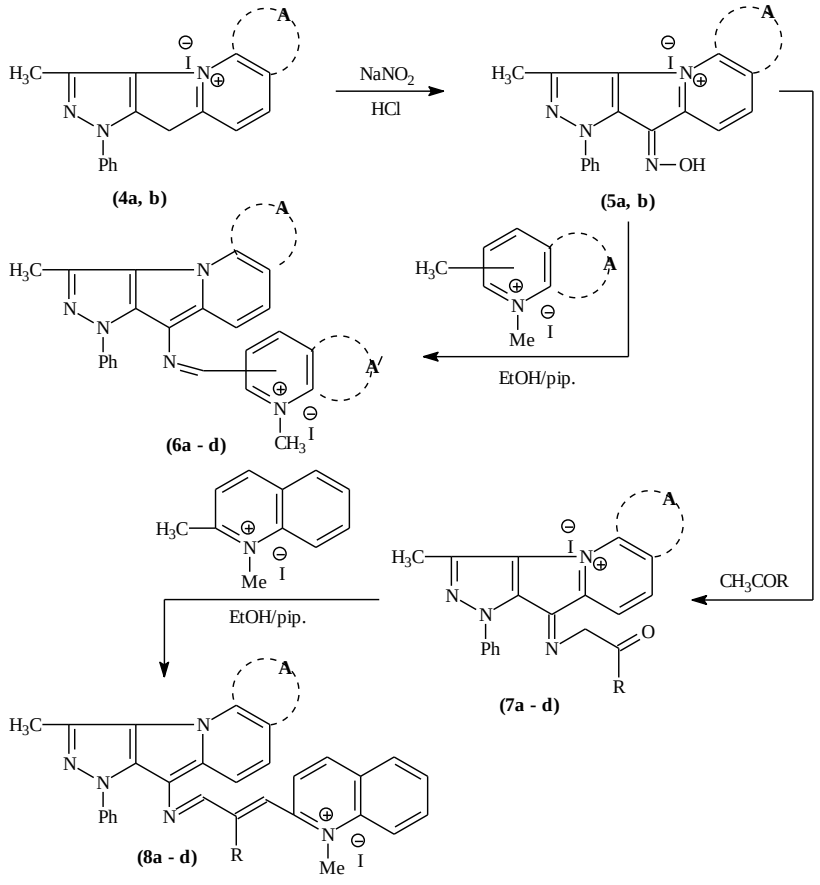

Fig. 2. Scheme 2

Substituents in Scheme 2:

(4a, b); (5a, b): A = indolizinium iodide (a); benzoindolizinium iodide (b).
(6a – d): A = indolizinium iodide, A′ = 1-methylpyridine-2-ium (a);
A = indolizinium iodide, A′ = 1-methyl quinoline-2-ium (b);
A = indolizinium iodide, A′ = 1-methyl-pyridine-4-ium (c);
A = benzoindolizinium iodide, A′ = 1-methyl-quinoline-2-ium (d).
(7a – d): A = indolizinium iodide, R = H (a);
A = indolizinium iodide, R = CH_3 (b);
A = indolizinium iodide, R = C_6H_5 (c);
A = benzoindolizinium iodide, R C_6H_5 (d).
(8a – d): A = indolizine, R = H (a);A = indolizine, R = CH_3 (b);
A = indolizine, R = C_6H_5 (c); A = benzoindolizine, R = C_6H_5 (d).
A series of monomethine cyanine dyes were synthesized (Abd El-Aal, Younis, 2004), Scheme 3.

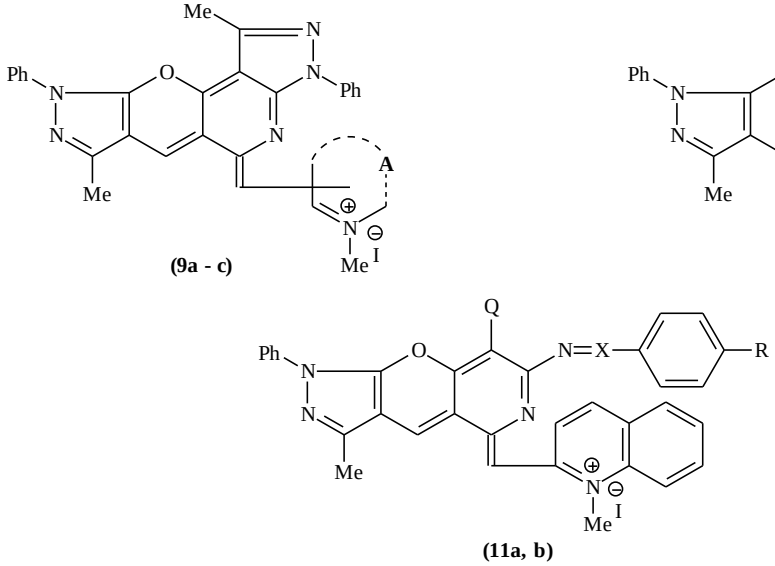

Fig. 3. Scheme 3

Substituents in Scheme 3:

(9a – c): A = 1-methyl-pyridinium-2-yl salt (a);
1-methyl-quinolinium-2-yl salt (b);
1-methyl-pyridinium-4-yl salt (c).
(10a – c): Q = imidazolyl, A = 1-methyl-pyridinium-2-yl salt (a);
Q = imidazolyl, A = 1-methyl-quinolinium-2-yl salt (b);
Q = imidazolyl, A = 1-methyl-pyridinium-4-yl salt (c).
(11a, b): X = N, R = OH (a); X = CH, R = OH (b).

Unsymmetrical 2[2(4)]-monomethine cyanine dyes derived from thiazolo-bis-[2,3-b; 5,4-d] pyrimidine were synthesized (Abd El-Motaleb, 2002), Scheme 4.

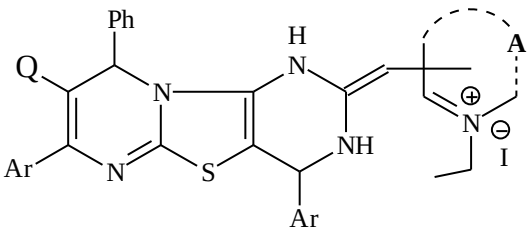

Fig. 4. Scheme 4

Substituents in Scheme 4:

(12a – f): Q = H; Ar = C_6H_5, A = 1-ethyl-pyridine-2-ium iodide (a);
Q = H; Ar = C_6H_5, A = 1-ethyl-quinoline-2-ium iodide (b);
Q = H; Ar = C_6H_5, A = 1-ethyl-pyridine-4-ium iodide (c);
Q = H; Ar = C_6H_4-p.OH, A = 1-ethyl-quinoline-2-ium iodide (d);
Q = H; Ar = C_6H_4-m.NO_2, A = 1-ethyl-quinoline-2-ium iodide (e);
Q= quinoline-4-ium ethiodide, Ar =C_6H_5, A = 1-ethyl-quinoline-2-ium iodide (f).

A number of monomethine merocyanine mixed cyanine dyes containing thiazole nucleus were prepared (Fedotov, Romanov, 1989), Scheme 5.

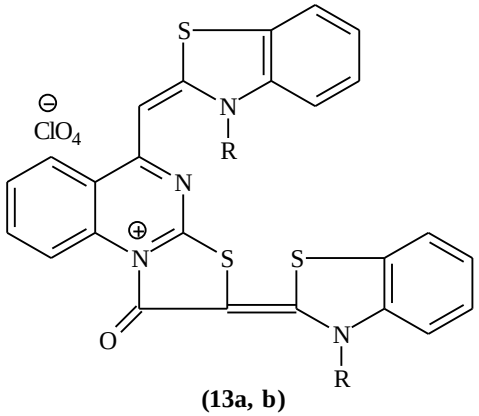

(13a, b)

Fig. 5. Scheme 5

Substituents in Scheme 5:

(13a, b): R = Me (a); Et (b).

A series of unsymmetrical pyrazolo[4,5-d]thiazolo/oxazolo [2,3-b]pyrimidine-5[2(4)]-monomethine cyanine dyes and pyrazolo[4,5-d]thiazolo[2,3-b]pyrimidine-5[4(1)]-cyclic mero cyanine dyes were synthesized (Mohamed, 1998), Scheme 6.

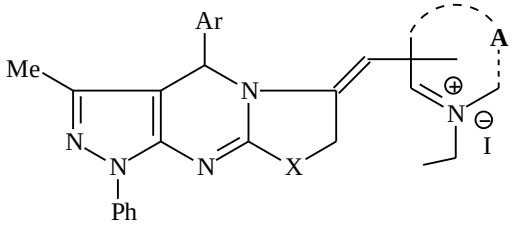

(14a - h)

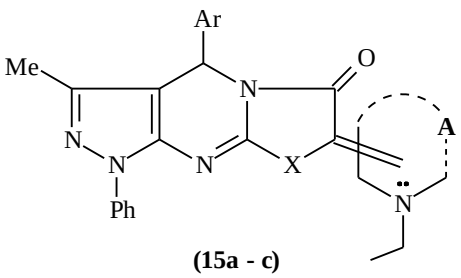

(15a - c)

Fig. 6. Scheme 6

Substituents in Scheme 6:

(14a – h): Ar = C_6H_5, A = 1-methylpyridine-2-ium, X = S (a);
Ar = C_6H_5, A = 1-methylquinoline-2-ium, X = S (b);
Ar = C_6H_5, A = 1-methylpyridine-4-ium, X = S (c);
Ar = C_6H_4- p.OH, A = 1-methylquinoline-2-ium, X = S (d);
Ar = C_6H_4-p.OCH_3, A = 1-methylquinoline-2-ium, X = S (e);
Ar = C_6H_4-p.NO_2, A = 1-methylquinoline-2-ium, X = S (f);
Ar = C_6H_4-m.NO_2, A = 1-methylquinoline-2-ium, X = S (g);
Ar = C_6H_5, A = 1-methylquinoline-2-ium, X = O (h).
(15a – c): Ar = C_6H_5, A = N-ethylpyridine (a);
Ar = C_6H_5, A = N-ethylquinoline (b);
Ar = C_6H_5, A = N-ethylisoquinoline (c).

A number of hemicyanine dyes with multi-carboxyl group in the accepter part and used them to sensitize TiO_2 electrode (Meng et al., 2003), Scheme 7.

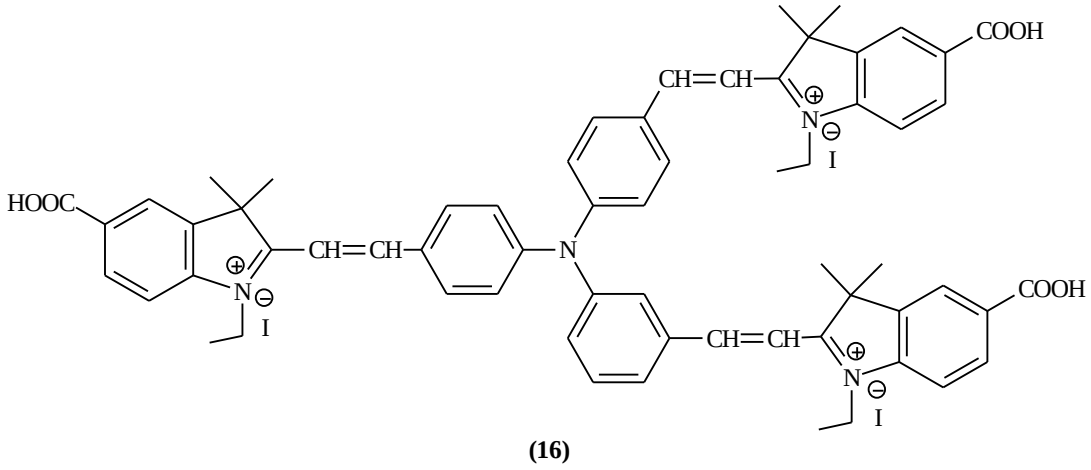

(16)

Fig. 7. Scheme 7

Dyes with two or three positive charged in the chromophere were synthesized by condensation of 4-chloroquinolinium salts with benzothiazolium salts and additional quaternization with ω-bromoalkyl substituents (Deligeogiev et al., 1989; Gadjev et al., 1999), Scheme 8.

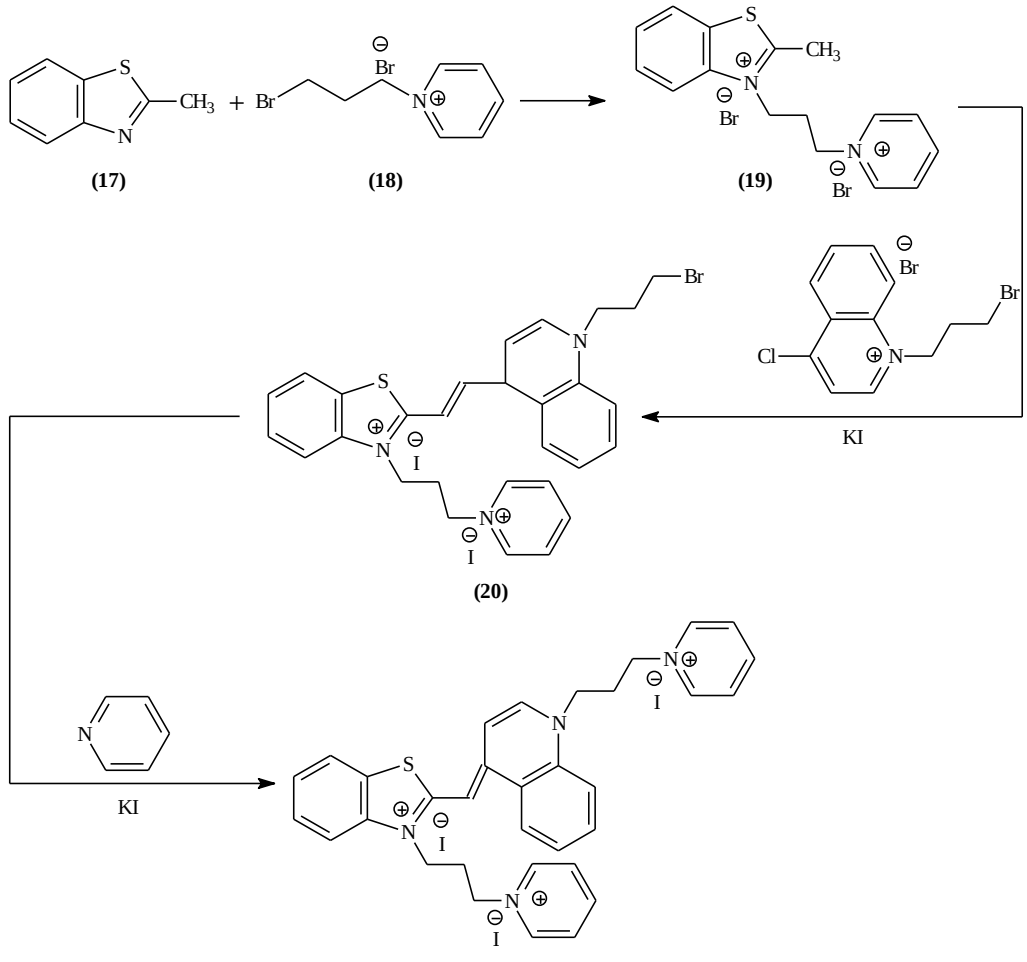

Fig. 8. Scheme 8

A number of monomethine cyanine dyes having three positive charges were prepared (Vasilev et al., 2005), Scheme 9.

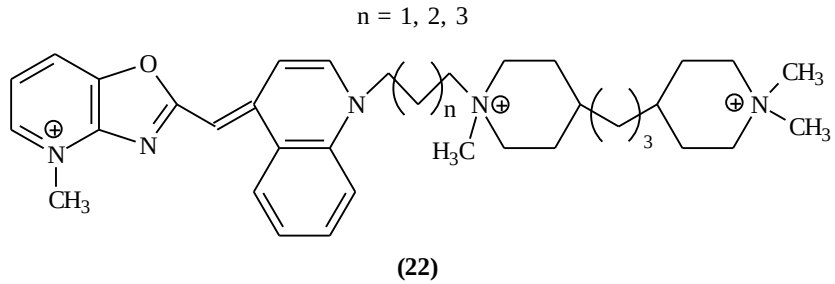

(22)

Fig. 9. Scheme 9

Trimethine cyanine dye (24) was synthesized through reaction of the quaternary salt (23) with sodium formate, ethylorthoformate or diphenylformamidine in the presence of acetic anhydride (Osman, Khalil, 1975), Scheme 10.

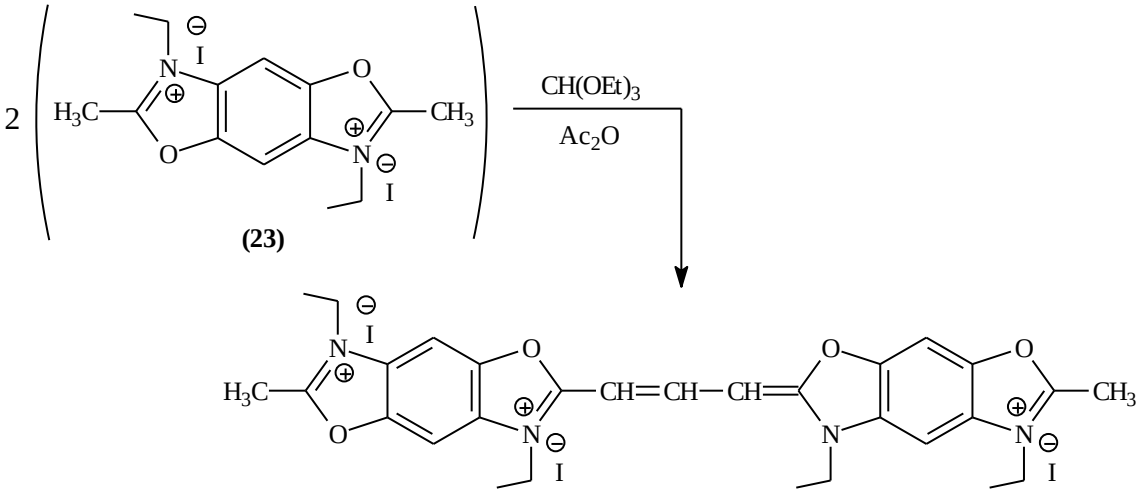

(23)

(24)

Fig. 10. Scheme 10

A series of monomethine meso-substituted pentamethine mixed cyanine dyes were prepared (Abd El-Aal, Koraiem, 2002), Scheme 11.

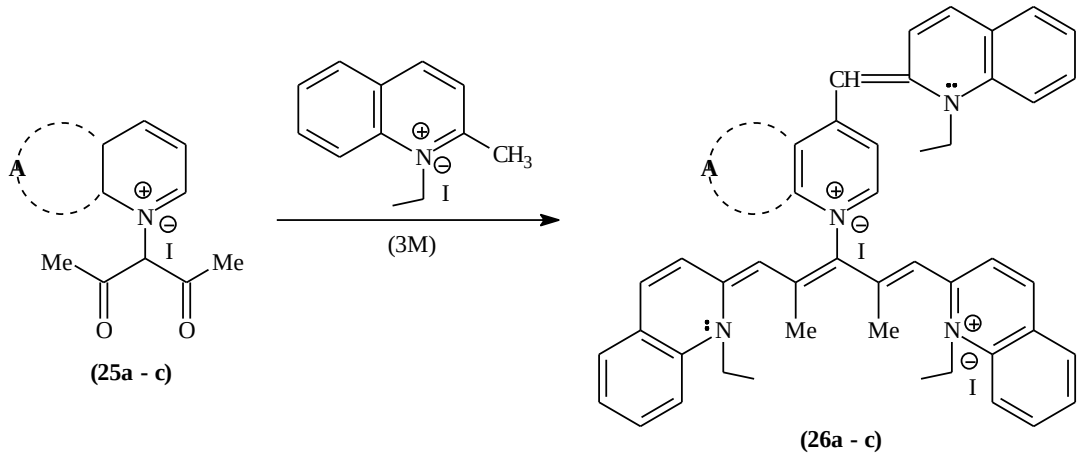

(25a - c)

(26a - c)

Fig. 11. Scheme 11

Substituents in Scheme 11:

(25a – c), (26a – c): A = N-pyridinium (a); N-quinolinium (b);
N-isoquinolinium (c).

A number of monomethine cyanine dyes containing thiozole and/or oxazole nucleus were synthesized (Deligeorgiev et al., 2000), Scheme 12.

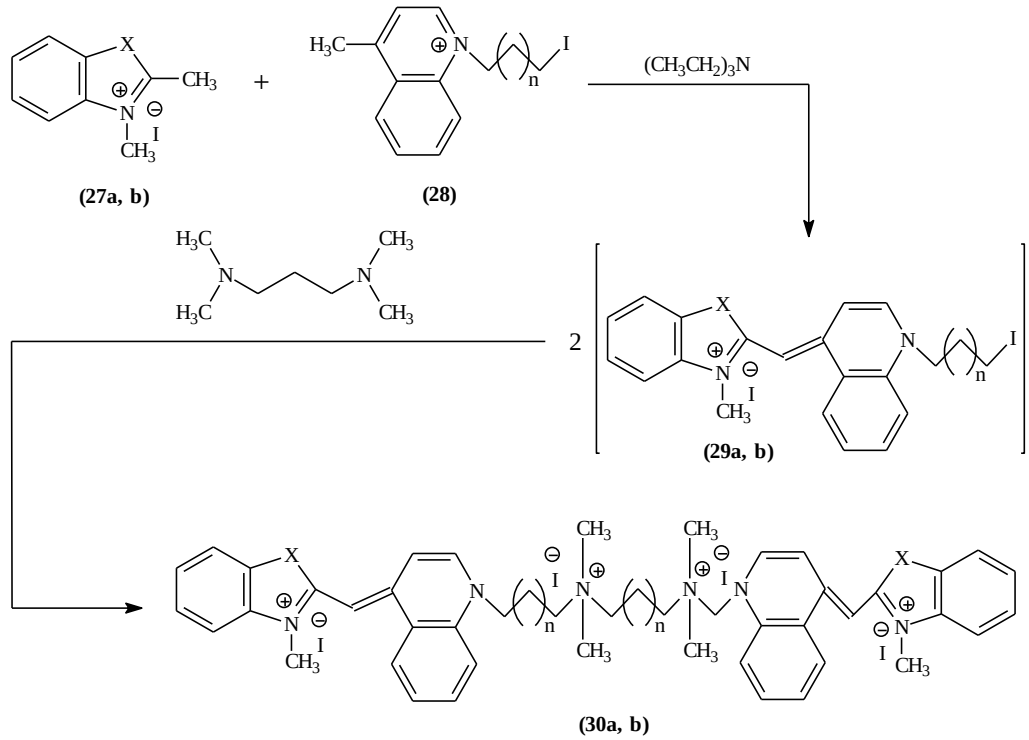

Fig. 12. Scheme 12

Substituents in Scheme 12:

(27a, b); (29a, b); (30a, b): n = 1, X = S (a); O (b).

Bis cyclic merocyanine dye linked by a 1,8-Naphthalene Skeleton were synthesized (Takashi et al., 1998), Scheme 13.

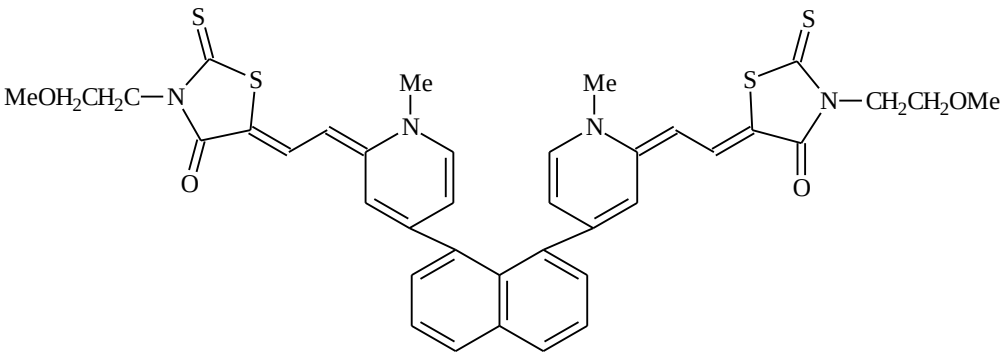

Fig. 13. Scheme 13

A number of hemicyanine dyes and bis hemicyanine dyes with a benzo[2,3-b; 2',3'-b']bis-furo[3,2-d]pyrazolium nucleus were prepared (Shindy, koraiem, 2008), Scheme 14.

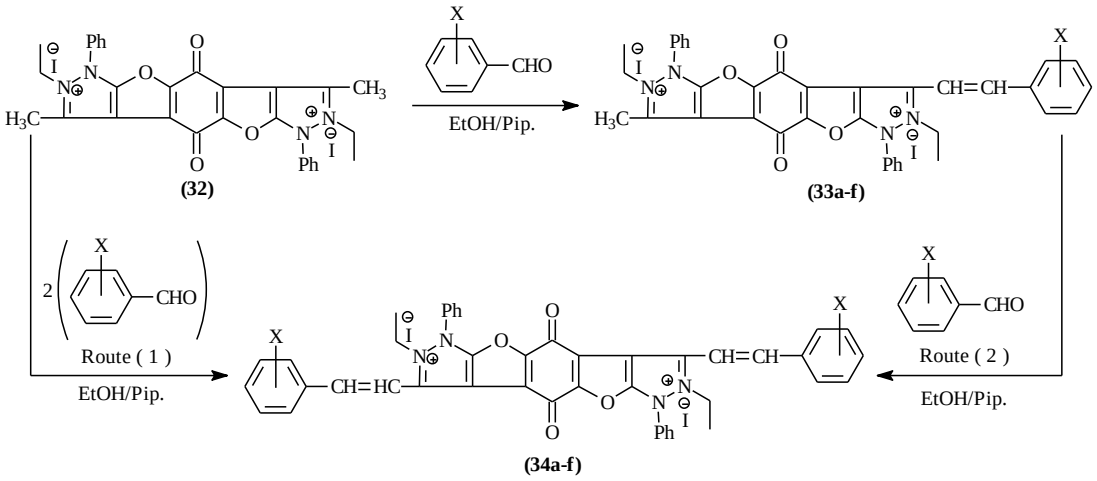

Fig. 14. Scheme 14

Substituents in Scheme 14:
(33a-f); (34a-f): X = H (a); *p*-OH (b); *p*-OCH_3 (c); *p*-$N(CH_3)_2$ (d);
p-NO_2 (e); p-Cl (f).

A series of tetramethine cyanine dyes and bis tetramethine cyanine dyes derived from benzo[2,3-b; 2',3'-b']bispyrazolo[4,5-b]-1,4-(oxa, thia, and pyra)-zine-6,12-dione nucleus were synthesized (Shindy et al., 2009), Scheme 15.

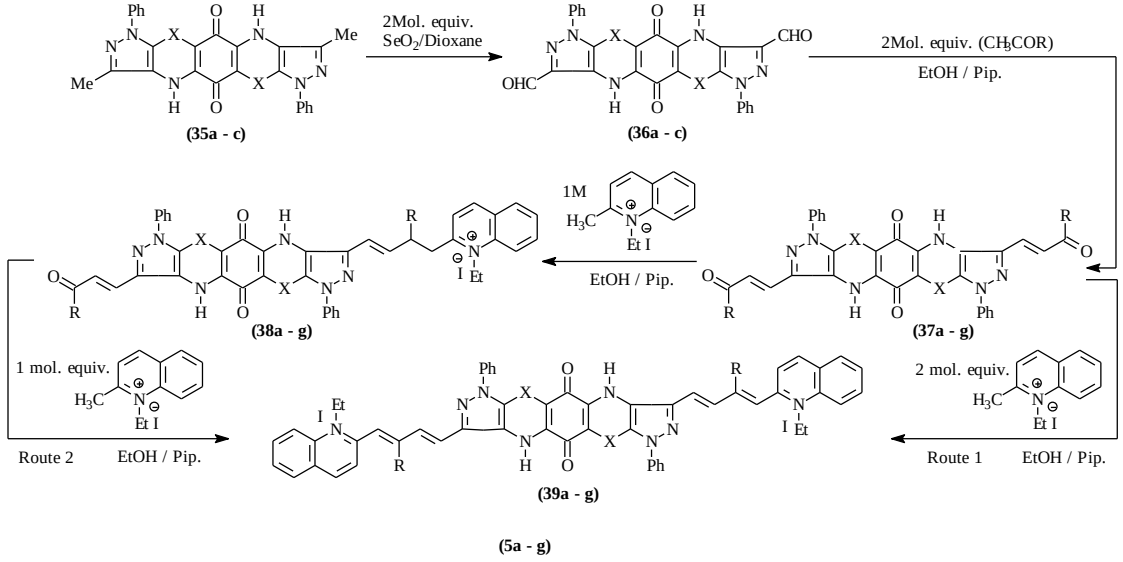

Fig. 15. Scheme 15

Substituents in Scheme 15
(37a-g); (38a-g) & (39a-g): X = O, R = H (a); X = O, R = CH_3 (b);
X = O, R = C_6H_5 (c); X = O, R = C_6H_4-*p*.OCH_3 (d);
X = O, R = C_6H_4-*p*.NO_2 (e); X = S, R = H (f);
X = NH, R = H (g).

A number of merocyanine dyes including a cyclic merocyanine dyes and cyclic merocyanine dyes incorporating benzo[2,3-b, 2',3'-b']bispyrazolo[4,5-b]-1,4-(oxa-, thia- and pyra-)-zine-6,12-dione were prepared (Shindy et al., 2012), Scheme 16.

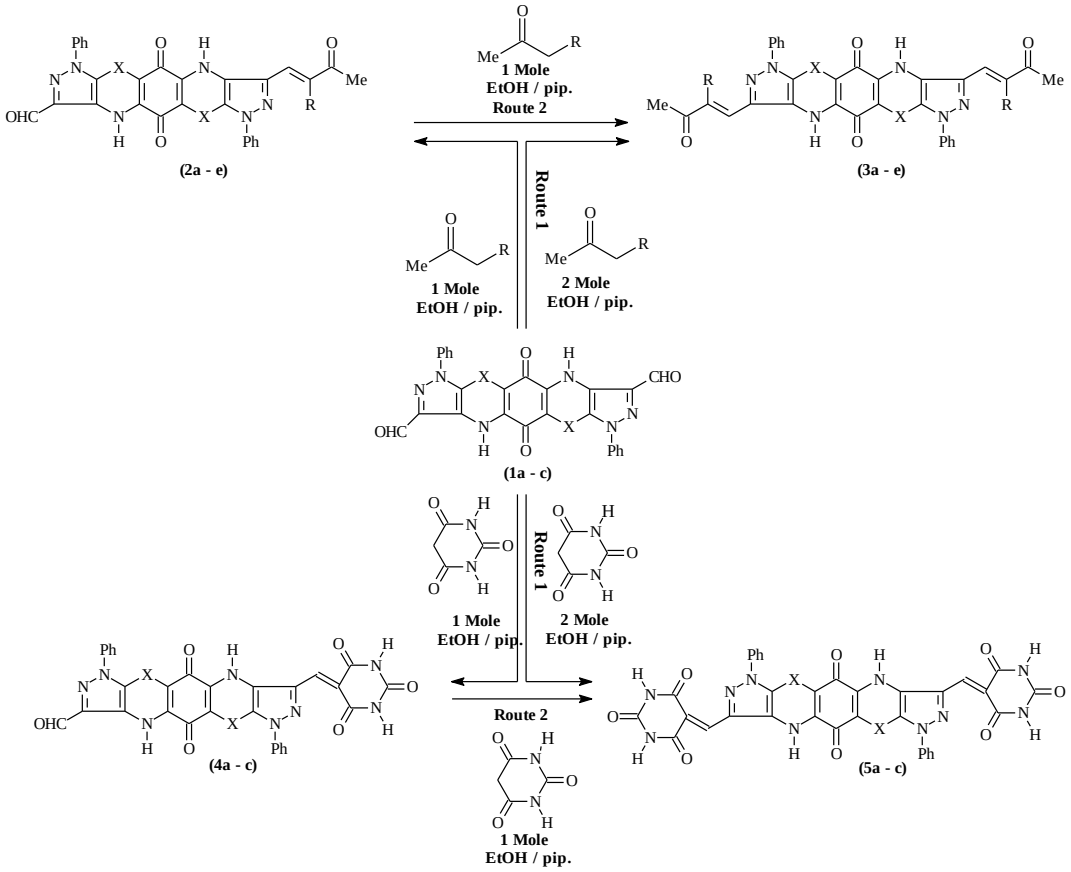

1a-c, 4a-c, 5a-c: a, X = O
b, X = S
c, X = NH

2a-e; 3a-e: a, X = O, R = H
b, X = O, R = $COCH_3$
c, X = O, R = COOEt
d, X = S, R = H
e, X = NH, R = H

Fig. 16. Scheme 16. A series of dimethine and *bis*-dimethine, cyanine dyes derived from benzo[2,3-b; 2`,3`-b`]*bis*-pyrazolo[4,5-*b*]-l,4-(oxa-, thia-, and pyra-)-zine-6,12-dione were synthesized (Shindy et al., 2014), Scheme 17.

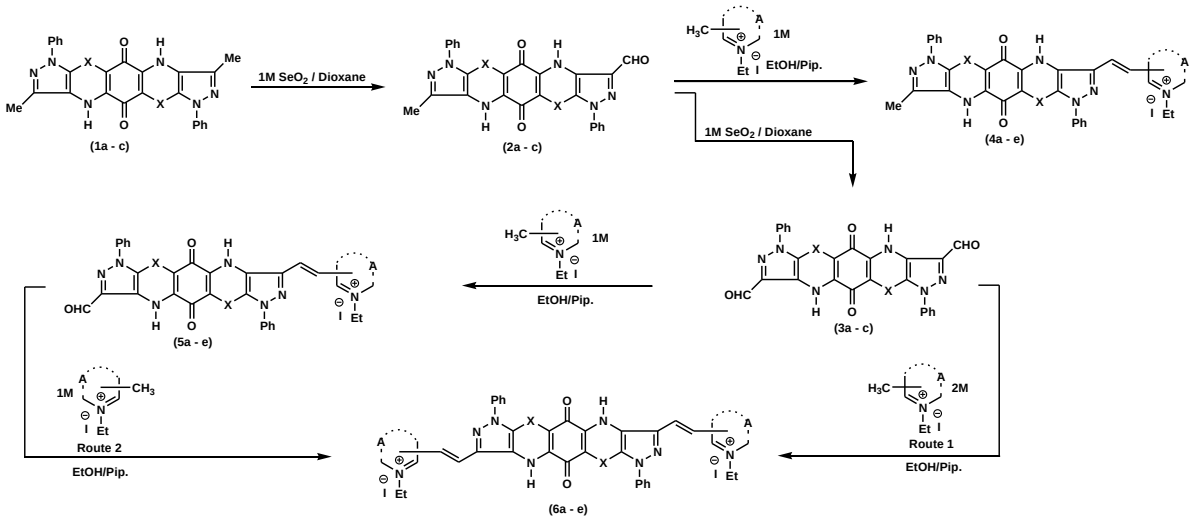

(1a-c); (2a-c);(3a-c): (a), X = O; (b), X = S; (c), X= NH. (4a-e); (5a-e) & (6a-e): (a) X = O, A = 1-ethyl pyridinium-2-yl salt; (b) X = O, A = 1-ethyl quinolinium-2-yl salt; (c) X = O, A = 1-ethyl pyridinium-4-yl salt; (d) X = S, A = 1-ethyl quinolinium-2-yl salt; (e) X = NH, A = 1-ethyl quinolinium-2-yl salt

Fig. 17. Scheme 17

3. Conclusion

1. The structure of cyanine dyes are consists of two heterocycles containing nitrogen linked together by a number of methine groups. If one methine unit, the cyanine named monomethine cyanine dyes, if two methine units, the cyanine called dimethine cyanine dyes, if three methine units, the cyanine termed trimethine cyanine dyes, and so on. The two heterocycles one is acts as electron donor (the basic center of the dye) and the other is acts as electron acceptor (the acidic center of the dye) and vice versa, creating and/or generating an push-pull system throughout the conjugated structure system of the cyanine dyes molecules, Scheme (18).

2. The intensity of the colour of the cyanine dyes is illustrated according to suggested two mesomeric electronic transitions structures (two resonance forms) (A) and (B) producing a delocalized positive charges over the conjugated chromophoric group system of the dyes structures, Scheme 18.

3. Cyanine dyes are electronic charge transfer pathways dyes. These charge transfer pathways is due to transfer of lone pair of electrons from the N •• -B-hetero nitrogen atom of the dyes (the electron donor and/or the basic center of the dyes) to the quaternary +N-A- hetero nitrogen atom of the dyes (the electron acceptor and/or the acidic center of the dyes), and vice versa, Scheme 18.

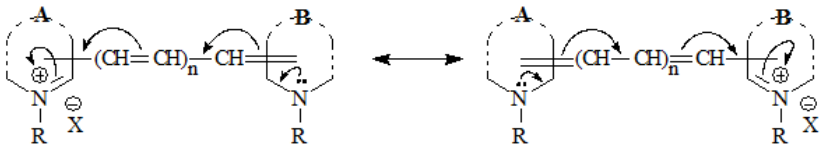

(A) (B)

(n = 0, 1, 2, 3, etc.); R=CH_3, CH_3CH_2;
X=I; Br, ClO_4; A = Heterocyclic nucleus; B = Heterocyclic nucleus

General structure, colour intensity and electronic charge transfer pathways illustration of cyanine dyes.

Fig. 18. Scheme 18

4. Cyanine dyes are solid state organic solar cell dyes (Kim, 2006). The appropriate electrochemical properties of cyanine make it possible to be used both as donor and acceptor in thin film heterojunction solar cells. Another property of cyanine is that it can be spin coated from solution to form good film, which is of great interest for large area photovoltaic production. The effect of counter ion on the properties of solid state solar cells have been discussed before. The covalently linked cyanine-fullerene dyad is also an promising materials for photovoltaic devices due to the photo induced intramolecular electron transfer from cyanine to fullerene.

5. Cyanine dyes are pH sensitive dyes, and so, their ethanolic solutions give changeable colours in acid and base media being yellow or colourless on acidification. and getting back (restore) their permanent intense colour on basification, Scheme 19.

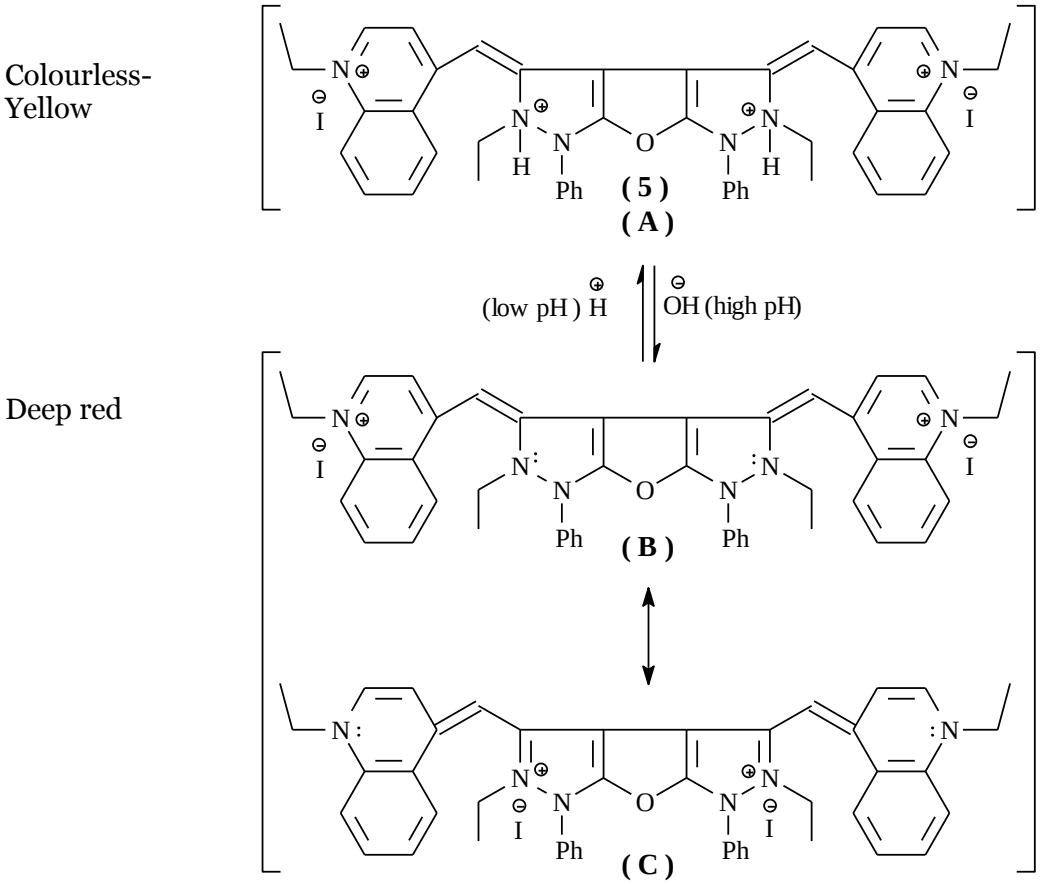

Fig. 19. Scheme 19. Decolourization (protonation) and colourization (deprotonation) of the bis mnomethine cyanine dye (5) in acid and base media, respectively (acido-basic equilibrium)

6. This review paper is recommended for chemists and researchers in the field of heterocyclic and/or cyanine dyes chemistry.

7. This paper review is recommended to all who are keen to have and know different methods in the synthesis of various classes of polyheterocyclic cyanine dyes and/or to get some basic applications, properties and characterization in the chemistry of cyanine dyes.

8. Because cyanine dyes have multi purposes uses and applications in various fields and different research area, this review paper is recommended not only for heterocyclic and/or cyanine dyes chemists but also for other scientists in other fields like biology, biotechnology, biochemistry, physics, engineering, pharmacology and medicine.

9. This review paper is recommended for all whom interested in the light absorbing systems in their research, labeling of biomolecules and/or in the synthesis and characterization of complex organic compounds.

10. This paper review is recommended to anyone interested in the subject, to chemistry libraries and also for the personal bookshelves of every organic heterocyclic and cyanine dyes chemist.

Current future development

The current and the future research developments aim to provide novel synthetic methods for the preparation of different classes of highly antimicrobial (antibacterial and anti-fungi) active, anti-tumor, anti-cancer, p-H sensitive, highly photographic sensitizers, non-toxic, high stability, light fastness, near IR (Infrared), fluorescent, anti-corrosion, strong labeled DNA and extra conjugated cyanine dyes. Such as oxadiazine cyanine dyes, thiazole cyanine dyes, metal stabilized cyanine dyes, pentamethine cyanine dyes, heptamethine cyanine dyes, nonamethine cyanine dyes, undecamethine cyanine dyes and tridecamethine cyanine dyes.

Also, the current and/or the future research developments aimed to provide new, novel and/or patent review papers in the field of color, dyes and pigments chemistry. The aimed review papers will covers and/or includes topics like the origin of color, the relation between color and constitutions, synthesis of dyes, properties of dyes, classification of dyes, uses and/or applications of dyes. Also, additional important topics for the current and/or the future research developments for the aimed review papers will includes methine cyanine dyes, hemicyanine dyes (styryl cyanine dyes), merocyanine dyes, apocyanine dyes, monoheterocyclic cyanine dyes, biheterocyclic cyanine dyes, polyheterocyclic cyanine dyes, six membered heterocyclic cyanine dyes, five/six membered heterocyclic cyanine dyes, five membered heterocyclic cyanine dyes and benz(naphth)/five membered heterocyclic cyanine dyes.

A very bright future for cyanine dyes chemistry can be expected through joint efforts (collaboration) of a large heterogenous community groups composed of synthetic cyanine dyes chemists, molecular biologists, physicists, biotechnologists, pharmacologists, technological engineerists and medical scientists.

4. Conflict of interest

There is no conflict of interest.

5. Acknowledgements

I am thankful to the Chemistry department, Faculty of Science, Aswan University, Aswan, Egypt for supporting this work.

References

Abd El-Aal, Koraiem, 2002 – *Abd El-Aal, R.M., Koraiem, A.I.M.* (2002). Synthesis, photophysics in organic solvents of meso substituted pentamethine, related metal complexes cyanine dyes. *Dyes and Pigments*. 54: 121-129.

Abd El-Aal, Younis, 2004 – *Abd El-Aal, R.M., Younis, M.* (2004). Synthesis and antimicrobial activity of certain novel monomethine cyanine dyes. *Dyes and Pigments*. 60: 205-214.

Abd El-Motaleb, 2002 – *Abd El-Motaleb, M.A.* (2002). M. Sc. Thesis, Aswan Faculty of Science, South Valley University.

Deligeogiev et al., 1989 – *Deligeogiev, T.G., Zaneva, D., Kim, S.M.* (1989). *Dyes and Pigments*. 17: 205.

Deligeorgiev et al., 2000 – *Deligeorgiev, T.G., Gadjev N.I., Timtcheva, I.I., Maximova, V.A., Katerinopoulos, H.E., Foukaraki, E.* (2000). *Dyes and Pigments*. 44: 131-136.

Ephardt, Fromhers, 1989 – Ephardt, H., Fromherz, P. (1989). Fluorescence and photoisomerization of an amphiphilic aminostilbazohum dye as controlled by the sensitivity of radiationless deactivation to polarity and viscosity. *J. Phys Chem*. 93: 7717-25.

Fedotov, Romanov, 1989 – *Fedotov, K.V., Romanov, N.N.* (1989). Khim Geterotsikl, Soedin, 6: 817-822.

Gadjev et al., 1999 – *Gadjev, N., Deligeorgiev, T., Kim, S.H.* (1999). *Dyes and Pigments*. 40, 181.

Gromov et al., 1992 – *Gromov, S.P., Fedorova, O.A., Ushakov, E.N., Buevich, A.V., Baskin, I.I., Pershina, Y.V.* (1992). Total synthesis of the mycotoxin (-)-zearalenone based on macrocyclisation using a cinnamyl radical intermediate. *J Chem Soc Perkin Trans*. 2: 1323-8.

Hamer, 1964 – *Hammer, F.M.* (1964). The cyanine dyes and related compounds, Interscience, wiley, New York, London.

He et al., 1995 – *He, G.S., Bhawalkar, J.D., Zhao, C.F., Prasad, P.N.* (1995). Optical limiting effect in a two-photon absorption dye doped solid matrix. *Appl Phys Lett*. 67: 2433-5.

Hyun et al., 2015 – *Hyun, H., Owens, E.A., Wada, H., Levitz, A., Park, G., Park, M.H., Frangioni, J.V., Henary, M., Choi, H.S.* (2015). Cartilage-Specific Near-Infrared Fluorophores for Biomedical Imaging. Angew. *Chem. Int. Ed. Engl.* 54, 8648-8652.

Keisar et al., 2014 – *Keisar, O.R., Finfer, E.K., Ferber, S., Finaro, R., Shabat, D.* (2014). Synthesis and use of QCY7-derived modular probes for the detection and imaging of biologically relevant analytes. *Nature Protocols*. 9 (1): 27-36.

Kim, 2006 – *Kim, S.H.* (2006). Functional dyes, Oxford, Elsevier B. V., Chapter 2, 58-61.

Komljenovic et al., 2016 – *Komljenovic, D., Wiessler, M., Waldeck, W., Ehemann, V., Pipkorn, R., Shrenk, H., Debus, J., Braun, R.* (2016). NIR-cyanine dye linker: a promising candidate for isochronic fluorescence imaging in molecular cancer diagnostics and therapy monitoring. *Theranostics*. 6 (1): 131-141.

Koraiem et al., 2006 – *Koraiem, A.I.M., Abd El-Aal, R.M., Salah El-Deen, N.M.* (2006). The use of N-bridgehead heterocyclic indolizinium ylide in the synthesis of aza-cyanine dyes. *Dyes and Pigments*. 68: 235-242.

Meng et al., 2003 – *Meng, F.S., Yao, Q.H., Sheng, J.G., Li, F.L., Huang, C.H., Chen. K.C., Tian, H.* (2003). *Synth. Met*. 137: 1543.

Mishra et al., 2000 – *Mishra, A., Behera, R.K., Behera, P.K., Mishra, B.K., Behera, G.B.* (2000). Cyanines during the 1990s: A review. *Chem. Rev*. 100: 1973-2012.

Mohamed, 1998 – *Mohamed, F.S.* (1998). M. Sc. Thesis, Aswan Faculty of Science, South Valley University.

Njiojob et al., 2015 – *Njiojoh, C.N., Owens, E.A., Narayana, L., Hyun, H., Choi, H.S., Henary, M.* (2015). Tailored Near-Infrared Contrast Agents for Image Guided Surgery. *J. Med. Chem*. 58: 2845-2854.

Osman et al., 1978 – *Osman, A.M., Khalil, Z.H., Youssef, M.S.K.* (1978). *Indian Journal of Chemistry*. 168: 865-868.

Osman, Khalil, 1975 – *Osman, A.M., Khalil, Z.H.* (1975). Studies on cyanine dyes. I. Synthesis of new oxacyanine dyes. *J. Appl. Chem. Biotechnol*. 25: 683-693.

Shindy et al., 2009 – *Shindy, H.A., El-Maghraby, M.A., Eissa. F.M.* (2009). Synthesis, absorption spectra studies, solvatochromism and halochromism of polymethine cyanine dyes. *Coloration Technology*. 125 (2): 104-110.

Shindy et al., 2014 – *Shindy, H.A., El-Maghraby, M.A., Eissa. F.M.* (2014). Effects of Chemical structure, solvent and solution pH on the visible spectra of some new methine cyanine dyes. *European Journal of Chemistry*. 5 (3): 451-456.

Shindy et al., 2017 – *Shindy, H.A., Khalafalla, A.K., Goma, M.M., Eed, A.H.* (2017). Synthesis and studies on some new dimethine and tetramethine cyanine dyes. *European Reviews of Chemical Research*. 4 (2): 52-65.

Shindy et al., 2018 – *Shindy, H.A., El-Maghraby, M.A., Goma, M.M., Harb, N.A.* (2018). Synthesis, electronic transitions and antimicrobial activity evaluation of novel monomethine and trimethine cyanine dyes. *European Journal of Molecular Biotechnology*. 6 (2): 83-95.

Shindy et al., 2019 – *Shindy, H.A., El-Maghraby, M.A., Goma, M.M., Harb, N.A.* (2019). Novel styryl and aza-styryl cyanine dyes: synthesis and spectral sensitization evaluation. *Chemistry International*. 5 (2): 117-125.

Shindy et al., 2019a – *Shindy, H.A., El-Maghraby, M.A., Goma, M.M., Harb, .N.A.* (2019). Polynuclear heterocyclic monomethine and trimethine cyanine dyes: synthesis and various absorption spectra studies. *European Journal of Molecular Biotechnology*. 7 (1): 25-39.

Shindy, 2012 – *Shindy, H.A.* (2012). Basics, Mechanisms and Properties in the Chemistry of Cyanine Dyes: A Review Paper. *Mini-Reviews in Organic Chemistry*. 9 (4): 352-360.

Shindy, 2016 – *Shindy, H.A.* (2016). Characterization, Mechanisms and Applications in the Chemistry of Cyanine Dyes: A Review. *European Journal of Molecular Biotechnology*, 14 (4), 158-170.

Shindy, 2017 – *Shindy, H.A.* (2017). Fundamentals in the Chemistry of Cyanine Dyes: A Review. *Dyes and Pigments*. 145: 505-513.

Shindy, 2018 – *Shindy, H.A.* (2018). Structure and solvent effects on the electronic transitions of some novel furo / pyrazole cyanine dyes. *Dyes and Pigments*. 149: 783-788.

Shindy, 2018a – *Shindy, H.A.* (2018). Novel polyheterocyclic cyanine dyes: synthesis, photosensitiztion and solvent/electronic transitions correlation. *European Reviews of Chemical Research*. 5 (1): 30-39.

Shindy, 2019 – *Shindy, H.A.* (2019). Synthesis of different classes of polyheterocyclic cyanine dyes: A review. *European Reviews of Chemical Research*. 6 (1): 29-46.

Shindy, et al., 2012 – *Shindy, H.A., El-Maghraby, M.A., Eissa, F.M.* (2012). Synthesis and Colour Spectrophotometric Measurements of some Novel Merocyanine Dyes. *Dyes and Pigments*. 92 (3): 929-935.

Shindy, koraiem, 2008 – *Shindy, H.A., Koraiem, A.I.M.* (2008). Synthesis and Colour Spectroscopic Investigation of Some Hemicyanine Dyes. *Coloration Technology*. 124 (5): 290-294.

Solomon et al., 2014 – *Solomon, R.V., Jagadeesan, R., Vedha, S.A., Venuvanalingam, P.* (2014). ADFT/TDDFT modelling of bithiophene azo Chromophores for optoelectronic applicatons. *Dyes and Pigment*. 100: 261-268.

Sun et al., 2013 – *Sun, R., Yan, B., Ge, J., Xu, Q., Li, N., Wu, X., Song, Y., Lu, J*. (2013). Third-order nonlinear optical properties of unsymmetric petamethine cyanine dyes possessing benzoxazolyl and benzothiazolyl groups. *Dyes and Pigments*. 96: 189-195.

Takashi et al., 1998 – Takashi, K., Yoshio, I., Renji, O. (1998). *J. Am. Chem. Soc.* 120 (15): 3623-3628.

Vasilev et al., 2005 – *Vasilev, A., Deligeorgiev, T., Gadjev, N., Drexhage, K.H*. (2005). Synthesis of novel monomeric and homodimeric cyanine dyes based on oxazolo[4,5-b]pyridinium and quinolinium end groups for nucleic acid detection. *Dyes and Pigments*. 66: 135-142.

Wada et al., 2015 – *Wada, H., Hyun, H., Vargas, C., Gravier, J., Park, G., Gioux, S., Frangioni, J.V., Henary, M., Choi, H.S.* (2015). Pancreas-Targeted NIR Fluorophores for Dual-Channel Image-Guided Abdominal Surgery. *Theranostics*. 5: 1-11.

Wang et al., 2003 – *Wang, Q-C, Qu, D., Ren J., Xu, L., Liu, M., Tian, H.* (2003). New benzo[e]indolinium cyanine dyes with two different fluorescence wavelengths. *Dyes Pigments*. 59: 163-72.

Wang et al., 2003a – *Wang, J., Cao, W-F., Su, J-H., Tian, H., Huang, Y-H., Sun, Z-R.* (2003). Synthesis and nonlinear absorption of novel unsymmetrical cyanine. *Dyes Pigments*. 57: 171-9.

Yi et al., 2014 – *Yi, X., Wang, F., Qin, W., Yang, X., Tuan, J*. (2014). Near-Infrared fluorescent probes in Cancer imaging and therapy: an emerging field. *International Journal of Nanomedicine*. 9, 1347-1365.

Zhang, et al., 2016 – *Zhang, H., Niesen, B., Hack, E., Jenatasch, S., Wang, L., Veron, A.C., Makha, M., Schneider, R., Arroyo, Y., Hany, R., Nuesch, F.* (2016). Cyanine tandem and triple-junction solar cells. *Organic Electronics*. 30: 191-199.

Zhao et al., 1996 – *Zhao, C.F., Gvishi, R., Narang, U., Rutand, G., Prasad, P.N*. (1996). Structures, spectra and lasing properties of new (aminostyryl)pyridinium laser dyes. *J. Phys Chem*. 100: 4526-32.

Zhao et al., 2013 – *Zhao J., Lv, Y., Ren, H., Sun, W., Liu, Q., Fu, Y., Wang, L*. (2013). Synthesis, spectral properties of cyanine dyes β-cyclodextrin and their application as the supramolecular host with spectroscopic probe. *Dyes and Pigments*. 96: 180-188.

Published in the Slovak Republic
European Journal of Molecular Biotechnology
Has been issued since 2013.
E-ISSN: 2409-1332
2019, 7(2): 123-125

DOI: 10.13187/ejmb.2019.2.123
www.ejournal8.com

Letters to the Editorial

Distribution Trends of African Swine Fever Virus (ASFV) through Water

Stoil Karadzhov [a], Ignat Ignatov [b, *], Hristo Najdenski [c], Teodora Popova [d], Wolfgang Luepcke [e], Georgi Gluhchev [c], Nik Kolev [f], Stefan Balabanov [f]

[a] Bulgarian Association of Activated Water, Sofia, Bulgaria
[b] Scientific Research Center of Medical Biophysics (SRCMB), Sofia, Bulgaria
[c] Bulgarian Academy of Sciences (BAS), Sofia, Bulgaria
[d] University of Forestry, Faculty of Veterinary Medicine, Sofia, Bulgaria
[e] University of Agribusiness and Rural Development, Regiowelr, Germany
[f] ADVA international, Stara Zagora, Bulgaria, London, UK

Abstract

The places for spreading of viruses in ground water are mostly in non-porous media aquifers. They are karst (limestone) aquifers and fractured bedrock (metamorphic rock) (Fong et al., 2007). Different authors have proved the spreading of the viruses in ground water. The Berger's study has dealt with Enteric virus (Berger, 2007). Norwalk-like virus has detected in ground water (Anderson, 2001).

The African swine fever (ASF) is contagious and rapidly spreading swine disease. The great virulence and continuous resilience in the environment, including in the natural water sources as an activator of African swine fever virus (ASFV), are a prerequisite for a seamless cross-border transmission of the disease, defining it as a main threat for the world's pig meat production. In 2007 ASFV infected pigs in Georgia, and in 2014 it reached the European Union (Boklund et al., 2018). In 2019 it has been observed in Bulgaria and has had serious economic consequences. The Tissue Culture Infectious Dose (TCID) for pigs is $10^{1.0}$ $TCID_{50}$ in liquids, and is $10^{6.8}$ $TCID_{50}$ in dried fodder (Niederwerder et al., 2019).

Contaminated water from the Danube River has been implicated in introducing ASF onto the ≈140,000 pig-breeding farms.

Keywords: virus, water, swine disease, hydrodynamic and antibacterial effect.

1. Introduction

In 2019 the African swine fever virus (ASFV) was registered in Bulgaria. The first farms infected with it were in the region of Ruse which borders Romania on the Danube. There are numerous small surface and underground rivers and streams on the territory of Bulgaria. A significant part of the farms are using their own water sources which is precondition for a possible breach with the technological bio-security, and as a consequence could infect the animals with doses larger than $10^{1.0}$ $TCID_{50}$.

* Corresponding author
E-mail addresses: mbioph@abv.bg (I. Ignatov)

The possibility for this are as follows.
1. Groundwater for closely positioned farms.
2. Excrements and decomposing carcasses of feral pigs.
3. Rainfall and run-off flows that leach into the soil.
4. Infected meat of wild boars carried by jackals.
5. Rats and other rodents.

2. Materials and methods

Research of drinking water in pig holdings is conducted. The physical parameters pH and ORP (Oxidation Reduction Potential) of the water are measured using HANNA Instruments HI221 meter equipped with Sensorex sensors. Analysis of the infection of closely positioned pig-breeding complexes is prepared.

Range of HANNA Instruments HI221 meter:

2.1. Parameters of pH

pH - (2.00-16.00)

For pH range the statistical error is 0.01

2.2. Parameters of Oxidation Reduction Potentail

ORP (±699.9- ±2000) mV

For ORP range (±699.9) the statistical error is ±0.01 mV

For ORP range **(**±2000) the statistical error is ±0.1 mV

3. Results

The potable waters in the pig-breeding farms are with pH from 6.5 to 8, and ORP from +230 to +350 mV. With such parameters the water is a conductive medium for the development of micro-organisms, including ASFV. (Karadzov et al., 2014; Popova, 2016).

Figure 1 shows the area of the bio-sphere of microorganisms as a function of pH and ORP. It is defined with the intervals from 3 to 10 for pH and -400 mV to +900 mV for ORP. The microorganisms will hardly survive outside these ranges (Karadzhov et al., 2015).

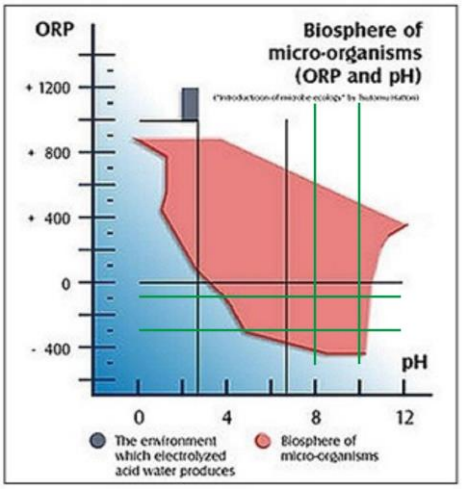

Fig. 1. Biosphere of microorganisms depending on pH and ORP of the water

The above data determine the water as a possible factor for the distribution of ASFV. In order to protect the animals from diseases transferred through water, there is a need for thorough antimicrobial control on each drop of water.

4. Conclusion

The authors point to the possibility of ASFV spread through water, which requires taking of emergency measures for its elimination as a risk factor for the appearance and transmission of African swine fever. The disinfectants in the drinking water for animals cannot guarantee its full bio-safety. Furthermore, they alter the organoleptic properties of the water and the animals drink it reluctantly.

There is a possibility of using the installations for bio-safety assurance of the water by its structuring (Ignatov, Mosin, 2013), where its organoleptic properties improve substantially, and at the same time the pathogenic micro-organisms get disintegrated as a result of the hydrodynamic effect (Suslick et al., 2004; Dular et al., 2016; Bandala, Rodriguez-Narvaez, 2019).

According to (Ignatov, Mosin et al., 2013) the combination of hydrodynamic and antibacterial effect, expressed by local extremum at (E = -0.1212 eV)(λ=10.23 μm)(ṽ=978 cm^{-1}) enables the bio-safety of the water.

References

Fong et al., 2007 – *Fong, T-T, et al.* (2007). Massive Microbiological Groundwater Contamination Associated with a Waterborne Outbreak in Lake Erie, South Bass Island, OH. *Environmental Health Perspectives*. 15 (6): 856-64.

Berger, 2007 – *Berger, Ph.* (2007). Viruses in Ground Water, Dangerous Pollutants (Xenobiotics) in Urban Water Cycle: 131-149.

Anderson et al., 2001 – *Anderson, A.D. et al.* (2001). A Waterborne Outbreak of Norwalk-like Virus among Snowmobilers-Wyoming. *Jour. Infect. Dis.* 187: 303-306.

Boklund et al., 2018 – *Boklund A. et al.* (2018). Epidemiological Analyses of African Swine Fever in the European Union (November 2017 until November 2018). *EFSA J.* 16: 5494.

Niederwerder et al., 2019 – *Niederwerder, M. et al.* (2019). Infectious Dose of African Swine Fever Virus When Consumed Naturally in Liquid or Feed. *Emerg Infect Dis.* 25 (5): 891-897.

Karadzhov et al., 2014 – *Karadzhov, S., Atanasov, A., Ivanova, E., Mosin, O. V., Ignatov, I.* (2014). Mathematical Models of Electrochemical Aqueous Sodium Chloride Solutions (Anolyte and Catholyte) as Types of Water. Study of the Effects of Anolyte on the Virus of Classical Swine Fever Virus. *Journal of Health, Medicine and Nursing*. 5: 30-55.

Popova, 2016 – *Popova, T.* (2016). Microbiology, Publ.house at FTU. Sofia: 311.

Gluhchev et al., 2015 – *Gluhchev, G., Ignatov, I., Karadzhov, S., Miloshev, G., Ivanov, N., Mosin, O.V.* (2015). Studying of Virucidal and Biocidal Effects of Electrochemically Activated Anolyte and Catholyte Types of Water on Classical Swine Fever Virus (CSF) and Bacterium E. coli DH5, Journal of Medicine, Physiology and Biophysics, 13: 1-17.

Ignatov, Mosin, 2013 – *Ignatov, I., Mosin, O.V.* (2013). Structural Mathematical Models Describing Water Clusters. *Journal of Mathematical Theory and Modeling*. 3 (11): 72-87.

Suslick et al., 1997 – *Suslick, K.S, Mdleleni, M.M, Ries, J.T.* (1997). Chemistry Induced by Hydrodynamic Cavitation. *J Am Chem Soc.* 119: 9303-9304.

Trenchev, 2004 – *Trenchev, K.* (2004). Studies on the influence of the hydrodynamic effect on certain microorganisms. *Proceedings of the Fifth International Symposium "Ecology and Sustainable Development"*, Vratsa, 21-22.10.2004, 161-166.

Dular et al., 2016 – *Dular, M. et al.* (2016). Use of Hydrodynamic Cavitation in (waste) Water Treatment. *Ultrasonics Sonochemistry*. 29: 577-88

Bandala, Rodriguez-Narvaez, 2019 – *Bandala, E., Rodriguez-Narvaez, O.* (2019). On the Nature of Hydrodynamic Cavitation Process and Its Application for the Removal of Water Pollutants. *Air, Soil and Water Research*. 12.

Valcheva et al., 2020 – *Valcheva, N., Ignatov, I., Dinkov, G.* (2020). Microbiological and Physicochemical Research of Thermal Spring and Mountain Spring Waters in the District of Sliven, Bulgaria. *Journal of Advances in Microbiology*. 20 (2): 9-17.

Ignatov et al., 2020 – *Ignatov, I., Gluhchev, G., Karadzhov, S. et al.* (2020). Dynamic Nano Clusters of Water on Waters Catholyte and Anolyte. Electrolysis with Nano Membranes, Manuscript: Dynamic Nano Clusters of Water on Waters Catholyte and Anolyte. *Electrolysis with Nano Membranes, Physical Science International Journal*. 24 (1): 46-54.

Velichkova et al., 2018 – *Velichkova, K., Sirakov, I., Rusenova, N., Beev, G., Denev, S., Valcheva, N., Denev, T.* (2018). In vitro Antimicrobial Activity on LemnaMinuta, Chlorella Vulgaris and Spirulina Sp. Extracts. *Fresenius Environmental Bulletin*. 27 (8): 5736-5741.

Tumbarski et al., 2014 – *Tumbarski, Y., Valcheva, N., Denkova, Z., Koleva, I.* (2014). Antimicrobial activity against Some Saprophytic and Pathogenic Microorganisms of Bacillus species Strains Isolated from Natural Sping Waters in Bulgaria. *British Microbiology Research Journal*. 4 (12): 1353-1369.